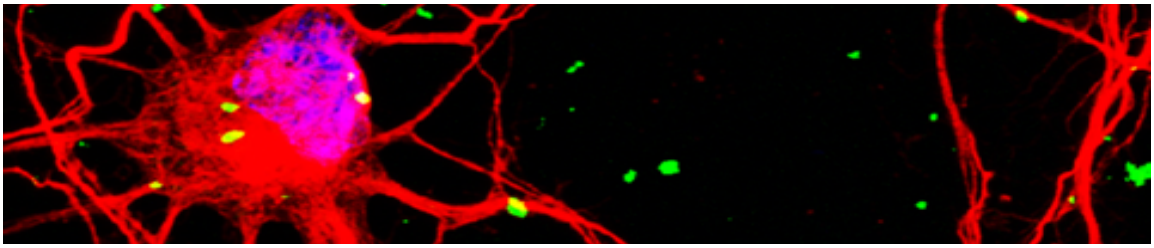

Corso di Dottorato in Neuroscienze
Curriculum Neuroscienze e Neurotecnologie
Ciclo XXX

Evaluating the impact of intracortical microstimulation on distant cortical brain regions for neuroprosthetic applications

Author: Alberto Averna
Supervisor: Dr Michela Chiappalone

ISTITUTO ITALIANO DI TECNOLOGIA

UNIVERSITÀ DEGLI STUDI DI GENOVA

ABSTRACT 7

CHAPTER 1 INTRODUCTION 10

CHAPTER 2 SCIENTIFIC AND TECHNICAL BACKGROUND 18

2.1. ORGANIZATION OF MOTOR AND SENSORY CORTICES 19

2.1.1. ORGANIZATION OF THE MOTOR CORTEX 19

2.1.2. ORGANIZATION OF THE SOMATOSENSORY CORTEX 23

2.1.3. CORTICO-CORTICAL CONNECTIONS 24

2.2. A BRIEF OVERVIEW ON STROKE 26

2.2.1. IN VIVO MODELS OF STROKE 30

2.2.2. LIMITATIONS OF IN VIVO MODELS OF STROKE 32

2.3. COMMUNICATING WITH CORTICAL TISSUE 34

2.3.1. STIMULATION OF MOTOR CORTEX 34

2.3.2. RECORDING NEURONAL ACTIVITY 37

2.4. NEUROPROSTHESIS FOR BRAIN REPAIR 44

ELECTROCEUTICAL CONCEPT 45

2.4.1. OPEN AND CLOSED LOOP SYSTEMS 48

CHAPTER 3 MATERIALS AND METHODS 72

3.1. IN VIVO RECORDING AND STIMULATION PROCEDURE 73

3.1.1. ANESTHESIA AND SURGERY 75

3.1.2. CORTICAL MAPS 76

3.1.3. Implantation of MEAs **78**
3.1.4. Model of Brain Injury (Stroke) **78**
3.1.5. Recording and Stimulation Protocols **79**
Healthy Anesthetized Protocol 79
Injured Anesthetized Protocol 80
Healthy Awake Protocol 82
Ethical Statement 83
3.2. DATA RECORDING AND PROCESSING 84
3.2.1. Acquisition system **84**
Tucker Davis System (TDT) 84
Intan System 86
3.2.2. Data Analysis **87**
Analysis of SUA 89
Analysis of LFPs 94
CHAPTER 4 EFFECT OF ICMS ON HEALTHY ANAESTHETIZED ANIMALS 99
4.1. INTRODUCTION 100
4.2. METHODS 103
4.2.1. Animals **103**
4.2.2. Surgical Procedures **103**
4.2.3. Mapping Cortical Areas **104**
4.2.4. Experimental Protocol **105**
4.2.5. Data Processing **108**
Mean Firing Rate (MFR) 108

LOCAL VARIATION COMPENSATE FOR REFRACTORINESS 108

POST-STIMULUS TIME HISTOGRAM 109

STATISTICAL MODEL 109

4.3. RESULTS 111

4.3.1. ICMS RESULTS IN INCREASED FIRING RATE IN A DISTANT CORTICAL AREA 111

4.3.2. ICMS MODULATES NEURONAL FIRING PATTERNS IN A DISTANT CORTICAL AREA 118

4.3.3. ADS AND RS EXHIBIT DIFFERENT EFFECTS ON STIMULUS-ASSOCIATED ACTION POTENTIALS IN A DISTANT CORTICAL AREA 123

4.4. DISCUSSION 127

CHAPTER 5 EFFECT OF ICMS ON STROKE INJURED ANESTHETIZED ANIMALS 141

5.1. INTRODUCTION 142

5.2. METHODS 144

5.2.1. ANIMALS 144

5.2.2. SURGICAL PROCEDURES 144

5.2.3. MAPPING CORTICAL AREAS 145

5.2.4. EXPERIMENTAL PROTOCOL 146

5.2.5. DATA PROCESSING 149

5.3. RESULTS 150

5.3.1. LFP POWER CHANGES AFTER STROKE 150

5.3.2. ADS MODULATES LFP POWER 151

5.3.3. STROKE MANIPULATES FUNCTIONAL CONNECTIONS BETWEEN S1 AND RFA 154

5.3.4. ADS INDUCES FUNCTIONAL CONNECTIVITY CHANGES BOTH WITHIN (RFA, S1) AND BETWEEN AREAS 156

5.4. DISCUSSION 161

CHAPTER 6 EFFECT OF ICMS ON HEALTHY BEHAVING ANIMALS 165

6.1. INTRODUCTION 166

6.2. METHODS 168

6.2.1. ANIMALS 168
6.2.2. SURGICAL PROCEDURES 168
6.2.3. MAPPING CORTICAL AREAS 169
6.2.4. EXPERIMENTAL PROTOCOL 170
6.2.5. DATA PROCESSING 172
SUA 172
LFP 174

6.3. RESULTS 176

6.3.1. ICMS INDUCES NO CHANGES IN FIRING RATE IN AWAKE ANIMALS 176
6.3.2. ADS PRODUCES MORE SIGNIFICANT STIMULUS-ASSOCIATED RESPONSES THAN RS 179
6.3.3. ICMS INDUCES CHANGES IN LFP OSCILLATORY ACTIVITY 181

6.4. DISCUSSION 183

CONCLUSIONS 189

CHAPTER 7 APPENDIX 194

Abstract

Enhancing functional motor recovery after localized brain injury is a widely recognized priority in healthcare as disorders of the nervous system that cause motor impairment, such as stroke, are among the most common causes of adult-onset disability. Restoring physiological function in a dysfunctional brain to improve quality of life is a primary challenge in scientific and clinical research and could be driven by innovative therapeutic approaches. Recently, techniques using brain stimulation methodologies have been employed to promote post-injury neuroplasticity for the restitution of motor function. One type of closed-loop stimulation, i.e., activity-dependent stimulation (ADS), has been shown to modify existing functional connectivity within either healthy or injured cerebral cortices and used to increase behavioral recovery following cortical injury.

The aim of this PhD thesis is to characterize the electrophysiological correlates of such behavioral recovery in both healthy and injured cortical networks using in vivo animal models.

We tested the ability of two different intracortical micro-stimulation protocols, i.e., ADS and its randomized open-loop version (RS), to potentiate cortico-cortical connections between two distant cortical locations in both anaesthetized and awake behaving rats. Thus, this dissertation has the following three main goals: 1) to investigate the ability of ADS to induce changes in intra-cortical activity in healthy anesthetized rats, 2) to characterize the electrophysiological signs of brain injury and evaluate the capability of ADS to promote electrophysiological changes in the damaged network, and 3) to investigate the long-term effects of stimulation by repeating the treatment for 21 consecutive days in healthy awake behaving animals.

The results of this study indicate that closed-loop activity-dependent stimulation induced greater changes than open-loop random stimulation, further strengthening the idea that Hebbian-inspired protocols might potentiate cortico-cortical connections between distant brain areas. The implications of these results have the potential to lead

to novel treatments for various neurological diseases and disorders and inspire new neurorehabilitation therapies.

Chapter 1 Introduction

Neurological disorders have a substantial impact on public health and are among the most important causes of mortality, constituting 12% of all deaths globally (Organization, 2006). Among these disorders, stroke and traumatic brain injury (TBI) are two of the top ten causes of death and disability in children and young adults worldwide, frequently affecting individuals' ability to function and resulting in disabilities or limited activities and restricted participation. Although the incidence of stroke is decreasing, its prevalence in the population appears to be increasing because of increased stroke survival and the growing elderly population (Silvoni, 2011; Nichols, 2012). During a stroke, oxygen- and energy-hungry neurons are deprived of their normal metabolic substrates, cease to function within a time frame of seconds and show signs of structural damage after only two minutes. Although stroke damage can be devastating, many patients survive the initial event and undergo some spontaneous recovery, which can be further promoted by rehabilitative therapy.

Currently, one of the most widely adopted rehabilitation techniques for stroke or injury recovery involves the use of different electrical stimulation modalities, such as Transcranial Direct Current Stimulation (TDCS) (Schlaug, 2008), repetitive Transcranial Magnetic Stimulation (rTMS), and Epidural Cortical Stimulation (ECS) (Kopell, 2011; Edwardson, 2012), but the results are often controversial (Hummel *et al.*, 2008). These techniques apply electrical stimulation to large groups of cells without focusing only on the affected area and primarily modulate the excitability of focal regions in uninjured parts of the brain (Webster *et al.*, 2006). Intracortical Microstimulation (ICMS) of human brain tissue has been used in many different cases, including for the treatment of epileptic seizures (Kerrigan *et al.*, 2004; Lee *et al.*, 2006; Fisher *et al.*, 2010; Morrell, 2011), therapies for Parkinson's disease (Anderson *et al.*, 2005; Deuschl *et al.*, 2006; Bronstein *et al.*, 2011; Weaver *et al.*, 2012; Little *et al.*, 2013), basic research investigating the properties of different cortical cell types and networks (Ranck Jr, 1975; Cohen & Newsome, 2004; Tehovnik *et al.*, 2006; Histed *et al.*, 2013; Tehovnik & Slocum, 2013) and visual (Dobelle & Mladejovsky, 1974; Schmidt *et al.*, 1996; Bradley *et al.*, 2005; Torab *et al.*, 2011; Davis *et al.*, 2012) or somatosensory

(Berg *et al.*, 2013; Tabot *et al.*, 2013; Thomson *et al.*, 2013) neuroprosthetic devices. Moreover, recent studies (Kleim *et al.*, 2003; Jackson *et al.*, 2006; Guggenmos *et al.*, 2013) have demonstrated that in animal models, ICMS can be successfully used to manipulate neuronal functional connectivity, representing a potentially powerful tool for steering neuroplasticity occurring after brain injury. Specifically, the adopted technique, i.e., activity-dependent stimulation (ADS), utilizes the neural activity recorded at one site as a trigger for electrical stimulation at another site and has shown success in promoting behavioral recovery by re-establishing an artificial connection between the somatosensory cortex and pre-motor cortex following primary motor cortical injury (Guggenmos *et al.*, 2013). This technique is based on Hebbian neural conditioning, according to which neurons firing synchronously have an increased probability of enhancing connectivity through the long term potentiation (LTP) or long-term depression (LTD) of existing synapses and could potentially create new connections through axodendritic sprouting (Jackson *et al.*, 2006). Although the efficacy of this technique in promoting behavioral recovery has already been demonstrated (Guggenmos *et al.*, 2013), the impact of pairing neuronal populations using ADS on the network firing properties remains unclear.

The purpose of this PhD thesis is to investigate the ability of ICMS to alter the physiological cortical firing patterns in both injured and healthy rats. To reach this ambitious objective, this PhD thesis is divided into three main parts.

The first part addresses the scientific and technical background describing the already available technological tools that have been exploited in the context of this thesis project.

The second part reports the experimental procedures applied to acquire electrophysiological signals in vivo.

Finally, the third part describes the main results obtained by the characterization of the changes induced by ADS treatment in intra-cortical neuronal activity using the following: i) healthy anesthetized procedures using a single four-hour experiment

involving healthy brains, ii) injury anesthetized procedures in which a potent vasoconstrictor is injected to induce a focal lesion, and iii) chronic procedures in which the treatment of healthy brains is repeated for 21 consecutive days.

The final goal of this work is to understand whether ADS can potentiate cortico-cortical connections by altering the normal patterns of neuronal activity and thus to provide a foundation for assessing the optimal stimulus parameters for implementing ADS protocols in the most effective way. Thus, these investigations are critical for inspiring new neurorehabilitation therapies.

References

Anderson, V.C., Burchiel, K.J., Hogarth, P., Favre, J. & Hammerstad, J.P. (2005) Pallidal vs subthalamic nucleus deep brain stimulation in Parkinson disease. *Archives of neurology*, **62**, 554-560.

Berg, J., Dammann III, J., Tenore, F., Tabot, G., Boback, J., Manfredi, L., Peterson, M., Katyal, K., Johannes, M. & Makhlin, A. (2013) Behavioral demonstration of a somatosensory neuroprosthesis. *IEEE Transactions on Neural Systems and Rehabilitation Engineering*, **21**, 500-507.

Bradley, D.C., Troyk, P.R., Berg, J.A., Bak, M., Cogan, S., Erickson, R., Kufta, C., Mascaro, M., McCreery, D. & Schmidt, E.M. (2005) Visuotopic mapping through a multichannel stimulating implant in primate V1. *Journal of neurophysiology*, **93**, 1659-1670.

Bronstein, J.M., Tagliati, M., Alterman, R.L., Lozano, A.M., Volkmann, J., Stefani, A., Horak, F.B., Okun, M.S., Foote, K.D. & Krack, P. (2011) Deep brain stimulation for Parkinson disease: an expert consensus and review of key issues. *Archives of neurology*, **68**, 165-165.

Cohen, M.R. & Newsome, W.T. (2004) What electrical microstimulation has revealed about the neural basis of cognition. *Current opinion in neurobiology*, **14**, 169-177.

Davis, T., Parker, R., House, P., Bagley, E., Wendelken, S., Normann, R. & Greger, B. (2012) Spatial and temporal characteristics of V1 microstimulation during chronic implantation of a microelectrode array in a behaving macaque. *Journal of neural engineering*, **9**, 065003.

Deuschl, G., Schade-Brittinger, C., Krack, P., Volkmann, J., Schäfer, H., Bötzel, K., Daniels, C., Deutschländer, A., Dillmann, U. & Eisner, W. (2006) A randomized trial of deep-brain stimulation for Parkinson's disease. *New England Journal of Medicine*, **355**, 896-908.

Dobelle, W. & Mladejovsky, M. (1974) Phosphenes produced by electrical stimulation of human occipital cortex, and their application to the development of a prosthesis for the blind. *The Journal of physiology*, **243**, 553-576.

Edwardson, M.A., Lucas, T.H., Carey, J. R., Fetz, E. E. (2012) New modalities of brain stimulation for stroke rehabilitation. *Exp. Brain Res.*, **224**, 335-358.

Fisher, R., Salanova, V., Witt, T., Worth, R., Henry, T., Gross, R., Oommen, K., Osorio, I., Nazzaro, J. & Labar, D. (2010) Electrical stimulation of the anterior nucleus of thalamus for treatment of refractory epilepsy. *Epilepsia*, **51**, 899-908.

Guggenmos, D.J., Azin, M., Barbay, S., Mahnken, J.D., Dunham, C., Mohseni, P. & Nudo, R.J. (2013) Restoration of function after brain damage using a neural prosthesis. *Proc Natl Acad Sci U S A*, **110**, 21177-21182.

Histed, M.H., Ni, A.M. & Maunsell, J.H. (2013) Insights into cortical mechanisms of behavior from microstimulation experiments. *Progress in neurobiology*, **103**, 115-130.

Hummel, F.C., Celnik, P., Pascual-Leone, A., Fregni, F., Byblow, W.D., Buetefisch, C.M., Rothwell, J., Cohen, L.G. & Gerloff, C. (2008) Controversy: noninvasive and invasive cortical stimulation show efficacy in treating stroke patients. *Brain stimulation*, **1**, 370-382.

Jackson, A., Mavoori, J. & Fetz, E.E. (2006) Long-term motor cortex plasticity induced by an electronic neural implant. *Nature*, **444**, 56-60.

Kerrigan, J.F., Litt, B., Fisher, R.S., Cranstoun, S., French, J.A., Blum, D.E., Dichter, M., Shetter, A., Baltuch, G. & Jaggi, J. (2004) Electrical stimulation of the anterior nucleus of the thalamus for the treatment of intractable epilepsy. *Epilepsia*, **45**, 346-354.

Kleim, J.A., Bruneau, R., VandenBerg, P., MacDonald, E., Mulrooney, R. & Pocock, D. (2003) Motor cortex stimulation enhances motor recovery and reduces peri-infarct dysfunction following ischemic insult. *Neurol Res*, **25**, 789-793.

Kopell, B.H., Halverson, J., Butson, C. R., Dickinson, M., Bobholz, J., Harsch, H., Rainey, C., Kondziolka, D., Howland, R., Eskandar, E., Evans, K. C., Dougherty, D. D. (2011)

Epidural Cortical Stimulation of the Left Dorsolateral Prefrontal Cortex for Refractory Major Depressive Disorder. *Neurosurgery*, **69**, 1015-1029.

Lee, K., Jang, K. & Shon, Y. (2006) Chronic deep brain stimulation of subthalamic and anterior thalamic nuclei for controlling refractory partial epilepsy *Advances in functional and reparative neurosurgery*. Springer, pp. 87-91.

Little, S., Pogosyan, A., Neal, S., Zavala, B., Zrinzo, L., Hariz, M., Foltynie, T., Limousin, P., Ashkan, K. & FitzGerald, J. (2013) Adaptive deep brain stimulation in advanced Parkinson disease. *Annals of neurology*, **74**, 449-457.

Morrell, M.J. (2011) Responsive cortical stimulation for the treatment of medically intractable partial epilepsy. *Neurology*, **77**, 1295-1304.

Nichols, M., Townsend, N., Scarborough, P., Rayner, M., Leal, J., Luengo-Fernandez, R. (2012) European Cardiovascular Disease Statistics. European Heart Network and European Society of Cardiology, Brussels, belgium.

Organization, W.H. (2006) *Neurological disorders: public health challenges*. World Health Organization.

Ranck Jr, J.B. (1975) Which elements are excited in electrical stimulation of mammalian central nervous system: a review. *Brain research*, **98**, 417-440.

Schlaug, G., Renga, V., Nair, D. (2008) Transcranial Direct Current Stimulation in Stroke Recovery. *Arch. Neurol.*, **65**, 1571-1576.

Schmidt, E., Bak, M., Hambrecht, F., Kufta, C., O'rourke, D. & Vallabhanath, P. (1996) Feasibility of a visual prosthesis for the blind based on intracortical micro stimulation of the visual cortex. *Brain*, **119**, 507-522.

Silvoni, S., Ramos-Murguialday, A., Calvinato, M., Volpato, C., Cisotto, G., Turolla, A., Piccione, F., Birbaumer, N. (2011) Brain-Computer Interface in Stroke: a Review of Progress. *Clinical EEG and Neuroscience*, **42**, 245-252.

Tabot, G.A., Dammann, J.F., Berg, J.A., Tenore, F.V., Boback, J.L., Vogelstein, R.J. & Bensmaia, S.J. (2013) Restoring the sense of touch with a prosthetic hand through a brain interface. *Proceedings of the National Academy of Sciences*, **110**, 18279-18284.

Tehovnik, E.J. & Slocum, W.M. (2013) Electrical induction of vision. *Neuroscience & Biobehavioral Reviews*, **37**, 803-818.

Tehovnik, E.J., Tolias, A.S., Sultan, F., Slocum, W.M. & Logothetis, N.K. (2006) Direct and indirect activation of cortical neurons by electrical microstimulation. *J Neurophysiol*, **96**, 512-521.

Thomson, E.E., Carra, R. & Nicolelis, M.A. (2013) Perceiving invisible light through a somatosensory cortical prosthesis. *Nature communications*, **4**, 1482.

Torab, K., Davis, T., Warren, D., House, P., Normann, R. & Greger, B. (2011) Multiple factors may influence the performance of a visual prosthesis based on intracortical microstimulation: nonhuman primate behavioural experimentation. *Journal of neural engineering*, **8**, 035001.

Weaver, F.M., Follett, K.A., Stern, M., Luo, P., Harris, C.L., Hur, K., Marks, W.J., Rothlind, J., Sagher, O. & Moy, C. (2012) Randomized trial of deep brain stimulation for Parkinson disease Thirty-six-month outcomes. *Neurology*, **79**, 55-65.

Webster, B.R., Celnik, P.A. & Cohen, L.G. (2006) Noninvasive brain stimulation in stroke rehabilitation. *NeuroRx*, **3**, 474-481.

Chapter 2 Scientific and technical background

2.1. Organization of Motor and Sensory Cortices

2.1.1. Organization of the Motor Cortex

Mammalian species have at least one area in the neocortex devoted to the output of volitional control movement (Kaas, 1987; Nudo *et al.*, 1995; Kaas, 2004) that is commonly referred to as the primary motor cortex (M1). M1 contains most cell bodies that have axons that descend into the spinal cord and synapse on spinal motoneurons and directly control skeletal muscles. In primates, in its simplest form, the control of the distal musculature consists of a two-neuron pathway that allows for the fine control of motor movement. In lower mammals, such as rodents, the action of cortical motoneurons is similar, but the pathway to the skeletal muscles typically includes additional interneurons within the spinal cord. This pathway reduces the ability of fine movements, such as pinching movements or individual digit movements, in these animals.

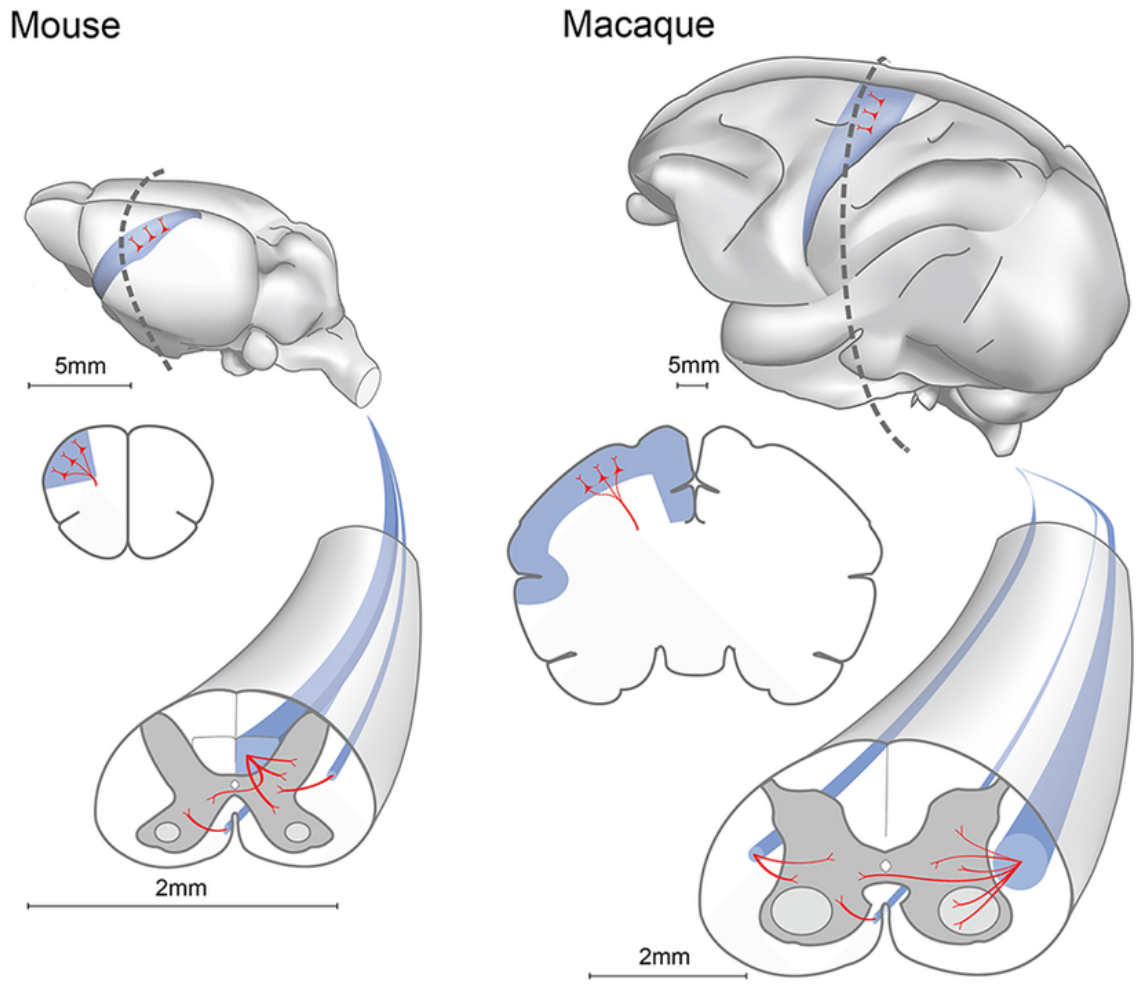

Figure 2.1.1: Comparative corticospinal projections between rodents and primates. Primary motor cortex is indicated by shaded region in the brain. In the rodent, most corticospinal axons project primarily within the contralateral ventral aspect of the dorsal column and terminate within the dorsal horn onto premotor spinal circuits. Notably, the minor components of the corticospinal tract reside within the contralateral lateral column and the ipsilateral ventral column. In primates, the corticospinal tract projects mainly within the dorsal aspect of the contralateral lateral column, and a minor component resides in the ipsilateral ventral column and terminates widely within the spinal gray matter (Serradj et al., 2017).

M1 has a roughly somatotopic organization that generally represents the motor movements of the lower lip to the face as one moves medial to lateral anterior to the central sulcus. The forelimb or arm movement representations typically constitute the largest area of responses within M1. In contrast to the somatosensory cortex, great overlap exists among the muscles within a limb that respond to stimulation. Both recording and stimulation studies have found that individual neurons within M1 can

facilitate the activation of multiple muscles, typically within muscle synergies (Fetz & Cheney, 1980; Cheney *et al.*, 1985). Similarly, multiple separate individual neurons can activate the same motor unit or muscle (Asanuma & Rosen, 1972; Andersen *et al.*, 1975; Jankowska *et al.*, 1975a; Strick & Preston, 1982; Sato & Tanji, 1989; Donoghue *et al.*, 1992).

In addition to the primary motor cortex, some mammals have additional cortical areas responsible for controlling motor movements. These areas are typically referred to as pre-motor areas because they send direct projections to M1 and the spinal cord (Dum & Strick, 2002). Primates have several specialized cortical areas responsible for planning and coordinating movement. There is a pre-motor cortex (PMA), a supplementary motor cortex (SMA), and a cingulate motor cortex (CMA). These areas can be further subdivided based on their location, anatomical projections, and cytoarchitecture. Typically, pre-motor areas are involved in coordinating visually guided movement, pattern and sequence generation, synchronizing bilateral movements, integration of body representation and target and somatosensory guided movements (Hoshi & Tanji, 2004).

Rodents have a single pre-motor cortex that contains only forelimb movement representations. This area, which is known as the rostral forelimb area (RFA), is believed to be involved in motor planning functions; however, its exact function is still under investigation.

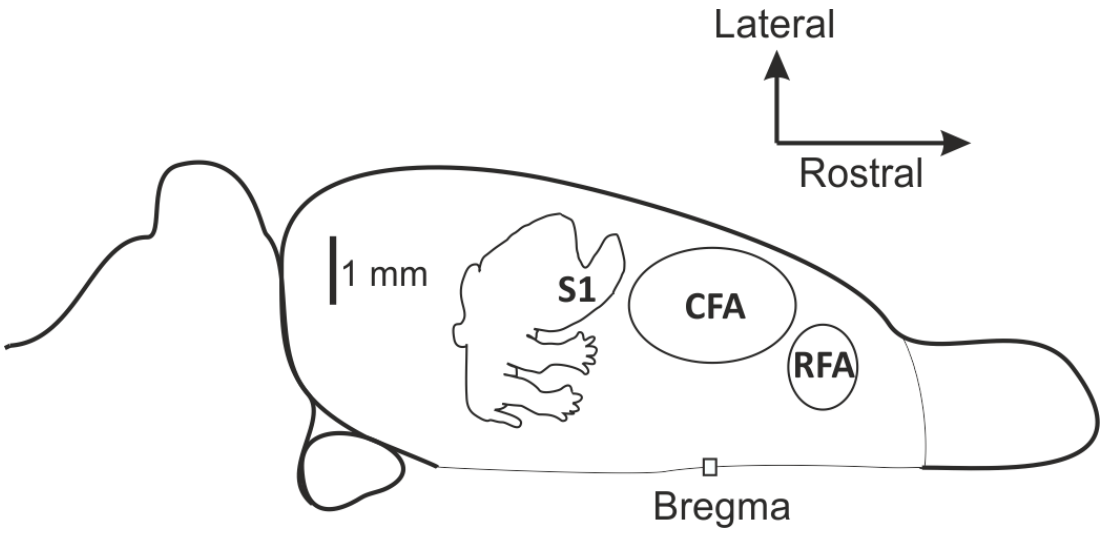

Figure 2.1.2: Locations of the RFA and CFA. A schematic dorsal view of the left hemisphere of the rat neocortex and olfactory bulb. The square denotes the location of bregma. The approximate locations of the RFA and CFA are labeled and indicated in gray.

Many research studies have explored how the primary motor cortex encodes motor movements, especially in primates. Evarts (Evarts, 1968) initially showed that the activity detected in the primary motor cortex could be correlated to both EEG activity and the force generated on the wrist of a macaque monkey. Using both spike- and stimulus-triggered averaging EMG signals, it has been shown that neurons within the primary motor cortex can activate multiple motor units in separate muscles, controlling not only single responses but also complex movements (Fetz & Cheney, 1980; Cheney *et al.*, 1985).

In addition to decoding the way the motor cortex codes movements at the level of the spinal cord and muscles, studies have attempted to decode and predict movement based on activity within M1. Humphrey (Humphrey *et al.*, 1970a) was one of the original investigators to predict motor movement based on cortical activity, and Georgopoulos *et al*. expanded on this work by proving evidence that the motor cortex can code the movement direction. These authors showed that some cells in M1 preferentially respond to joint movement in a certain direction (Georgopoulos *et al.*, 1986). Fetz (Fetz, 1969) operantly conditioned a monkey to alter the firing activity of a neuron in M1 to receive a reward. These studies laid the groundwork for the idea that

it is possible to predict the output of firing neurons and that this output (namely, the firing of individual units) could be volitionally modulated. The idea underlying some brain machine interfaces (O'Doherty *et al.*, 2009) stems from these studies.

2.1.2. Organization of the Somatosensory Cortex

The somatosensory cortex receives cutaneous, proprioceptive, and tactile information from the periphery. The primary somatosensory cortex (S1) includes areas 3a, 3b, 1 and 2. These areas correspond to large sensory field cutaneous responses, small sensory field cutaneous responses, and deep cutaneous responses. Wilder Penfield initially described the area posterior to the central sulcus as generating perceived peripheral sensation when stimulated with a ball electrode (Penfield & Boldrey, 1939). By systematically stimulating the post-central gyrus, he was able to map a full body representation from the foot to the head onto this strip of cortex. The sensory cortex showed a highly ordered response, directly mapping the cutaneous responses from the periphery to the cortex.

In rodents, the areas of S1 are typically divided based on the cytoarchitecture into the granular zone, peri-granular zone and dysgranular (or agranular) zone, roughly corresponding to areas 3, 1 and 2 (Donoghue & Wise, 1982); however, some disagreement exists regarding whether rodents have areas 1 and 2 (Kaas, 2004).

The granular zone can be visualized with Nissl or cytochrome oxidase staining to reveal the complete ratunculus. This area overlaps with the caudal portion of M1 to varying degrees. In practice, nearly the entirety of the hindlimb motor and sensory areas overlap, and a small portion of the M1 forelimb representation overlaps the sensory forelimb representation.

The primary sensory inputs into S1 project from the ventral posterior thalamus into layer IV. There are also other thalamic projections to S1 and several cortico-cortical connections from both the ipsilateral and contralateral cortices. Unfortunately, the staining techniques used to visualize these connections tend to label a volume of

tissue rather than individual neurons. Because of the overlap between M1 and S1 in the rat, the observed projections may arise from M1 and innervate all three zones of the rat S1, especially between the hindlimb and forelimb motor and sensory areas. Therefore, some S1 projections may coincide or overlap with M1 projections, especially in these overlapping zones.

In general, S1 is primarily considered the endpoint of sensory information, but there are many projections from S1 to other areas of the CNS. Similar to M1, S1 has descending corticospinal projections. While these projections do not terminate on motoneurons, they are likely to play some modulatory role in movement. The aforementioned reciprocal connections to M1 and connections to the secondary motor cortex exist in the cortex (Killackey *et al.*, 1989; Koralek *et al.*, 1990; Cauller *et al.*, 1998; Kaas, 2004). S2 is an association cortex that likely receives inputs from other sensory areas, including some sparse connections from premotor areas. S2 integrates this additional sensory information and projects strongly back to S1.

2.1.3. Cortico-Cortical Connections

Cortical areas are usually described by their individual properties, but any function, such as movement, involves multiple motor areas, sensory feedback, visual feedback, activation and modulation by subcortical structures, the cerebellum, etc. These interactions, rather than only the output, drive the function of the cortex. Thus, this communication is critical for discussions related to both the normal and injured cortex.

These cortico-cortical interactions have typically been described as a function of their anatomical projections. In the 1960s and 1970s, several histochemical staining procedures, such as horseradish peroxidase and PHA-L, were applied to retrogradely and anterogradely label populations of cells. Using these and more modern neuronal labeling techniques, it is possible to locate the soma of fibers in an area of interest or observe the projections of labeled cells. Based on a combination of many anatomical

studies and advanced fluorescent staining and imaging techniques, such as the Brainbow (Livet *et al.*, 2007) in which various fluorescent genes are spliced into developing neurons, it is readily apparent that the brain has an extraordinary complex system of connections. Complete circuit diagrams of the nervous system show the extent of these connections, and more pathways are constantly identified (Sporns *et al.*, 2005; Lichtman *et al.*, 2008; Eisenstein, 2009).

Unfortunately, the function of all these connections is more difficult to determine than visualizing the anatomy. Studies have attempted to determine the connectivity of cortical areas by performing recordings in multiple areas in search of correlated activity or stimulating one area and searching for the evoked output (Stevenson *et al.*, 2008; Stevenson *et al.*, 2009; Stevenson & Kording, 2011). Recently, functional magnetic resonance imaging (fMRI) studies have explored the interaction among different regions in the cortex (Deco & Corbetta, 2011). The authors termed this approach functional connectivity mapping. These studies show the extent to which these cortico-cortical connections are important for normal functionality.

2.2. A brief overview on stroke

Stroke related disorders are among the most frequent causes of disability and represent the second leading cause of death worldwide (Organization, 2006). Each year, approximately 795,000 people experience a new or recurrent stroke (ischemic or hemorrhagic). In 2010, stroke caused approximately 1 of 19 deaths in the United States. On average, every 40 seconds, someone in the United States has a stroke, and someone dies of stroke approximately every 4 minutes (Go *et al.*, 2014).

Although the incidence of stroke is decreasing, its prevalence in the population appears to be increasing because of increased stroke survival and the growing elderly population (Silvoni, 2011; Nichols, 2012). More than 60% of stroke survivors suffer from persistent neurological deficits (Gresham *et al.*, 1975) that impair activities of daily living (i.e., dressing, eating, self-care and personal hygiene)(Gresham *et al.*, 1975; Carod-Artal *et al.*, 2000; Clarke *et al.*, 2002), highlighting the need for the development of new neurorehabilitative treatments (Nudo & Milliken, 1996; Nudo, 2003); despite recent progress, the recovery of motor function after stroke is usually incomplete.

The brain is highly dependent on the constant blood flow supplied by the Circle of Willis (Figure 2.2.1). This formation of arteries allows the distribution of blood entering from the internal carotid artery or vertebral artery to any part of both hemispheres. Cortical and central branches arise from the circle and further supply the brain.

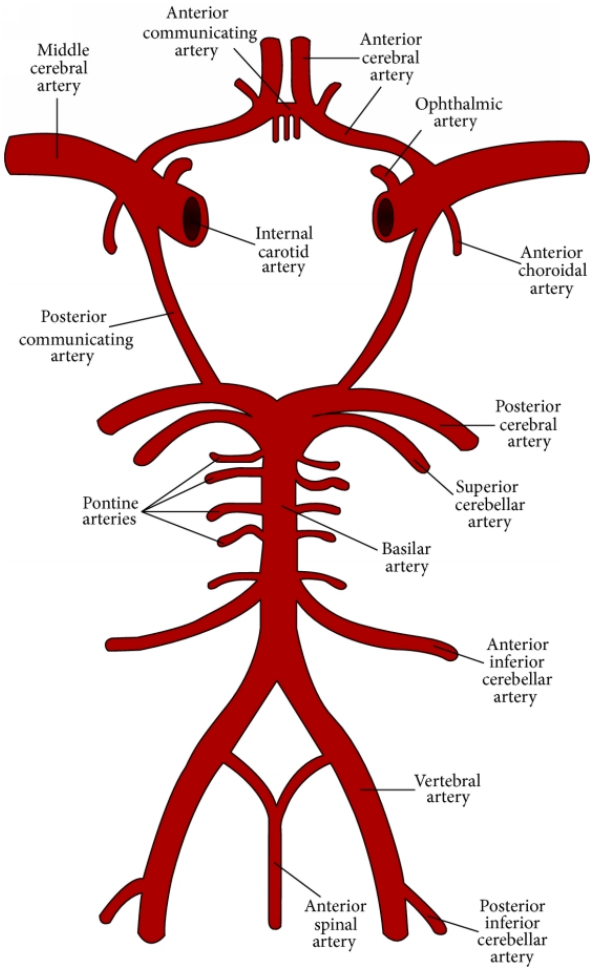

Figure 2.2.1: Vertebral-basilar arteries and circle of Willis.

The cerebral circulation supplies blood to the brain through multiple interconnected channels and is endowed with powerful control mechanisms, whose function is to ensure that the brain always receives adequate blood flow. When this mechanism is altered, oxygen- and energy-hungry neurons deprived of their normal metabolic substrates cease to function in a time frame of seconds and show signs of structural damage after only two minutes.

The following factors could cause such alterations:

- Atherosclerosis blocks cerebral arteries at multiple sites, limiting the possible alternative routes for the delivery of blood (ischemic stroke, Figure 2.2.2).

- Cardiovascular risk factors, e.g., hypertension and diabetes, impair the cerebrovascular control mechanisms.
- Aging increases the brain's susceptibility to injury and reduces the repair potential.

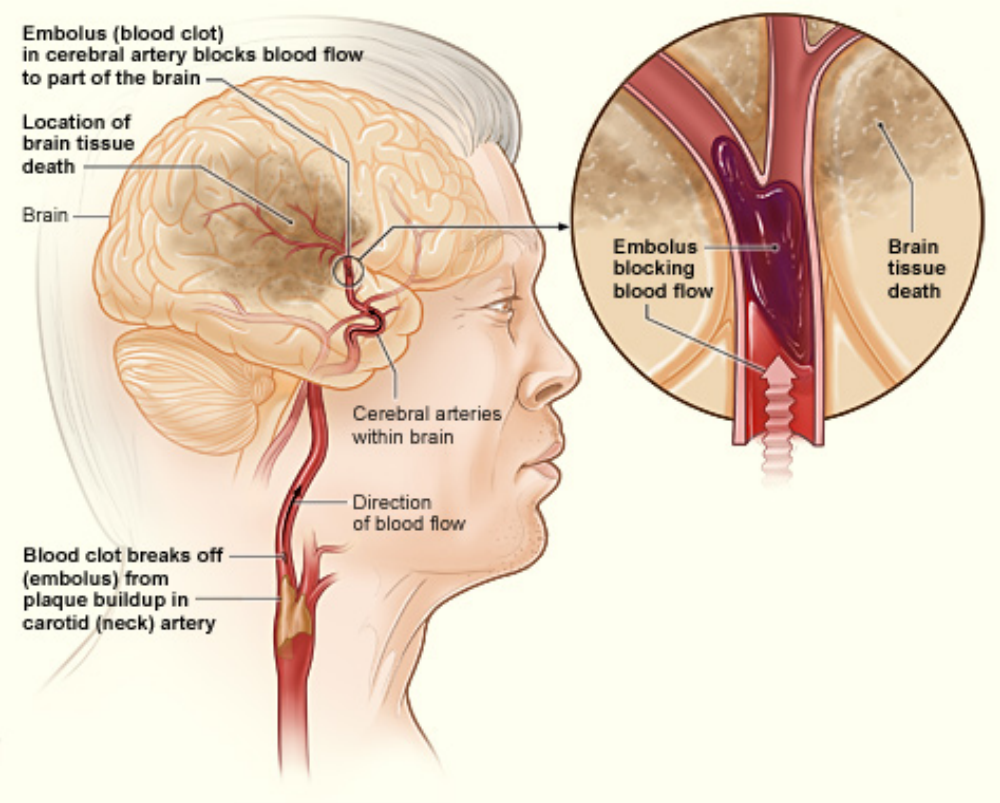

Figure 2.2.2: Illustration showing how an ischemic stroke can occur in the brain. If a blood clot breaks away from plaque buildup in a carotid (neck) artery, it can travel to and lodge in an artery in the brain. The clot can block blood flow to a part of the brain, causing brain tissue death (https://www.nhlbi.nih.gov).

Within the ischemic cerebrovascular zone, there are two major zones of injury as follows: the core ischemic zone and the "ischemic penumbra" (tissue is functionally impaired but still viable, Figure 2.2.3).

In the core zone, which is the area of severe ischemia (blood flow below 10% to 25%), the loss of oxygen and glucose results in the rapid depletion of energy stores. Severe ischemia can result in necrosis in neurons and supporting cellular elements (glial cells) within the severely ischemic area. Brain cells within the penumbra, which

is a rim of mild to moderately ischemic tissue lying between tissue that is normally perfused and the area in which the infarction is evolving, may remain viable for several hours because the penumbral zone is supplied with blood by collateral arteries anastomosing with branches of the occluded vascular tree. However, even cells in this region die if reperfusion is not established during the early hours since collateral circulation is inadequate to indefinitely maintain the neuronal demand for oxygen and glucose.

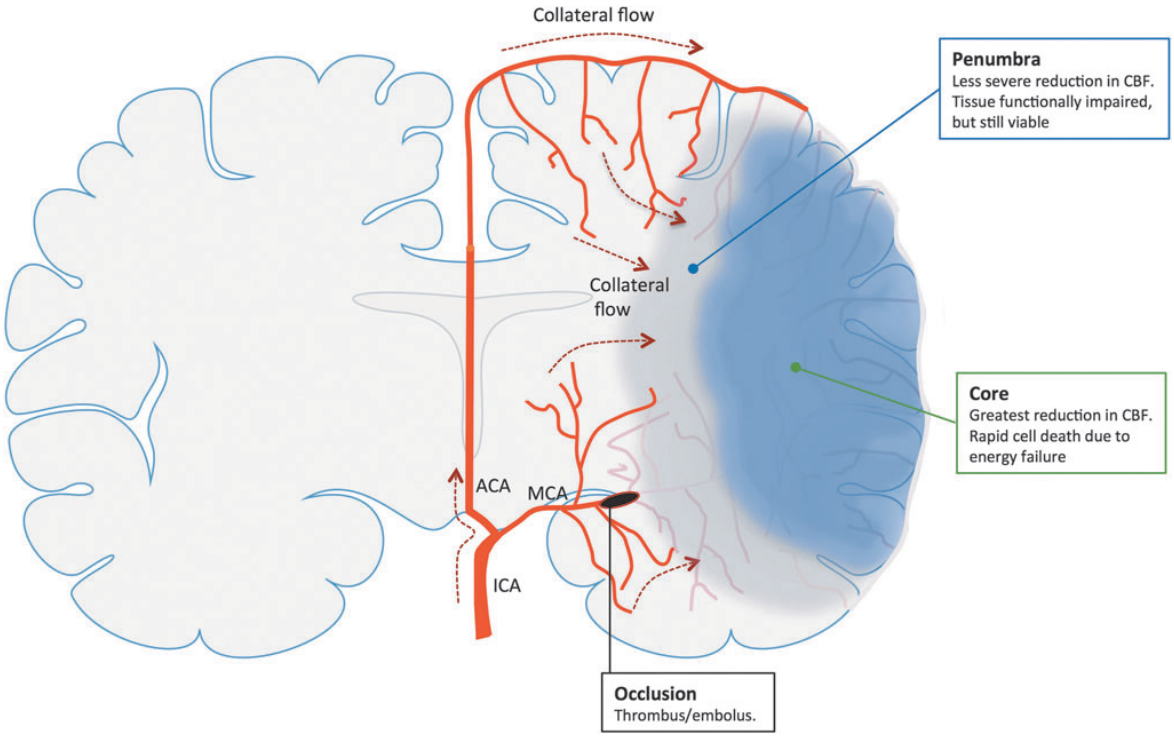

Figure 2.2.3: Collateral perfusion in the brain after focal cerebral ischemia. After ischemic stroke, there is a central region (ischemic core) where the reduction in cerebrovascular blood flow (CBF) is most severe, resulting in rapid cell death. In contrast, the area surrounding the core (ischemic penumbra) receives sufficient flow to remain vital but has impaired functionality. The fate of the ischemic penumbra is largely dependent on the efficiency of collateral circulation. Supplied by vessels from adjacent vascular territories unaffected by the vascular occlusion, collateral flow mitigates the CBF reduction in regions peripheral to the ischemic territory, which, if adequate, prevents the recruitment of penumbral tissue into the ischemic core. ACA, anterior communicating artery; ICA, internal carotid artery; MCA, middle cerebral artery (Jackman & Iadecola, 2015).

Recent findings have revealed that synapses and their networks express a high degree of functional and structural plasticity in the penumbra around a focal infarction (Lüscher *et al.*, 2000), thus suggesting the existence of a therapeutic window for

neuronal recovery in the early stages of damage during which pharmacologic interventions are most likely to be effective.

Although the impairment caused by such disease can be devastating, the possibility of surviving the initial event enables many spontaneous recovery processes, which can be further augmented by neurorehabilitative therapy.

2.2.1. In Vivo models of Stroke

The development of primate and higher mammal stroke models is an important goal, but without institutional change in animal facilities and costs, rodents will continue to provide the predominant basic science research model for explorations of the mechanisms of neuroprotection and neural repair after stroke (Carmichael, 2005). Several recent animal models have been specifically designed to determine reparative events in the brain after stroke, and many standard rodent models are best suited for testing neuroprotective therapies. Animal models of cell death in stroke are designed to generate reproducible infarcts in a high throughput manner with minimum surgical manipulation to determine the mechanisms of cell death and test neuroprotective therapies.

Animal ischemic stroke models can be characterized by the type of ischemic cerebral injury created. These models can be categorized into one of the following three categories: (1) global, (2) focal, or (3) multifocal cerebral ischemia (Graham *et al.*, 2004).

1) In global cerebral ischemia, Cerebral Blood Flow (CBF) is reduced throughout the brain. In complete global ischemic models, global flow ceases completely for a period. In incomplete models, CBF is sufficiently reduced, preventing normal metabolism and function from being adequately maintained. Animal species other than the gerbil have a complete Circle of Willis, and therefore, bilateral or unilateral occlusion of the common carotid artery alone cannot be used to induce complete or incomplete global stroke, respectively. For example, incomplete global

cerebral ischemia can be induced in rats by four-vessel occlusion (bilateral vertebral and common carotid arteries (Pulsinelli & Brierley, 1979; Pulsinelli & Duffy, 1983; Pulsinelli & Buchan, 1988)). A reduction in blood flow to a specific brain region is observed in focal stroke models.

2) Most focal stroke models involve middle cerebral artery occlusion (MCAO) (Garcia, 1993; Fukuda & del Zoppo, 2003; Traystman, 2003; Saita, 2004; Murphy, 2009; Tsuji, 2013; Zhang, 2013). In this case, a blood clot is introduced through the internal carotid to occlude the MCA and reduce or stop blood flow to a specific hemisphere of the brain for a limited time (transient MCAO) or permanently. This model closely resembles human ischemic stroke. Other methods used to induce focal ischemic infarcts can be fairly precisely localized to specific brain regions and leave substantial tissue intact to support functional recovery. One method consists of a stereotaxic injection of a vasoconstrictive peptide, i.e., endothelin-1 (ET-1), into the cortex to create a very focal ischemic infarct (Frost *et al.*, 2006; Fang *et al.*, 2010).
3) A patchy pattern of reduced CBF is observed in multifocal cerebral ischemic models (McAuley, 1995). In these models, multiple sites of ischemia result from the use of embolization of autologous or heterologous blood clots (Traystman, 2003), microspheres (Kiyota *et al.*, 1986), or photochemically induced thrombi (Photothrombosis model) (Watson, 1998).

In the present study, I used the following model of focal ischemia: the Endolthelin-1 (ET-1) model.

ET-1 is a strong and long-acting vasoconstrictive peptide (Yanagisawa *et al.*, 1988). ET-1 can be applied directly to the exposed MCA (Robinson *et al.*, 1990) as an intracerebral (stereotactic) injection (Hughes *et al.*, 2003) or the cortical surface (Fuxe *et al.*, 1997), leading to a dose-dependent ischemic lesion with marginal ischemic edema (Fuxe *et al.*, 1997; Hughes *et al.*, 2003). The first two modes of delivery produce an ischemic lesion comparable to that induced by permanent MCAO (Sharkey, 1993),

whereas a cortical injection provides a semicircular infarct that involves all cortical layers (Fuxe *et al.*, 1997). After ET-1 administration, a rapid CBF reduction (70%–90%) is observed, followed by reperfusion that occurs over several hours (Biernaskie *et al.*, 2001). Notably, ET-1 is approximately four times more potent in conscious rats than in anesthetized rats (Bogaert *et al.*, 2000). The advantages of the ET-1 model include a less invasive technique, low mortality, and the possibility of inducing direct focal ischemia in deep and superficial brain regions.

2.2.2. Limitations of in vivo models of stroke

Importantly, all models presented above differ from human stroke, which particularly affects elderly people who have a multiplicity of cerebrovascular risk factors. Here, I report some of the most important differences found among the most widely used animal models of stroke. In MCAO of a 60-minute duration, damage to the hypothalamus always occurs (Dietrich & Kuluz, 1999), but this damage rarely occurs in human stroke. Hypothalamic ischemia results in a hyperthermic response in rats that persists for at least 1 day after MCAO (Dietrich & Kuluz, 1999) and thus may affect further analysis. There are also concerns regarding the different pathophysiologies of the permanent and transient MCAO models (Hossmann, 2012). In the transient MCAO model, primary core damage may recover, and a secondary delayed injury evolves after a free interval of up to 12 hours. There is a long therapeutic window that is not observed in human stroke. In contrast, permanent MCAO is characterized by primary core damage that expands to peripheral brain regions and reaches its maximum approximately 3 hours after MCAO (Hossmann, 2012).

The disadvantages of the photothrombosis model are due to its end-arterial occlusive nature. The rapidly evolving ischemic damage and endothelial injury are associated with early cytotoxic (intracellular) and simultaneous vasogenic (extracellular) edema formation (Lee *et al.*, 1996).

The ET-1 model is limited by the fact that ET-1 receptors and ET-1-converting enzyme are also expressed by neurons and astrocytes (Nakagomi *et al.*, 2000). ET-1 has been shown to induce astrocytosis and facilitate axonal sprouting (Uesugi *et al.*, 1998), which may interfere with the interpretation of neural repair experiments (Carmichael, 2005).

In addition, in all animal models of stroke, only slight or no ischemic penumbra and local collateral flow/reperfusion occur, thus demonstrating their limitation. However, optimizing the study design used in preclinical trials might increase the translational potential of animal stroke models (Fluri *et al.*, 2015).

2.3. Communicating with Cortical Tissue

2.3.1. Stimulation of Motor Cortex

The stimulation of the motor cortex has been performed in animals since Fritsch and Hitzig in the late 1800s (Eduard & Gustav, 1870). The first studies involving humans were performed by Wilder Penfield, who evoked motor responses with surface stimulation using a ball electrode in an area anterior to the central sulcus (Penfield & Boldrey, 1939). This research showed that motor movements (EMG, muscle twitch, or whole muscle movement) could be elicited through stimulation and that the pattern within the cortex showed a rough somatotopic organization. Further refinement and experimentation using surface stimulation in primates and other species were performed over several decades (Welker *et al.*, 1957). There are several technical problems with using surface stimulation to study the output of the motor cortex. The current levels required to generate responses in skeletal muscles are on the order of tens of millivolts, which is potentially damaging to cortical tissue. Furthermore, the spread of current diffuses along the pial surface and does not allow for fine resolution within the cortex. Thus, studies using surface stimulation to obtain information about motor outputs are limited to general maps of muscle responses.

In the 1960s, researchers, particularly Stoney, Thompson, and Asanuma, developed a technique for the more focal stimulation of cortical tissue (Stoney *et al.*, 1968). By placing an electrode within the cortical tissue and injecting small electrical currents (on the order of microvolts) through a microelectrode, it was possible to stimulate and activate much smaller volumes of tissue than with surface electrodes. Intracortical microstimulation (ICMS) represents one of the fundamental techniques used to obtain an understanding of the motor control of movement during the remainder of the 20th century. During the 1960s and 70s, this tool was further developed for analyses of the output properties of motor cortical neurons, and these analyses involved analyzing the stimulation effects through the pyramidal tract into

the spinal cord and ultimately out to skeletal muscles (Fetz, 1969; Jankowska *et al.*, 1975a; b; Gustafsson & Jankowska, 1976; Fetz *et al.*, 1979; Jankowska *et al.*, 1981). Currently, this technique is still extensively used for purposes as diverse as spike triggered averaging of EMG signals to understanding cortico-cortical communication within and between motor areas (Faggin *et al.*, 1997; Park *et al.*, 2004; Jackson *et al.*, 2006).

Additionally, the focal properties of ICMS (Tehovnik, 1996; Tolias *et al.*, 2005; Tehovnik *et al.*, 2006) enable investigations of the representation of motor movements within the cortex. While Penfield, Woolsey and other researchers were able to draw rudimentary maps of motor responses within the primary motor cortex, these maps are limited due to several problems with the resolution of the surface stimulation. By systematically mapping cortical tissue, the realization that in contrast to the sensory cortex, a one-to-one representation of motor cortical neurons to muscle responses is lacking emerged. While muscle responses are roughly laid out in the somatotopic orientation, there is great overlap among the movements generated by a limb, and the movements of multiple joints could be observed. These studies helped frame the idea that there is both convergence (multiple populations of neurons project onto a single muscle or spinal motoneuron) and divergence (a single neuron can contribute to the activation of more than one muscle). Cheney and other researchers have greatly expanded upon this fundamental property of the motor cortex.

Nudo *et al*. used the technique of mapping cortical responses to observe changes in the overall representations of different forelimb responses (Nudo *et al.*, 1996a; Nudo *et al.*, 1996b; Kleim *et al.*, 1998; Plautz *et al.*, 2000; Plautz *et al.*, 2003; Barbay *et al.*, 2006). A new field exploring the changes within the motor cortex as a result of training, injury and rehabilitation developed as a tool to measure cortical plasticity.

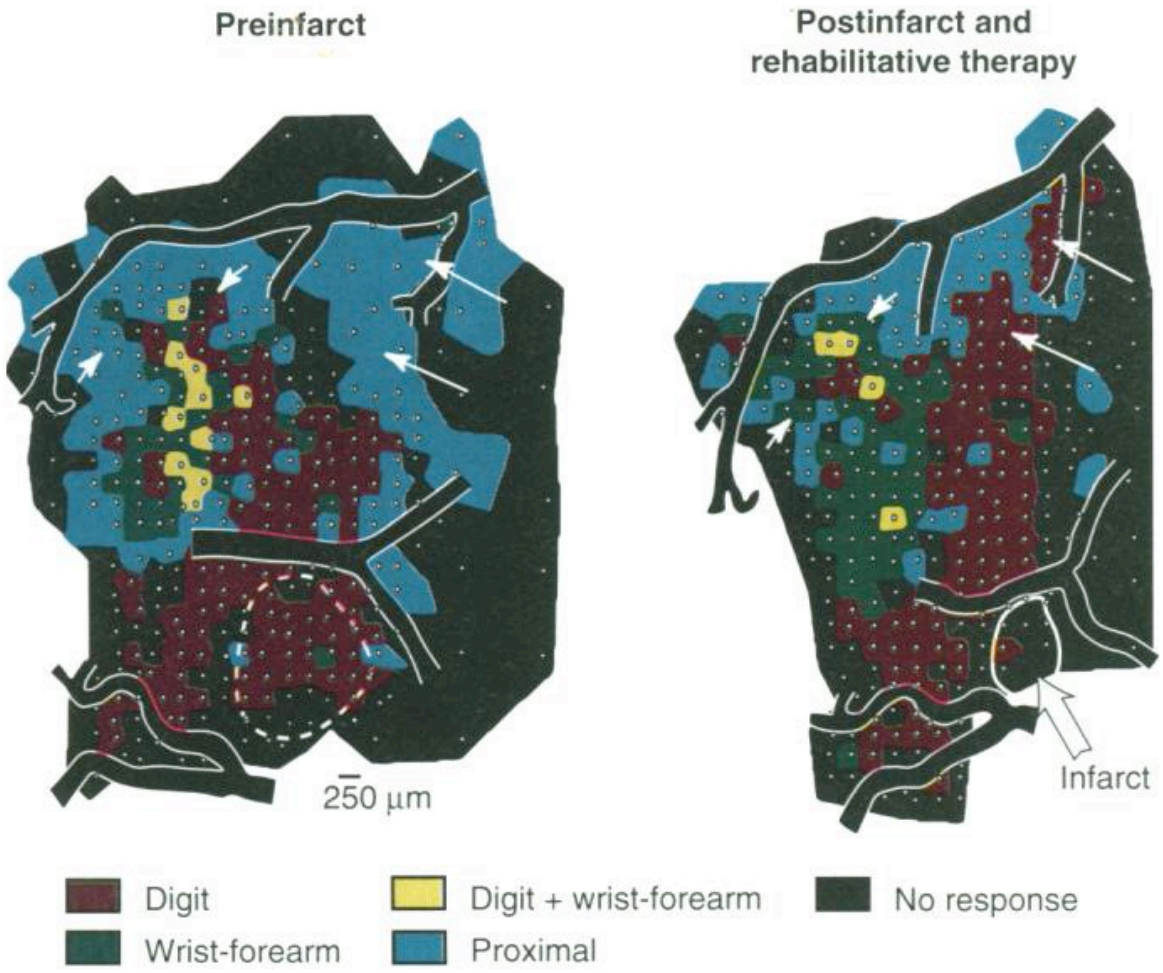

Figure 2.3.1: Reorganization of hand representations in the primary motor cortex before infarct (left) and after focal ischemic infarct and rehabilitative training (right). At each microelectrode penetration site (small white circles), ICMS techniques were used to define the movements evoked by near-threshold electrical stimulation (<30 μA). In this animal, the infarct destroyed 21.6% of digit and 4.1% of wrist-forearm representations. After rehabilitative training, the spared digit representational area increased by 14.9%, and the spared wrist-forearm representational area increased by 58.5%. The dashed circle in the preinfarct map encompasses the cortical territory targeted for ischemic infarct. The large white arrow in the postinfarct map indicates the infarcted region. The reduction in the size of the infarcted zone is attributable to tissue necrosis during the rehabilitation period. Long thin arrows point to adjacent, undamaged cortex in which digit representations (red) appear to have invaded regions formerly occupied by representations of the elbow and shoulder (blue). Short thin arrows point to wrist-forearm representations (green) that appear to have invaded digit, elbow, and shoulder representations (Nudo & Milliken, 1996).

Finally, several emerging stimulation techniques have been established to stimulate cortical tissue without having direct access to cortical tissue for use in humans. Transcranial direct current stimulation (tDCS) is similar to surface stimulation, but instead of stimulating the cortex directly, the current passes from an

electrode placed on the scalp to a return electrode located on the scalp somewhere distantly. While this technique exhibits even more resolution issues than ball electrodes, it has shown some efficacy as a therapeutic device for depression and a potential device for promoting attention and retention. Transcranial magnetic stimulation (TMS) is another non-invasive stimulation technology. By passing large voltages through a coil around a magnet, a strong temporary magnet field is produced. In turn, this field leads to the introduction of current through neurons near the surface of the cortex. This technique has a high safety margin and few side effects, making it ideal for studies involving human subjects. TMS has been refined to allow multiple trains of pulses (repetitive TMS or rTMS) that can lead to the excitation or inhibition of the tissue stimulated based on the rate of the pulses. In the motor cortex, this technique has been used to map EMG responses in the forelimb, and a variety of techniques have been used to explore interhemispheric inhibition after stroke.

2.3.2. Recording Neuronal Activity

While stimulation can activate neurons by forcing their discharge, the ability to record neural signals is critical for obtaining an understanding of how neural tissue naturally responds under various experimental conditions and tasks. Numerous techniques are used to acquire and determine activity within the CNS. Several techniques can be used to record low-frequency oscillations from the cortex, and these techniques are fundamentally similar (Buzsaki *et al.*, 2012) and can vary from more to less invasive techniques. These techniques include electroencephalogram (EEG), electrocorticography (ECoG), magnetoencephalography (MEG) and local field potentials (LFP). EEG signals are obtained from electrodes placed throughout the scalp; ECoG signals are obtained from electrodes placed either on the top of or underneath the dura; MEG uses superconducting quantum interference devices (SQUIDs) to measure tiny magnetic fields outside the skull from currents generated by neurons; and LFP signals are obtained from electrodes placed in neural tissue. The

main difference among these methods is the resolution and invasiveness of the procedure, both of which increase from EEG to ECoG to LFP.

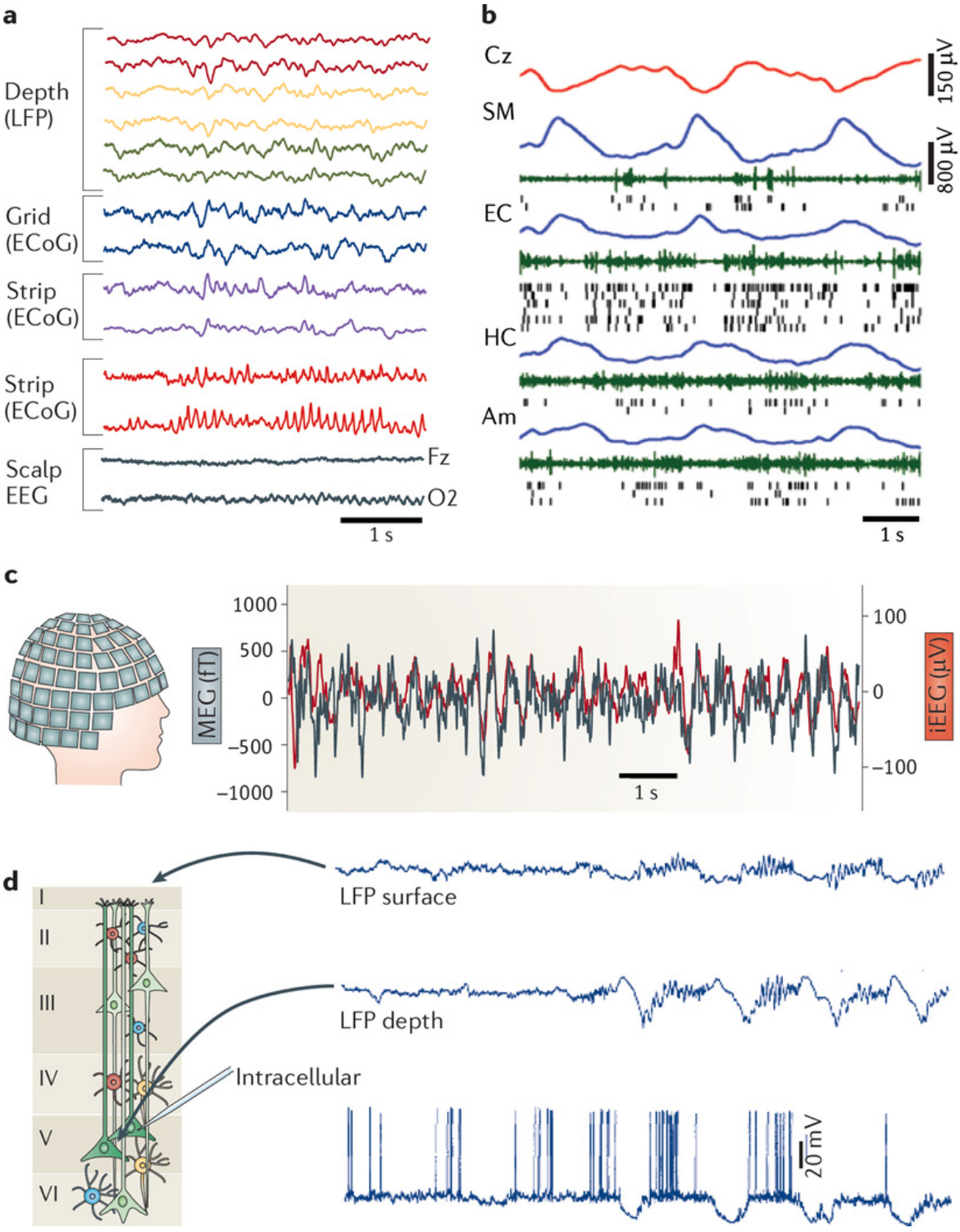

Figure 2.3.2: Extracellular traces using different fundamentally similar recording methods. a) Simultaneous recordings from three depth electrodes (two selected sites each) in the left amygdala and hippocampus (measuring the local field potential (LFP)); a 3 × 8 subdural grid electrode array placed over the lateral left temporal cortex (measuring electrocorticogram (ECoG); two four-contact strips placed under the inferior temporal surface

(measuring ECoG); an eight-contact strip placed over the left orbitofrontal surface (measuring ECoG); and scalp electroencephalography (EEG) over both hemispheres. The amplitude signals are larger, and the higher-frequency patterns have a greater resolution at the intracerebral (LFP) and ECoG sites compared to those of the scalp EEG. B) A 6 s epoch of slow waves recorded by scalp EEG (Cz, red), and LFP (blue) recorded by depth electrodes placed in the deep layers of the supplementary motor area (SM), entorhinal cortex (EC), hippocampus (HC) and amygdala (Am). Multiple-unit activity (green) and spikes of isolated neurons (black ticks) are also shown. c) Simultaneously recorded magnetoencephalogram (MEG; black) and anterior hippocampus depth EEG (red). d) Simultaneously recorded LFP traces from the superficial ('surface') and deep ('depth') layers of the motor cortex in an anaesthetized cat and an intracellular trace from a layer 5 pyramidal neuron. Note the alternation between hyperpolarization and depolarization (slow oscillation) in the layer 5 neuron and the corresponding changes in the LFP. The positive waves in the deep layer (close to the recorded neuron) are also known as delta waves. iEEG, intracranial EEG (Buzsaki et al., 2012).

These techniques amplify and filter all high-frequency signals (>250 Hz) in a large population of neurons. Then, the signal is typically analyzed to detect changes in power in various frequency bands. The following frequency bands are typically considered based on correlations between certain behavioral states and the LFP observed in cortex: delta or sharp waves (δ, 1-4 Hz), theta (θ, 4-11 Hz), beta (β, 11-30 Hz), low-gamma (γ_L, 30-55 Hz), and high-gamma (γ_H, 55-130Hz) (Colgin & Moser, 2010). These neural oscillations are temporally correlated; for example, the gamma band is known to be associated with communications in local cortical regions (Womelsdorf *et al.*, 2007), and the lower frequency bands seem to maintain synchronization between distant regions (Von Stein *et al.*, 2000). Furthermore, these temporal correlations are functionally related (Uhlhaas & Singer, 2010). The following list describes some of the functions of each band:

- Theta band: memory (Vertes, 2005), synaptic plasticity (Huerta & Lisman, 1993), top-down control and long-range synchronization (Von Stein *et al.*, 2000).
- Beta band: sensory gating (Hong *et al.*, 2008), motor control (Kilner *et al.*, 2000), attention (Gross *et al.*, 2004) and long-range synchronization (Kopell *et al.*, 2000).
- Gamma band: memory (Tallon-Baudry *et al.*, 1998), synaptic plasticity (Wespatat *et al.*, 2004), attention (Fries *et al.*, 2001), consciousness (Melloni *et al.*, 2007), and perception (Gray *et al.*, 1989).

These techniques suffer from the following two main flaws: the spatial resolution of the recorded is very low, and the frequency of the signals is slow.

Recent developments in the silicon micro-fabrication field have led to the introduction of multi-channel devices used for recording electrophysiological signals. These devices are known as Micro Electrode Arrays (MEAs) and are widely used in both in vitro (Chiappalone *et al.*, 2006) and in vivo (Chapin, 2004; Smith *et al.*, 2004; Donoghue *et al.*, 2007; Avestruz, 2008; Kayagil *et al.*, 2009; van Gerven *et al.*, 2009; Rothschild, 2010) experiments.

In vivo MEAs can be used to record neuronal action potentials or local field potentials (LFP) in several areas of the brain. These signals are in the micro- to millivolt range when recording intracortical signals in the form of (single) spike activity or local field potentials (Cheung *et al.*, 2007). These invasive methods achieve a high signal-to-noise ratio by eliminating the volume conduction problems caused by tissue and bone usually encountered with non-invasive methods, such as EEG. The electrodes are directly placed on the cortical matter, allowing for the excellent detection of high-frequency oscillatory activity (Rothschild, 2010). Therefore, these devices are widely used in the context of BMI (Brain Machine Interface) and BCI (Brain Computer Interface) research, particularly of chronic implants in humans (Sanes *et al.*, 1995; Hochberg *et al.*, 2006a; Donoghue *et al.*, 2007; Kim *et al.*, 2008; Simeral *et al.*, 2011; Hochberg *et al.*, 2012b), despite their relative problems of gliosis (Rothschild, 2010).

When an electrode array is inserted into the neural tissue, the recording of a single neuron action potential becomes possible. Thus, when an action potential occurs, the intracellular and extracellular ionic concentrations are both modified by the membrane transport properties as follows: the extracellular changes are localized near the membrane, and the currents entering or leaving the neuron generate voltage signals at the nearby electrode. These signals result from a resistive drop in the medium between the reference electrode and the recording electrode.

The amplification and bandpass filtering of the signal between 300 and 3000 Hz allows the activity of a single unit to be detected. Depending on the characteristics of the electrode used for the recording, individual neurons can be detected from up to 100 μm away. This method alleviates the problems of low-frequency signals as it is possible to obtain a high spatial resolution, and the signals occur very rapidly.

Instead of using power bands, it is possible to detect activity directly. This activity can be detected in real-time in several ways. The simplest form of detection is by thresholding, which determines whether the signal waveform passes above a certain value. A slightly more complex method is using time-amplitude windows in conjunction with thresholding. This technique requires the signal to pass above a threshold but also through one or more windows that are defined by both the voltage of the signal and the relative time from the threshold crossing. Another advanced method, which is used in one part of this study (see Chapter 4), is called PTSD and employs the following three parameters, which are based on the biophysical characteristics of spike waveforms to identify candidate spike profiles (Maccione *et al.*, 2009): (1) differential threshold (DT), (2) pulse lifetime period (PLP), and (3) refractory period (RP). Once a peak is found, the algorithm scans the signal to detect the maximum peak of opposite polarity. If these two peaks have an amplitude difference greater than or equal to the DT, these peaks are considered to correspond to a spike, and the algorithm searches for an RP to begin the search for a new spike.

Once the time occurrence of the spikes has been detected, a new process is required to determine the units from each single action potential. The consequent method, which is called 'spike sorting', allows for more than one spike profile to be detected on one channel, which is impossible with the other three methods. Thus, spike sorting is the grouping of detected spikes into clusters based on the similarity of their shapes using different clustering methods (e.g., PCA, SPC, etc.). The interpolated waveforms studies are sorted by employing wavelet transformation and superparamagnetic clustering (SPC) with Waveclus (Quiroga *et al.*, 2004).

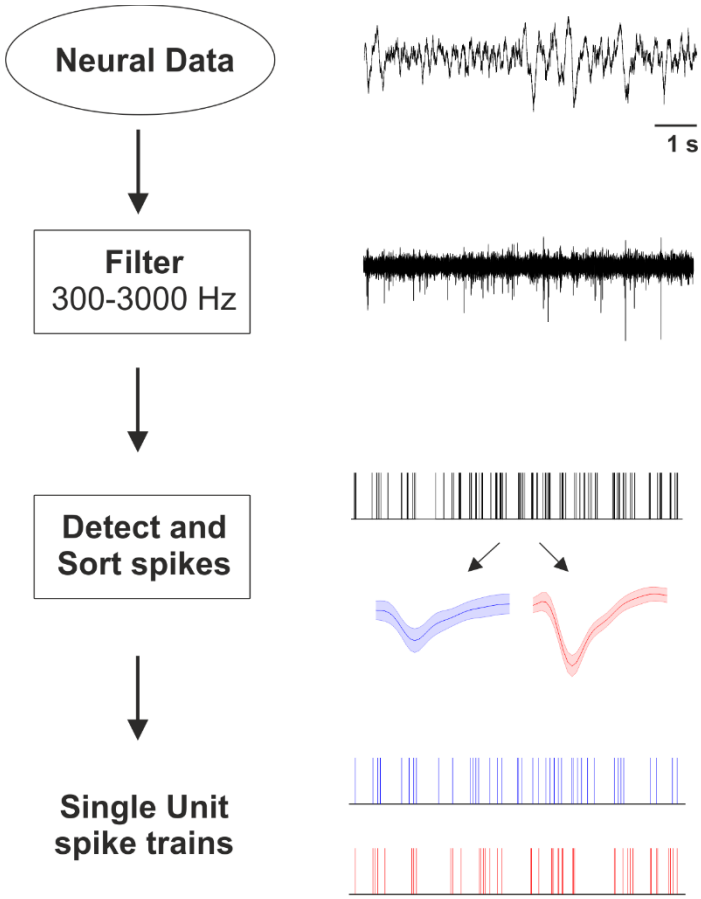

Figure 2.3.3: Overview of the pipeline used to produce the single unit spike trains procedure. Neural data are filtered in the bandwidth of the spikes, the spikes are detected by the PTSD algorithm and finally, the spikes are sorted using SPC.

Once a spike has been detected, it is possible to use this information to code the other parameters. The simplest method is to count the number of spikes that occur during some time range (10-20 ms) to obtain the spiking rate. This rate can be used to monitor relative activity in relation to a stimulus or control some other output. As more electrodes are introduced, it is possible to encode various decoding strategies to utilize the activity both independently and as a function of combinations of activity among the different channels. The ability to record the activity and decode some function of that activity has allowed the field of brain machine interfaces (BMI) to expand.

2.4. Neuroprosthesis for Brain Repair

Pioneering work conducted in the late 1960s by Fetz revealed that given feedback, monkeys could learn to consciously control the firing rate of their cortical neurons (Fetz, 1969). During the following year, Humphrey et al found that recordings from neurons could be used to predict and thus potentially drive arm movements (Humphrey *et al.*, 1970b). Subsequent groundbreaking studies have demonstrated this possibility; in 1999, Chapin *et al*. showed that rats could control a robot arm's trajectory via recordings from the motor cortex (Chapin *et al.*, 1999). These early works laid the foundation for the field of neuroprosthesis, and devices have been designed to interact with the nervous system and restore function. Their objective is the safe and efficient completion of functional tasks in people with severe paralysis when motor relearning strategies are no longer amenable (Cramer & Nudo, 2010).

Neuroprosthesis for brain repair, such as brain modulators, brain–machine interfaces (BMIs) and brain prosthesis, have been exponentially developed over recent years. Brain modulators are devices that modulate brain patterns by means of externally applied current or magnetic fields or by electrical stimulation of deep brain structures (deep brain stimulation - DBS) (Figure 2.4.1(a)). Traditionally, these devices were developed to treat movement disorders (e.g., Parkinson's disease (Duker & Espay, 2013; Collomb-Clerc & Welter, 2015)), epilepsy (Laxpati *et al.*, 2014) and psychiatric conditions (such as obsessive-compulsive disorder and major depression (Berlim *et al.*, 2014)). The term BMI refers to a device that interfaces the brain with a robotic end effector, such as a robotic limb. BMIs aim to restore missing motor functions in patients stricken by a disabling neurological condition, brain injury or limb amputation (Figure 2.4.1(b)). Following the pioneering demonstration of the feasibility of this approach (Chapin *et al*., 1999), BMIs have become increasingly sophisticated and have been successfully applied to paralyzed humans (Hochberg *et al.*, 2012a; Bouton *et al.*, 2016; Ajiboye *et al.*, 2017; Panuccio *et al.*, 2018). Brain prostheses are intended to be artificial systems directly connected with the brain to replace a

damaged area or bridge disconnected areas for the regaining of lost functionality (Figure 2.4.1(c)). For example, the device may be used to reconnect the somatosensory and motor cortical areas to restore forelimb movement impaired by brain injury. A brain prosthesis implementing an architecture following a closed-loop reactive policy has been presented for the first time by the Kansas University Medical Center (Guggenmos *et al.*, 2013). Another promising example is represented by a hippocampal memory prosthesis allowing the neural activity in specific hippocampal areas to be suitably processed, which can be used to manipulate and thus restore (through ad hoc electrical stimulation) cognitive mnemonic processes (Berger *et al.*, 2011; Berger *et al.*, 2012; Song & Berger, 2015).

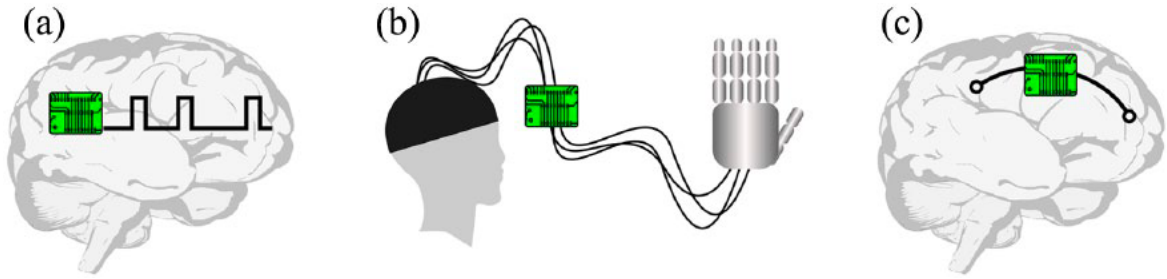

Figure 2.4.1: Neuroengineering devices used for brain repair. (a) Brain modulator for DBS. The device is implanted into deep brain structures and may be based on open- or closed-loop architecture. (b) A BMI conveys the electrical activity of the recorded brain area to a robotic end effector. In this rendition, the established system consists of the input brain area, the interface apparatus and the robotic hand. In this case, an open-loop strategy is implemented as follows: visual feedback aids movement planning, and in turn, the required adjustments influence the function of the interface apparatus. (c) A brain prosthesis is an artificial device implanted in the brain to replace brain activity or reconnect disconnected brain areas (Panuccio et al., 2018).

The development of brain prostheses is still at the preclinical stage.

The use of neuroprosthetic devices aiming to repair the central nervous system could benefit from exploitation of the so-called Electroceutical Concept.

Electroceutical Concept

Currently, drugs rule the roost, and conditions that cannot be treated by drugs are treated by interventions or surgery. All organs and functions are regulated through the brain and nervous system. Even the endocrine system is under the control of the central nervous system by a complex array of feedback mechanisms. Furthermore,

most drugs have their effects by either acting on final-receptors (neural) or endocrine mechanisms. However, all known drugs, surgeries and even non-surgical interventions have definite side-effects because their action cannot be exactly localized to the defective part or organ. In this context, electrical impulses become the mainstay of medical therapy. Indeed, the following new approach has been envisioned for the treatment of many diseases: the Electroceutical (Famm *et al.*, 2013; Reardon, 2014; MAGAZINE & RADAR'S, 2015). The Electroceutical is considered complementary and helps pharmaceutical interventions by using electrical stimulation to alleviate or mitigate symptomatology and pathology. Thus, instead of administering drugs or performing complex procedures, physicians or a specific portable device may simply administer electrical stimulation targeting individual nerve fibers or specific brain circuits to treat any condition (Mishra, 2017). Thus, the neural impulses that control the body will be entrained to regain the lost function and reestablish a healthy balance. Furthermore, a host of bodily activities could be regulated, including food intake, cardiac activity, pancreatic activity, and liver, kidney or spleen functions. In some cases, even inflammation could be controlled, and many pathologies, such as diabetes mellitus, obesity, hypertension, heart failure, and cerebrovascular and pulmonary diseases, could be corrected. Electroceutical's most promising results have been achieved in the neuromodulation field. Electroceutical in neuromodulation refers to interfacing and intervening with the nervous system through electrical and electromagnetic methodologies with the goal of long-term activation, inhibition, modification, and/or regulation of neural activity (Krames *et al.*, 2009). While oral medication and ablative neurosurgical procedures can achieve similar therapeutic outcomes, neuromodulation has the advantage of higher spatiotemporal precision than oral medication combined with reversibility, which is absent in ablative procedures. To date, neuromodulation has been used to treat movement disorders (Parkinson's disease, dystonia, and tremor), tics associated with Tourette syndrome, obsessive compulsive disorder, depression, tinnitus, sensory disabilities, bladder control, epilepsy, headache, chronic pain, spasticity, stroke, minimally conscious state,

spinal cord injury, etc. With these successes, there is tremendous impetus to refine the existing technologies and develop new approaches for the modulation of the nervous system for the treatment of existing indications and emerging indications, including memory disorders, schizophrenia, addiction, eating disorders, hyperacusis, and traumatic brain injury (Johnson *et al.*, 2013). The following are among the most important neuromodulation techniques:

- Deep Brain Stimulation (DBS): DBS is an intracranial, electrical neuromodulation therapy that has FDA approval for the treatment of medication-refractory Parkinson's disease and essential tremor and has humanitarian device exemption for the treatment of dystonia and severe obsessive-compulsive disorder. DBS therapy involves surgical implantation of a lead of electrodes into a nucleus or fiber tract within the brain.
- Intracranial Cortical Stimulation: This technique has become an increasingly popular investigational approach for the treatment of patients with epilepsy, tinnitus, pain, depression, stroke, tremor, dystonia, Parkinson's disease, etc. This approach first involves implanting an array of electrodes over or into the cortex and then delivering electrical stimulation through these electrodes using stimulation parameters comparable to those used in DBS therapy.
- Transcranial Direct Current Stimulation (tDCS): tDCS has emerged over the last decade as a noninvasive tool for modulating the excitability of the cortex. Current flows across the cortex from the negatively polarized cathode to the positively polarized anode. This technique has shown promising results in the treatment of several neuropsychiatric conditions, including schizophrenia, addiction and depression.
- Transcranial Magnetic Stimulation (TMS): TMS is a non-invasive neuromodulation therapy that is currently FDA approved for the treatment of medication-refractory depression and the stimulation of peripheral nerves. TMS is also emerging as a possible therapeutic intervention for stroke rehabilitation, schizophrenia, and other conditions affecting the brain. In

contrast to invasive neuromodulation techniques, TMS does not require surgical intervention. Instead, a pulsed current is discharged through a coil placed near the surface of the scalp, creating a time-varying magnetic field perpendicular to the plane of the coil with durations of approximately 1 ms.

Electroceutical therapy truly represents a breakthrough in medical technology that can improve the quality of life of innumerable individuals. Patients suffering from life-threatening conditions may experience improvements in their situations, while those afflicted with constant pain that causes daily complications might finally obtain relief.

2.4.1. Open and Closed loop systems

Neuroprosthetic systems can be implemented with different configurations (for a review, see (Greenwald *et al.*, 2016) depending on the modality used to interface the brain with the external device. First, a distinction should be made between open-loop and closed-loop architectures, both of which involve two systems, i.e., a device (D) and a brain or neural preparation (B), characterized by their specific I/O functions (ID/OD for the device and IB/OB for the brain) (Panuccio *et al.*, 2018). In open-loop systems (Figure 2.4.2A), the output of the device (OD) consists of a stimulus (e.g., electrical pulse), which is directly delivered to the brain (IB = OD). The brain processes the incoming information (IB) and produces an output response (OB). The input to the device (ID) can be any function determining the features of the stimulation sequence; however, this input is not modulated by any feedback from the brain. Closed-loop devices are based on feedback as follows (Figure 2.4.2B): the output of the brain (OB), which consists of ongoing brain activity or its processed version, serves as the input for the device (ID = OB), which triggers the device operation. The output of the device (OD) is the input to the brain (IB = OD). This system generates an I/O loop, which continues indefinitely.

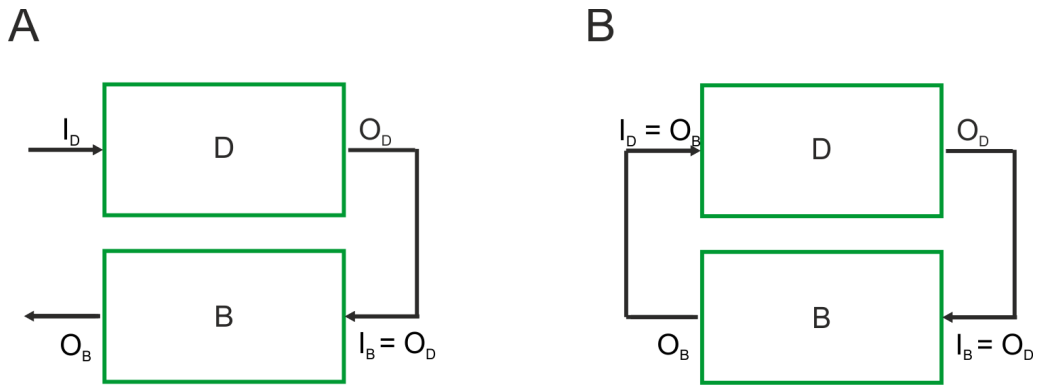

Figure 2.4.2: Schematic representation of open- and closed-loop architectures. A. Open-loop configuration: the output of the device (OD) becomes the input of the biological counterpart (IB). B. Closed-loop configuration: the output of each block is the input of the other block. B = biological counterpart, D = artificial device, Ii = input of block i, Oi = output of block i. Modified from (Panuccio et al., 2018).

Many neuroprosthetic systems have an open-loop configuration (Moro *et al.*, 1999; Molinuevo *et al.*, 2000), which does not respond to unexpected internal or external perturbations (Blaha & Phillips, 1996; Lee *et al.*, 2006). Indeed, in open-loop neuroprosthetics, the system output has no effect on the input to the nervous system (Vassileva *et al.*, 2018), while in closed-loop configurations, the feedback signal can be used to both control and adjust the whole system behavior (Berenyi *et al.*, 2012; Xu *et al.*, 2014; Miao & Koomson, 2018; Sisterson *et al.*, 2018). Recently, closed-loop stimulation strategies have been successfully introduced to Deep Brain Stimulation (DBS) systems (Rosin *et al.*, 2011; Little *et al.*, 2013; Cagnan *et al.*, 2017; Arlotti *et al.*, 2018).

In the future, investigations of the feasibility and efficacy of closed-loop systems for the treatment of neurological conditions will likely emerge. Such conditions include epilepsy and Parkinson's disease and potentially stroke, traumatic brain injury, and spinal cord injury. Thus, obtaining an understanding of how such systems interact with the neural circuitry and how communication may be altered is critical.

Another critical step for the development of neuroprosthetic devices was the introduction of multichannel electrodes. Recording the activity of one single unit allows for one degree of freedom (essentially the firing rate can be decoded as a binary state or linear motion). Recording from multiple units allows for many more degrees

of freedom. This recording could be extremely beneficial for driving a prosthetic limb with motion similar to that of a real limb or controlling complex computer user interfaces. Multiple electrodes have been in use as combinations of single metal electrodes, but over the prior two decades, there have been developments in electrode design adding both channels and dimensionality. Currently, 2D and 3D array electrodes allowing hundreds of channels to be positioned over a large area of cortical tissue are available. These electrodes are typically laid out in a grid pattern, such as 10x10, with a single electrode site at each shank. The shanks can be cut at different lengths to sample from different cortical layers. There are also silicon-based probes that can contain multiple electrode sites on a single shank, enabling recording from an entire cortical column.

The increase in the number of channels require a corresponding increase in the computing power. As more channel are used for algorithms used to determine output, it is necessary to record the output of each channel and then run the decoding algorithm and generate an output in near-real time. As the decoding strategies improved over time, the algorithms used for decoding became more complex, and the predictors of movement were refined. This improvement has resulted in an array of successful Brain Machine Interfaces (BMI's), including the control of robotic arms, computer cursors, and speech (Carmena *et al.*, 2003; Hochberg *et al.*, 2006b; Guenther *et al.*, 2009; Brumberg *et al.*, 2011; Hochberg *et al.*, 2012b). Usually, the decoding of signals in these devices occurs in mainly one direction, but their design includes a biological feedback mechanism. Directly observing the output of a robotic arm or cursor allows the subject to modulate the activity of those neurons.

As shown by the group of Fetz (Jackson *et al.*, 2006), it is possible to volitionally modulate neural activity, and visual feedback likely facilitates this modulation, leading to a pseudo-closed-loop brain machine interface. There has been a recent push to integrate closed-loop systems in the design of BMIs (O'Doherty *et al.*, 2009; Venkatraman *et al.*, 2009; O'Doherty *et al.*, 2011). Closed-loop systems that record

neuronal activity decode that activity and deliver stimulation to a peripheral target. This stimulation includes functional electrical stimulation (FES) to peripheral nerve fibers and direct stimulation of laminae within the spinal cord to evoke motor movements (Moritz *et al.*, 2008; Pohlmeyer *et al.*, 2009; Ethier *et al.*, 2012). Thus, these devices are able to bypass neural damage at the level of the spinal cord. There has also been a push for devices that allow communication within the cortex in normal subjects. Jackson *et al*. described altering the motor output of neurons in M1 through a design in which the activity of one M1 neuron tuned to a certain direction is paired with the stimulation of another neuron in M1 tuned to a different direction (Jackson *et al.*, 2006). These investigators were able to alter the trajectory of movement in the direction of the recorded neuron, indicating that activity-dependent pairing can be useful for making artificial connections within M1. Another set of studies have shown that non-human primates can use the activity in M1 to drive motion toward a target chosen by stimulation triggers in the somatosensory cortex (Dzirasa *et al.*, 2011; O'Doherty *et al.*, 2011). These studies created a method for a closed-loop system to target a section and movement potentially independent of external cues. These previous examples utilize BMBIs (brain machine to brain interfaces) for communication within a cortical area or between areas in normal subjects. This localized communication can potentially be altered by small changes in synaptic efficacy between the recorded and stimulated sites.

For the first time, Guggenmos *et al*. used a BMBI for the treatment of brain injury (TBI in that case) by bridging functional areas that have been disconnected by the injury.

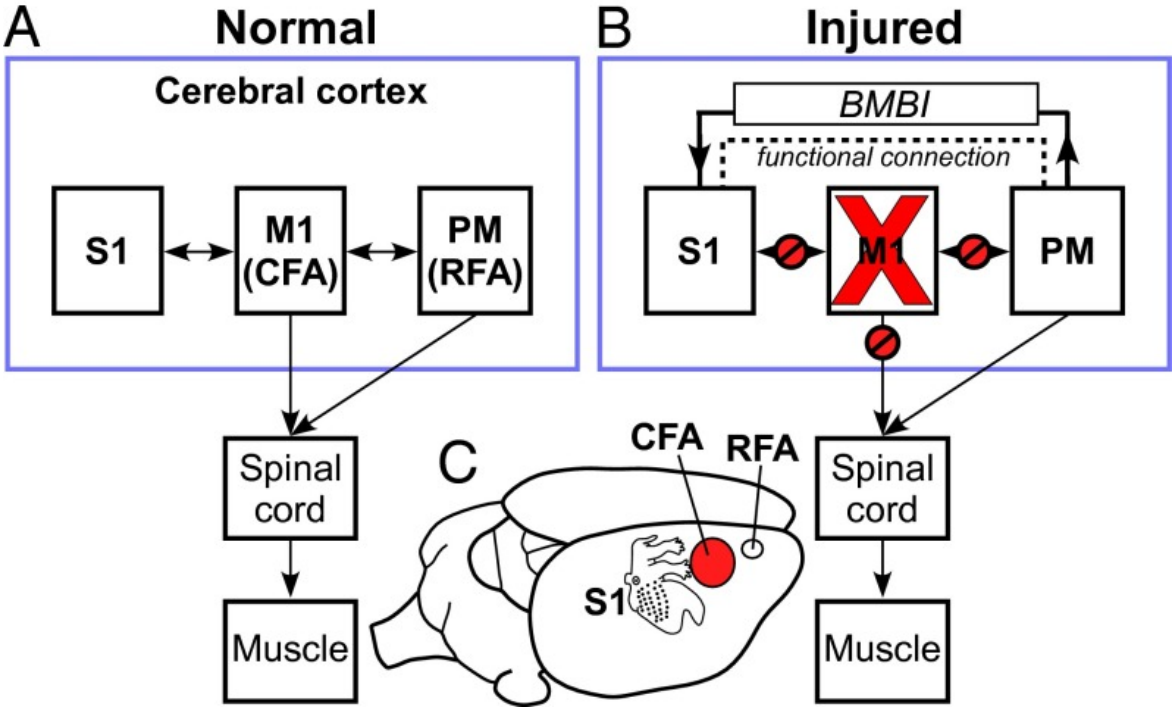

Figure 2.4.3: Theoretical model of the neuroprosthetic treatment approach after brain injury. (A) Normal connectivity of M1, S1, and PM. Both M1 (CFA in rat) and PM (RFA in rat) send substantial outputs to the spinal cord via the corticospinal tract. Additionally, extensive reciprocal connections exist between M1 and PM and between M1 and S1. (B) Effects of focal M1 injury on brain connectivity and the hypothetical effect of a BMBI to restore somatosensory-motor communication. An injury to M1, such as that occurring in stroke or brain trauma, results in a focal area of necrosis and the loss of M1 outputs to the spinal cord. Corticocortical communication between M1 and S1 (and between M1 and PM) is also disrupted, further contributing to functional impairment. Because the uninjured PM also contains corticospinal neurons, it might have the ability to play a vicarious role. The dotted line indicates enhanced functional connection between PM and S1, which we propose is established after treatment with a BMBI. (C) Location of target areas in rat cerebral cortex. A topographic map of the somatosensory representation in S1 is superimposed onto the cortex (Guggenmos et al., 2013).

The purpose of this work was to establish an alternative cortico-cortical communication between distant areas within the cortex. The authors demonstrated better efficacy in terms of behavioral recovery using a neuronal guided stimulation protocol called activity dependent stimulation (ADS) by comparing its performance with that of a randomized version of the protocol (random stimulation, RS) using a simple reaching pellet task in rats (Guggenmos *et al.*, 2013).

References

Ajiboye, A.B., Willett, F.R., Young, D.R., Memberg, W.D., Murphy, B.A., Miller, J.P., Walter, B.L., Sweet, J.A., Hoyen, H.A. & Keith, M.W. (2017) Restoration of reaching and grasping movements through brain-controlled muscle stimulation in a person with tetraplegia: a proof-of-concept demonstration. *The Lancet*, **389**, 1821-1830.

Andersen, P., Hagan, P.J., Phillips, C.G. & Powell, T.P. (1975) Mapping by microstimulation of overlapping projections from area 4 to motor units of the baboon's hand. *Proc R Soc Lond B Biol Sci*, **188**, 31-36.

Arlotti, M., Marceglia, S., Foffani, G., Volkmann, J., Lozano, A.M., Moro, E., Cogiamanian, F., Prenassi, M., Bocci, T., Cortese, F., Rampini, P., Barbieri, S. & Priori, A. (2018) Eight-hours adaptive deep brain stimulation in patients with Parkinson disease. *Neurology*, **90**, e971-e976.

Asanuma, H. & Rosen, I. (1972) Topographical organization of cortical efferent zones projecting to distal forelimb muscles in the monkey. *Exp Brain Res*, **14**, 243-256.

Avestruz, A.T., Santa, W., Carlson, D., Jensen, R., Stanslaski, S., Helfenstine, A., and Denison, T. (2008) A 5 μw/channel spectral analysis IC for chronic bidirectional brain-machine interfaces. *Solid State Circuits*, **43**, 3006-3024.

Barbay, S., Plautz, E.J., Friel, K.M., Frost, S.B., Dancause, N., Stowe, A.M. & Nudo, R.J. (2006) Behavioral and neurophysiological effects of delayed training following a small ischemic infarct in primary motor cortex of squirrel monkeys. *Exp Brain Res*, **169**, 106-116.

Berenyi, A., Belluscio, M., Mao, D. & Buzsaki, G. (2012) Closed-loop control of epilepsy by transcranial electrical stimulation. *Science*, **337**, 735-737.

Berger, T.W., Hampson, R.E., Song, D., Goonawardena, A., Marmarelis, V.Z. & Deadwyler, S.A. (2011) A cortical neural prosthesis for restoring and enhancing memory. *J Neural Eng*, **8**, 046017.

Berger, T.W., Song, D., Chan, R.H., Marmarelis, V.Z., LaCoss, J., Wills, J., Hampson, R.E., Deadwyler, S.A. & Granacki, J.J. (2012) A hippocampal cognitive prosthesis: multi-input, multi-output nonlinear modeling and VLSI implementation. *IEEE Transactions on Neural Systems and Rehabilitation Engineering*, **20**, 198-211.

Berlim, M.T., McGirr, A., Van den Eynde, F., Fleck, M.P. & Giacobbe, P. (2014) Effectiveness and acceptability of deep brain stimulation (DBS) of the subgenual cingulate cortex for treatment-resistant depression: a systematic review and exploratory meta-analysis. *Journal of affective disorders*, **159**, 31-38.

Biernaskie, J., Corbett, D., Peeling, J., Wells, J. & Lei, H. (2001) A serial MR study of cerebral blood flow changes and lesion development following endothelin‐1‐induced ischemia in rats. *Magnetic Resonance in Medicine: An Official Journal of the International Society for Magnetic Resonance in Medicine*, **46**, 827-830.

Blaha, C. & Phillips, A. (1996) A critical assessment of electrochemical procedures applied to the measurement of dopamine and its metabolites during drug-induced and species-typical behaviours. *Behavioural pharmacology*, **7**, 675-708.

Bogaert, L., Scheller, D., Moonen, J., Sarre, S., Smolders, I., Ebinger, G. & Michotte, Y. (2000) Neurochemical changes and laser Doppler flowmetry in the endothelin-1 rat model for focal cerebral ischemia. *Brain research*, **887**, 266-275.

Bouton, C.E., Shaikhouni, A., Annetta, N.V., Bockbrader, M.A., Friedenberg, D.A., Nielson, D.M., Sharma, G., Sederberg, P.B., Glenn, B.C. & Mysiw, W.J. (2016) Restoring cortical control of functional movement in a human with quadriplegia. *Nature*, **533**, 247.

Brumberg, J.S., Wright, E.J., Andreasen, D.S., Guenther, F.H. & Kennedy, P.R. (2011) Classification of intended phoneme production from chronic intracortical microelectrode recordings in speech motor cortex. *Frontiers in neuroscience*, **5**, 65.

Buzsaki, G., Anastassiou, C.A. & Koch, C. (2012) The origin of extracellular fields and currents - EEG, ECoG, LFP and spikes. *Nat Rev Neurosci*, **13**, 407-420.

Cagnan, H., Pedrosa, D., Little, S., Pogosyan, A., Cheeran, B., Aziz, T., Green, A., Fitzgerald, J., Foltynie, T., Limousin, P., Zrinzo, L., Hariz, M., Friston, K.J., Denison, T. & Brown, P. (2017) Stimulating at the right time: phase-specific deep brain stimulation. *Brain*, **140**, 132-145.

Carmena, J.M., Lebedev, M.A., Crist, R.E., O'Doherty, J.E., Santucci, D.M., Dimitrov, D.F., Patil, P.G., Henriquez, C.S. & Nicolelis, M.A. (2003) Learning to control a brain–machine interface for reaching and grasping by primates. *PLoS biology*, **1**, e42.

Carmichael, S.T. (2005) Rodent models of focal stroke: size, mechanism, and purpose. *NeuroRx*, **2**, 396-409.

Carod-Artal, J., Egido, J.A., González, J.L. & Varela de Seijas, E. (2000) Quality of life among stroke survivors evaluated 1 year after stroke: experience of a stroke unit. *Stroke*, **31**, 2995-3000.

Cauller, L.J., Clancy, B. & Connors, B.W. (1998) Backward cortical projections to primary somatosensory cortex in rats extend long horizontal axons in layer I. *J Comp Neurol*, **390**, 297-310.

Chapin, J.K. (2004) Using multi-neuron population recordings for neural prosthetics. *Nature Neuroscience*, **7**, 452-455.

Chapin, J.K., Moxon, K.A., Markowitz, R.S. & Nicolelis, M.A. (1999) Real-time control of a robot arm using simultaneously recorded neurons in the motor cortex. *Nature neuroscience*, **2**, 664.

Cheney, P.D., Fetz, E.E. & Palmer, S.S. (1985) Patterns of facilitation and suppression of antagonist forelimb muscles from motor cortex sites in the awake monkey. *J Neurophysiol*, **53**, 805-820.

Cheung, K.C., Renaud, P., Tanila, H. & Djupsund, K. (2007) Flexible polyimide microelectrode array for in vivo recordings and current source density analysis. *Biosens Bioelectron*, **22**, 1783-1790.

Chiappalone, M., Bove, M., Vato, A., Tedesco, M. & Martinoia, S. (2006) Dissociated cortical networks show spontaneously correlated activity patterns during in vitro development. *Brain research*, **1093**, 41-53.

Clarke, P., Marshall, V., Black, S.E. & Colantonio, A. (2002) Well-being after stroke in Canadian seniors: findings from the Canadian Study of Health and Aging. *Stroke*, **33**, 1016-1021.

Colgin, L.L. & Moser, E.I. (2010) Gamma oscillations in the hippocampus. *Physiology*, **25**, 319-329.

Collomb-Clerc, A. & Welter, M.-L. (2015) Effects of deep brain stimulation on balance and gait in patients with Parkinson's disease: a systematic neurophysiological review. *Neurophysiologie Clinique/Clinical Neurophysiology*, **45**, 371-388.

Cramer, S.C. & Nudo, R.J. (2010) *Brain repair after stroke*. Cambridge University Press.

Deco, G. & Corbetta, M. (2011) The dynamical balance of the brain at rest. *The Neuroscientist*, **17**, 107-123.

Dietrich, W.D. & Kuluz, J.W. (1999) Spontaneous Hyperthermia and its Mechanism in the Intraluminal Suture Middle Cerebral Artery Occlusion Model of Rats. *Stroke*, **30**, 2470-2471.

Donoghue, J.P., Leibovic, S. & Sanes, J.N. (1992) Organization of the forelimb area in squirrel monkey motor cortex: representation of digit, wrist, and elbow muscles. *Exp Brain Res*, **89**, 1-19.

Donoghue, J.P., Nurmikko, A., Black, M. & Hochberg, L.R. (2007) Assistive technology and robotic control using motor cortex ensemble-based neural interface systems in humans with tetraplegia. *Journal of Physiology-London*, **579**, 603-611.

Donoghue, J.P. & Wise, S.P. (1982) The motor cortex of the rat: cytoarchitecture and microstimulation mapping. *J Comp Neurol*, **212**, 76-88.

Duker, A.P. & Espay, A.J. (2013) Surgical treatment of Parkinson disease: past, present, and future. *Neurologic clinics*, **31**, 799-808.

Dum, R.P. & Strick, P.L. (2002) Motor areas in the frontal lobe of the primate. *Physiol Behav*, **77**, 677-682.

Dzirasa, K., Fuentes, R., Kumar, S., Potes, J.M. & Nicolelis, M.A. (2011) Chronic in vivo multi-circuit neurophysiological recordings in mice. *Journal of neuroscience methods*, **195**, 36-46.

Eduard, F. & Gustav, H. (1870) Uber die elektrische erregbarkeit des grosshims. *Arch Anat Physiol wiss Med*, **37**, 300-332.

Eisenstein, M. (2009) Neural circuits: Putting neurons on the map. *Nature*, **461**, 1149-1152.

Ethier, C., Oby, E.R., Bauman, M. & Miller, L.E. (2012) Restoration of grasp following paralysis through brain-controlled stimulation of muscles. *Nature*, **485**, 368.

Evarts, E.V. (1968) A technique for recording activity of subcortical neurons in moving animals. *Electroencephalogr Clin Neurophysiol*, **24**, 83-86.

Faggin, B.M., Nguyen, K.T. & Nicolelis, M.A. (1997) Immediate and simultaneous sensory reorganization at cortical and subcortical levels of the somatosensory system. *Proceedings of the National Academy of Sciences*, **94**, 9428-9433.

Famm, K., Litt, B., Tracey, K.J., Boyden, E.S. & Slaoui, M. (2013) Drug discovery: a jump-start for electroceuticals. *Nature*, **496**, 159.

Fang, P.-c., Barbay, S., Plautz, E.J., Hoover, E., Strittmatter, S.M. & Nudo, R.J. (2010) Combination of NEP 1-40 treatment and motor training enhances behavioral recovery after a focal cortical infarct in rats. *Stroke*, **41**, 544-549.

Fetz, E.E. (1969) Operant conditioning of cortical unit activity. *Science*, **163**, 955-958.

Fetz, E.E. & Cheney, P.D. (1980) Postspike facilitation of forelimb muscle activity by primate corticomotoneuronal cells. *J Neurophysiol*, **44**, 751-772.

Fetz, E.E., Jankowska, E., Johannisson, T. & Lipski, J. (1979) Autogenetic inhibition of motoneurones by impulses in group Ia muscle spindle afferents. *J Physiol*, **293**, 173-195.

Fluri, F., Schuhmann, M.K. & Kleinschnitz, C. (2015) Animal models of ischemic stroke and their application in clinical research. *Drug design, development and therapy*, **9**, 3445.

Fries, P., Reynolds, J.H., Rorie, A.E. & Desimone, R. (2001) Modulation of oscillatory neuronal synchronization by selective visual attention. *Science*, **291**, 1560-1563.

Frost, S.B., Barbay, S., Mumert, M.L., Stowe, A.M. & Nudo, R.J. (2006) An animal model of capsular infarct: endothelin-1 injections in the rat. *Behavioural brain research*, **169**, 206-211.

Fukuda, S. & del Zoppo, G.J. (2003) Models of focal cerebral ischemia in the nonhuman primate. *ILAR journal*, **44**, 96-104.

Fuxe, K., Bjelke, B., Andbjer, B., Grahn, H., Rimondini, R. & Agnati, L.F. (1997) Endothelin-1 induced lesions of the frontoparietal cortex of the rat. A possible model of focal cortical ischemia. *Neuroreport*, **8**, 2623-2629.

Garcia, J.H., Yoshida, Y., Chen, H., Li, Y., Zhang, Z. G., Lian, J., Chen, S., Chopp, M. (1993) Progression from Ischemic In jury to Infarct Following Middle Cerebral Artery Occlusion in the Rat. *American Journal of Pathology*, **142**, 623-635.

Georgopoulos, A.P., Schwartz, A.B. & Kettner, R.E. (1986) Neuronal population coding of movement direction. *Science*, 1416-1419.

Go, A.S., Mozaffarian, D., Roger, V.L., Benjamin, E.J., Berry, J.D., Blaha, M.J., Dai, S., Ford, E.S. & Fox, C.S. (2014) Heart disease and stroke statistics—2014 update: A report from the American Heart Association. *Circulation*, **129**, e28.

Graham, S.M., McCullough, L.D. & Murphy, S.J. (2004) Animal models of ischemic stroke: balancing experimental aims and animal care. *Comparative medicine*, **54**, 486-496.

Gray, C.M., König, P., Engel, A.K. & Singer, W. (1989) Oscillatory responses in cat visual cortex exhibit inter-columnar synchronization which reflects global stimulus properties. *Nature*, **338**, 334.

Greenwald, E., Masters, M.R. & Thakor, N.V. (2016) Implantable neurotechnologies: bidirectional neural interfaces—applications and VLSI circuit implementations. *Medical & biological engineering & computing*, **54**, 1-17.

Gresham, G.E., Fitzpatrick, T.E., Wolf, P.A., McNamara, P.M., Kannel, W.B. & Dawber, T.R. (1975) Residual disability in survivors of stroke—the Framingham study. *New England journal of medicine*, **293**, 954-956.

Gross, J., Schmitz, F., Schnitzler, I., Kessler, K., Shapiro, K., Hommel, B. & Schnitzler, A. (2004) Modulation of long-range neural synchrony reflects temporal limitations of visual attention in humans. *Proceedings of the national Academy of Sciences*, **101**, 13050-13055.

Guenther, F.H., Brumberg, J.S., Wright, E.J., Nieto-Castanon, A., Tourville, J.A., Panko, M., Law, R., Siebert, S.A., Bartels, J.L. & Andreasen, D.S. (2009) A wireless brain-machine interface for real-time speech synthesis. *PloS one*, **4**, e8218.

Guggenmos, D.J., Azin, M., Barbay, S., Mahnken, J.D., Dunham, C., Mohseni, P. & Nudo, R.J. (2013) Restoration of function after brain damage using a neural prosthesis. *Proceedings of the National Academy of Sciences of the United States of America*, **110**, 21177-21182.

Gustafsson, B. & Jankowska, E. (1976) Direct and indirect activation of nerve cells by electrical pulses applied extracellularly. *J Physiol*, **258**, 33-61.

Hochberg, L.R., Bacher, D., Jarosiewicz, B., Masse, N.Y., Simeral, J.D., Vogel, J., Haddadin, S., Liu, J., Cash, S.S. & van der Smagt, P. (2012a) Reach and grasp by people with tetraplegia using a neurally controlled robotic arm. *Nature*, **485**, 372.

Hochberg, L.R., Bacher, D., Jarosiewicz, B., Masse, N.Y., Simeral, J.D., Vogel, J., Haddadin, S., Liu, J., Cash, S.S., van der Smagt, P. & Donoghue, J.P. (2012b) Reach and grasp by people with tetraplegia using a neurally controlled robotic arm. *Nature*, **485**, 372-U121.

Hochberg, L.R., Serruya, M.D., Friehs, G.M., Mukand, J.A., Saleh, M., Caplan, A.H., Branner, A., Chen, D., Penn, R.D. & Donoghue, J.P. (2006a) Neuronal ensemble control of prosthetic devices by a human with tetraplegia. *Nature*, **442**, 164-171.

Hochberg, L.R., Serruya, M.D., Friehs, G.M., Mukand, J.A., Saleh, M., Caplan, A.H., Branner, A., Chen, D., Penn, R.D. & Donoghue, J.P. (2006b) Neuronal ensemble control of prosthetic devices by a human with tetraplegia. *Nature*, **442**, 164.

Hong, L.E., Buchanan, R.W., Thaker, G.K., Shepard, P.D. & Summerfelt, A. (2008) Beta (~ 16 Hz) frequency neural oscillations mediate auditory sensory gating in humans. *Psychophysiology*, **45**, 197-204.

Hoshi, E. & Tanji, J. (2004) Differential roles of neuronal activity in the supplementary and presupplementary motor areas: from information retrieval to motor planning and execution. *J Neurophysiol*, **92**, 3482-3499.

Hossmann, K.-A. (2012) The two pathophysiologies of focal brain ischemia: implications for translational stroke research. *Journal of Cerebral Blood Flow & Metabolism*, **32**, 1310-1316.

Huerta, P.T. & Lisman, J.E. (1993) Heightened synaptic plasticity of hippocampal CA1 neurons during a cholinergically induced rhythmic state. *Nature*, **364**, 723.

Hughes, P., Anthony, D., Ruddin, M., Botham, M., Rankine, E., Sablone, M., Baumann, D., Mir, A. & Perry, V. (2003) Focal lesions in the rat central nervous system induced by endothelin-1. *Journal of Neuropathology & Experimental Neurology*, **62**, 1276-1286.

Humphrey, D.R., Schmidt, E. & Thompson, W. (1970a) Predicting measures of motor performance from multiple cortical spike trains. *Science*, **170**, 758-762.

Humphrey, D.R., Schmidt, E.M. & Thompson, W.D. (1970b) Predicting measures of motor performance from multiple cortical spike trains. *Science*, **170**, 758-762.

Jackman, K. & Iadecola, C. (2015) Neurovascular regulation in the ischemic brain. *Antioxidants & redox signaling*, **22**, 149-160.

Jackson, A., Mavoori, J. & Fetz, E.E. (2006) Long-term motor cortex plasticity induced by an electronic neural implant. *Nature*, **444**, 56-60.

Jankowska, E., Johannisson, T. & Lipski, J. (1981) Common interneurones in reflex pathways from group 1a and 1b afferents of ankle extensors in the cat. *J Physiol*, **310**, 381-402.

Jankowska, E., Padel, Y. & Tanaka, R. (1975a) The mode of activation of pyramidal tract cells by intracortical stimuli. *J Physiol*, **249**, 617-636.

Jankowska, E., Padel, Y. & Tanaka, R. (1975b) Projections of pyramidal tract cells to alpha-motoneurones innervating hind-limb muscles in the monkey. *J Physiol*, **249**, 637-667.

Johnson, M.D., Lim, H.H., Netoff, T.I., Connolly, A.T., Johnson, N., Roy, A., Holt, A., Lim, K.O., Carey, J.R. & Vitek, J.L. (2013) Neuromodulation for brain disorders: challenges and opportunities. *IEEE Transactions on Biomedical Engineering*, **60**, 610-624.

Kaas, J.H. (1987) The organization of neocortex in mammals: implications for theories of brain function. *Annu Rev Psychol*, **38**, 129-151.

Kaas, J.H. (2004) Evolution of somatosensory and motor cortex in primates. *Anat Rec A Discov Mol Cell Evol Biol*, **281**, 1148-1156.

Kayagil, T.A., Bai, O., Henriquez, C.S., Lin, P., Furlani, S.J., Vorbach, S. & Hallett, M. (2009) A binary method for simple and accurate two-dimensional cursor control from EEG with minimal subject training. *J Neuroeng Rehabil*, **6**, 14.

Killackey, H.P., Koralek, K.A., Chiaia, N.L. & Rhodes, R.W. (1989) Laminar and areal differences in the origin of the subcortical projection neurons of the rat somatosensory cortex. *J Comp Neurol*, **282**, 428-445.

Kilner, J.M., Baker, S.N., Salenius, S., Hari, R. & Lemon, R.N. (2000) Human cortical muscle coherence is directly related to specific motor parameters. *Journal of Neuroscience*, **20**, 8838-8845.

Kim, S.P., Simeral, J.D., Hochberg, L.R., Donoghue, J.P. & Black, M.J. (2008) Neural control of computer cursor velocity by decoding motor cortical spiking activity in humans with tetraplegia. *J Neural Eng*, **5**, 455-476.

Kiyota, Y., Miyamoto, M., Nagaoka, A. & Nagawa, Y. (1986) Cerebral embolization leads to memory impairment of several learning tasks in rats. *Pharmacology Biochemistry and Behavior*, **24**, 687-692.

Kleim, J.A., Barbay, S. & Nudo, R.J. (1998) Functional reorganization of the rat motor cortex following motor skill learning. *J Neurophysiol*, **80**, 3321-3325.

Kopell, N., Ermentrout, G., Whittington, M. & Traub, R. (2000) Gamma rhythms and beta rhythms have different synchronization properties. *Proceedings of the National Academy of Sciences*, **97**, 1867-1872.

Koralek, K.A., Olavarria, J. & Killackey, H.P. (1990) Areal and laminar organization of corticocortical projections in the rat somatosensory cortex. *J Comp Neurol*, **299**, 133-150.

Krames, E.S., Peckham, P.H., Rezai, A. & Aboelsaad, F. (2009) What is neuromodulation? *Neuromodulation*. Elsevier, pp. 3-8.

Laxpati, N.G., Kasoff, W.S. & Gross, R.E. (2014) Deep brain stimulation for the treatment of epilepsy: circuits, targets, and trials. *Neurotherapeutics*, **11**, 508-526.

Lee, K., Jang, K. & Shon, Y. (2006) Chronic deep brain stimulation of subthalamic and anterior thalamic nuclei for controlling refractory partial epilepsy *Advances in functional and reparative neurosurgery*. Springer, pp. 87-91.

Lee, V.M., Burdett, N.G., Carpenter, T.A., Hall, L.D., Pambakian, P.S., Patel, S., Wood, N.I. & James, M.F. (1996) Evolution of photochemically induced focal cerebral ischemia in the rat: magnetic resonance imaging and histology. *Stroke*, **27**, 2110-2119.

Lichtman, J.W., Livet, J. & Sanes, J.R. (2008) A technicolour approach to the connectome. *Nat Rev Neurosci*, **9**, 417-422.

Little, S., Pogosyan, A., Neal, S., Zavala, B., Zrinzo, L., Hariz, M., Foltynie, T., Limousin, P., Ashkan, K., FitzGerald, J., Green, A.L., Aziz, T.Z. & Brown, P. (2013) Adaptive deep brain stimulation in advanced Parkinson disease. *Ann Neurol*, **74**, 449-457.

Livet, J., Weissman, T.A., Kang, H., Draft, R.W., Lu, J., Bennis, R.A., Sanes, J.R. & Lichtman, J.W. (2007) Transgenic strategies for combinatorial expression of fluorescent proteins in the nervous system. *Nature*, **450**, 56.

Lüscher, C., Nicoll, R.A., Malenka, R.C. & Muller, D. (2000) Synaptic plasticity and dynamic modulation of the postsynaptic membrane. *Nat Neurosci*, **3**, 545.

Maccione, A., Gandolfo, M., Massobrio, P., Novellino, A., Martinoia, S. & Chiappalone, M. (2009) A novel algorithm for precise identification of spikes in extracellularly recorded neuronal signals. *J Neurosci Methods*, **177**, 241-249.

MAGAZINE, T. & RADAR'S, T. (2015) IEEE Spectrum - Front cover. *IEEE Spectrum*, **52**, c1-c1.

McAuley, M. (1995) Rodent models of focal ischemia. *Cerebrovascular and brain metabolism reviews*, **7**, 153-180.

Melloni, L., Molina, C., Pena, M., Torres, D., Singer, W. & Rodriguez, E. (2007) Synchronization of neural activity across cortical areas correlates with conscious perception. *Journal of neuroscience*, **27**, 2858-2865.

Miao, Y. & Koomson, V.J. (2018) A CMOS-Based Bidirectional Brain Machine Interface System With Integrated fdNIRS and tDCS for Closed-Loop Brain Stimulation. *IEEE transactions on biomedical circuits and systems*, **12**, 554-563.

Mishra, S. (2017) Electroceuticals in medicine–The brave new future. *Indian Heart Journal*, **69**, 685-686.

Molinuevo, J.L., Valldeoriola, F., Tolosa, E., Rumia, J., Valls-Solé, J., Roldán, H. & Ferrer, E. (2000) Levodopa withdrawal after bilateral subthalamic nucleus stimulation in advanced Parkinson disease. *Archives of neurology*, **57**, 983-988.

Moritz, C.T., Perlmutter, S.I. & Fetz, E.E. (2008) Direct control of paralysed muscles by cortical neurons. *Nature*, **456**, 639.

Moro, E., Scerrati, M., Romito, L., Roselli, R., Tonali, P. & Albanese, A. (1999) Chronic subthalamic nucleus stimulation reduces medication requirements in Parkinson's disease. *Neurology*, **53**, 85-85.

Murphy, T., Corbett, D. (2009) Plasticity during stroke recovery: from synapse to behaviour. *Nature Reviews*, **10**, 861-872.

Nakagomi, S., Kiryu-Seo, S. & Kiyama, H. (2000) Endothelin-converting enzymes and endothelin receptor B messenger RNAs are expressed in different neural cell species and these messenger RNAs are coordinately induced in neurons and astrocytes respectively following nerve injury. *Neuroscience*, **101**, 441-449.

Nichols, M., Townsend, N., Scarborough, P., Rayner, M., Leal, J., Luengo-Fernandez, R. (2012) European Cardiovascular Disease Statistics. European Heart Network and European Society of Cardiology, Brussels, belgium.

Nudo, R.J. (2003) Adaptive plasticity in motor cortex: implications for rehabilitation after brain injury. *Journal of rehabilitation medicine*, 7-10.

Nudo, R.J. & Milliken, G.W. (1996) Reorganization of movement representations in primary motor cortex following focal ischemic infarcts in adult squirrel monkeys. *J Neurophysiol*, **75**, 2144-2149.

Nudo, R.J., Milliken, G.W., Jenkins, W.M. & Merzenich, M.M. (1996a) Use-dependent alterations of movement representations in primary motor cortex of adult squirrel monkeys. *The Journal of neuroscience : the official journal of the Society for Neuroscience*, **16**, 785-807.

Nudo, R.J., Sutherland, D.P. & Masterton, R.B. (1995) Variation and evolution of mammalian corticospinal somata with special reference to primates. *J Comp Neurol*, **358**, 181-205.

Nudo, R.J., Wise, B.M., SiFuentes, F. & Milliken, G.W. (1996b) Neural substrates for the effects of rehabilitative training on motor recovery after ischemic infarct. *Science*, **272**, 1791-1794.

O'Doherty, J.E., Lebedev, M.A., Hanson, T.L., Fitzsimmons, N.A. & Nicolelis, M.A. (2009) A brain-machine interface instructed by direct intracortical microstimulation. *Frontiers in integrative neuroscience*, **3**, 20.

O'Doherty, J.E., Lebedev, M.A., Ifft, P.J., Zhuang, K.Z., Shokur, S., Bleuler, H. & Nicolelis, M.A. (2011) Active tactile exploration using a brain–machine–brain interface. *Nature*, **479**, 228.

Organization, W.H. (2006) *Neurological disorders: public health challenges*. World Health Organization.

Panuccio, G., Semprini, M., Natale, L., Buccelli, S., Colombi, I. & Chiappalone, M. (2018) Progress in Neuroengineering for brain repair: New challenges and open issues. *Brain and Neuroscience Advances*, **2**, 2398212818776475.

Park, M.C., Belhaj-Saif, A. & Cheney, P.D. (2004) Properties of primary motor cortex output to forelimb muscles in rhesus macaques. *J Neurophysiol*, **92**, 2968-2984.

Penfield, W. & Boldrey, E. (1939) Cortical spread of epileptic discharge and the conditioning effect of habitual seizures. *American Journal of Psychiatry*, **96**, 255-281.

Plautz, E.J., Barbay, S., Frost, S.B., Friel, K.M., Dancause, N., Zoubina, E.V., Stowe, A.M., Quaney, B.M. & Nudo, R.J. (2003) Post-infarct cortical plasticity and behavioral recovery using concurrent cortical stimulation and rehabilitative training: a feasibility study in primates. *Neurological research*, **25**, 801-810.

Plautz, E.J., Milliken, G.W. & Nudo, R.J. (2000) Effects of repetitive motor training on movement representations in adult squirrel monkeys: role of use versus learning. *Neurobiology of learning and memory*, **74**, 27-55.

Pohlmeyer, E.A., Oby, E.R., Perreault, E.J., Solla, S.A., Kilgore, K.L., Kirsch, R.F. & Miller, L.E. (2009) Toward the restoration of hand use to a paralyzed monkey: brain-controlled functional electrical stimulation of forearm muscles. *PloS one*, **4**, e5924.

Pulsinelli, W. & Buchan, A. (1988) The four-vessel occlusion rat model: method for complete occlusion of vertebral arteries and control of collateral circulation. *Stroke*, **19**, 913-914.

Pulsinelli, W. & Duffy, T. (1983) Regional energy balance in rat brain after transient forebrain ischemia. *Journal of neurochemistry*, **40**, 1500-1503.

Pulsinelli, W.A. & Brierley, J.B. (1979) A new model of bilateral hemispheric ischemia in the unanesthetized rat. *Stroke*, **10**, 267-272.

Quiroga, R.Q., Nadasdy, Z. & Ben-Shaul, Y. (2004) Unsupervised spike detection and sorting with wavelets and superparamagnetic clustering. *Neural Comput*, **16**, 1661-1687.

Reardon, S. (2014) Electroceuticals spark interest. *Nature*, **511**, 18.

Robinson, M., Macrae, I., Todd, M., Reid, J. & McCulloch, J. (1990) Reduction of local cerebral blood flow to pathological levels by endothelin-1 applied to the middle cerebral artery in the rat. *Neuroscience letters*, **118**, 269-272.

Rosin, B., Slovik, M., Mitelman, R., Rivlin-Etzion, M., Haber, S.N., Israel, Z., Vaadia, E. & Bergman, H. (2011) Closed-Loop Deep Brain Stimulation Is Superior in Ameliorating Parkinsonism. *Neuron*, **72**, 370-384.

Rothschild, R.M. (2010) Neuroengineering tools/applications for bidirectional interfaces, brain-computer interfaces, and neuroprosthetic implants - a review of recent progress. *Front Neuroeng*, **3**, 112.

Saita, K., Chen, M., Spratt, N. J., Porrit, M. J., Liberatore, G. T., Read, S. J., Levi, C. R., Donnan, A., Ackermann, U., Tochon-Danguy, H. J., Sachinidis, J. I., Howells, D. W. (2004) Imaging the Ischemic Penumbra with 18F-Fluoromisonidazole in a Rat Model of Ischemic Stroke. *Stroke*, **35**, 975-980.

Sanes, J.N., Donoghue, J.P., Thangaraj, V., Edelman, R.R. & Warach, S. (1995) Shared neural substrates controlling hand movements in human motor cortex. *Science*, **268**, 1775-1777.

Sato, K.C. & Tanji, J. (1989) Digit-muscle responses evoked from multiple intracortical foci in monkey precentral motor cortex. *J Neurophysiol*, **62**, 959-970.

Serradj, N., Agger, S.F. & Hollis II, E.R. (2017) Corticospinal circuit plasticity in motor rehabilitation from spinal cord injury. *Neuroscience letters*, **652**, 94-104.

Sharkey, J. (1993) Perivascular microapplication of endothelin-1: a new model of focal cerebral ischaemia in the rat. *Journal of Cerebral Blood Flow & Metabolism*, **13**, 865-871.

Silvoni, S., Ramos-Murguialday, A., Calvinato, M., Volpato, C., Cisotto, G., Turolla, A., Piccione, F., Birbaumer, N. (2011) Brain-Computer Interface in Stroke: a Review of Progress. *Clinical EEG and Neuroscience*, **42**, 245-252.

Simeral, J.D., Kim, S.P., Black, M.J., Donoghue, J.P. & Hochberg, L.R. (2011) Neural control of cursor trajectory and click by a human with tetraplegia 1000 days after implant of an intracortical microelectrode array. *J Neural Eng*, **8**, 025027.

Sisterson, N.D., Wozny, T.A., Kokkinos, V., Constantino, A. & Richardson, R.M. (2018) Closed-Loop Brain Stimulation for Drug-Resistant Epilepsy: Towards an Evidence-Based Approach to Personalized Medicine. *Neurotherapeutics*, 1-9.

Smith, S.L., Judy, J.W. & Otis, T.S. (2004) An ultra small array of electrodes for stimulating multiple inputs into a single neuron. *Journal of Neuroscience Methods*, **133**, 109-114.

Song, D. & Berger, T.W. (2015) Hippocampal memory prosthesis. *Encyclopedia of Computational Neuroscience*, 1324-1328.

Sporns, O., Tononi, G. & Kotter, R. (2005) The human connectome: A structural description of the human brain. *PLoS Comput Biol*, **1**, e42.

Stevenson, I.H. & Kording, K.P. (2011) How advances in neural recording affect data analysis. *Nature neuroscience*, **14**, 139-142.

Stevenson, I.H., Rebesco, J.M., Hatsopoulos, N.G., Haga, Z., Miller, L.E. & Kording, K.P. (2009) Bayesian inference of functional connectivity and network structure from spikes. *IEEE Trans Neural Syst Rehabil Eng*, **17**, 203-213.

Stevenson, I.H., Rebesco, J.M., Miller, L.E. & Körding, K.P. (2008) Inferring functional connections between neurons. *Current opinion in neurobiology*, **18**, 582-588.

Stoney, S.D., Jr., Thompson, W.D. & Asanuma, H. (1968) Excitation of pyramidal tract cells by intracortical microstimulation: effective extent of stimulating current. *J Neurophysiol*, **31**, 659-669.

Strick, P.L. & Preston, J.B. (1982) Two representations of the hand in area 4 of a primate. I. Motor output organization. *J Neurophysiol*, **48**, 139-149.

Tallon-Baudry, C., Bertrand, O., Peronnet, F. & Pernier, J. (1998) Induced γ-band activity during the delay of a visual short-term memory task in humans. *Journal of Neuroscience*, **18**, 4244-4254.

Tehovnik, E.J. (1996) Electrical stimulation of neural tissue to evoke behavioral responses. *J Neurosci Methods*, **65**, 1-17.

Tehovnik, E.J., Tolias, A.S., Sultan, F., Slocum, W.M. & Logothetis, N.K. (2006) Direct and indirect activation of cortical neurons by electrical microstimulation. *J Neurophysiol*, **96**, 512-521.

Tolias, A.S., Sultan, F., Augath, M., Oeltermann, A., Tehovnik, E.J., Schiller, P.H. & Logothetis, N.K. (2005) Mapping cortical activity elicited with electrical microstimulation using FMRI in the macaque. *Neuron*, **48**, 901-911.

Traystman, R.J. (2003) Animal models of focal and global cerebral ischemia. *ILAR journal*, **44**, 85-95.

Tsuji, M., Ohshima, M., Taguchi, A., Kasahara, Y., Ikeda, T., Matsuyama, T. (2013) A novel reproducible model of neonatal stroke in mice: Comparison with a hypoxia–ischemia model. *Experimental Neurology*, **247**, 218-225.

Uesugi, M., Kasuya, Y., Hayashi, K. & Goto, K. (1998) SB209670, a potent endothelin receptor antagonist, prevents or delays axonal degeneration after spinal cord injury. *Brain research*, **786**, 235-239.

Uhlhaas, P.J. & Singer, W. (2010) Abnormal neural oscillations and synchrony in schizophrenia. *Nat Rev Neurosci*, **11**, 100.

van Gerven, M., Farquhar, J., Schaefer, R., Vlek, R., Geuze, J., Nijholt, A., Ramsey, N., Haselager, P., Vuurpijl, L., Gielen, S. & Desain, P. (2009) The brain-computer interface cycle. *J Neural Eng*, **6**, 041001.

Vassileva, A., van Blooijs, D., Leijten, F. & Huiskamp, G. (2018) Neocortical electrical stimulation for epilepsy: Closed-loop versus open-loop. *Epilepsy research*.

Venkatraman, V., Payne, J.W., Bettman, J.R., Luce, M.F. & Huettel, S.A. (2009) Separate neural mechanisms underlie choices and strategic preferences in risky decision making. *Neuron*, **62**, 593-602.

Vertes, R.P. (2005) Hippocampal theta rhythm: A tag for short‐term memory. *Hippocampus*, **15**, 923-935.

Von Stein, A., Chiang, C. & König, P. (2000) Top-down processing mediated by interareal synchronization. *Proceedings of the National Academy of Sciences*, **97**, 14748-14753.

Watson, B. (1998) Animal models of photochemically induced brain ischemia and stroke. *Cerebrovascular disease. Pathophysiology, diagnosis, and management*, **1**, 52-74.

Welker, W.I., Benjamin, R.M., Miles, R.C. & Woolsey, C.N. (1957) Motor effects of stimulation of cerebral cortex of squirrel monkey (Saimiri sciureus). *J Neurophysiol*, **20**, 347-364.

Wespatat, V., Tennigkeit, F. & Singer, W. (2004) Phase sensitivity of synaptic modifications in oscillating cells of rat visual cortex. *Journal of Neuroscience*, **24**, 9067-9075.

Womelsdorf, T., Schoffelen, J.-M., Oostenveld, R., Singer, W., Desimone, R., Engel, A.K. & Fries, P. (2007) Modulation of neuronal interactions through neuronal synchronization. *science*, **316**, 1609-1612.

Xu, R., Jiang, N., Lin, C., Mrachacz-Kersting, N., Dremstrup, K. & Farina, D. (2014) Enhanced low-latency detection of motor intention from EEG for closed-loop brain-computer interface applications. *IEEE Transactions on Biomedical Engineering*, **61**, 288-296.

Yanagisawa, M., Kurihara, H., Kimura, S., Goto, K. & Masaki, T. (1988) A novel peptide vasoconstrictor, endothelin, is produced by vascular endothelium and modulates smooth muscle Ca2+ channels. *Journal of hypertension. Supplement: official journal of the International Society of Hypertension*, **6**, S188-191.

Zhang, P., Yu, H., Zhou, N., Zhang, J., Wu, Y., Zhang, Y., Bai, Y., Jia, J., Zhang, Q., Tian, S., Wu, J., Hu, Y. (2013) Early exercise improves cerebral blood flow through increased

angiogenesis in experimental stroke rat model. *journal of NeuroEngineering and Rehabilitation*, **10**, 43.

Chapter 3 Materials and Methods

This chapter describes how this study was conducted.

The materials and methods used during my PhD work, i.e., the experimental groups, the surgical procedures and the systems used to perform the in vivo experiments, are discussed. Finally, an overview of the data analysis that was implemented to evaluate the changes in neural activity under specific conditions is presented.

3.1. In vivo recording and stimulation procedure

Under the framework of this thesis work, I performed three different experimental in vivo procedures to evaluate and test the ability of different types of intracortical microstimulation to manipulate the electrophysiological response in a distant brain region. The following three experimental groups were considered:

I. Healthy Anesthetized (Acute)
II. Injured Anesthetized (Acute)
III. Healthy Awake (Chronic)

The different steps used to conduct each experimental procedure are briefly reported in Figure 3.1.1.

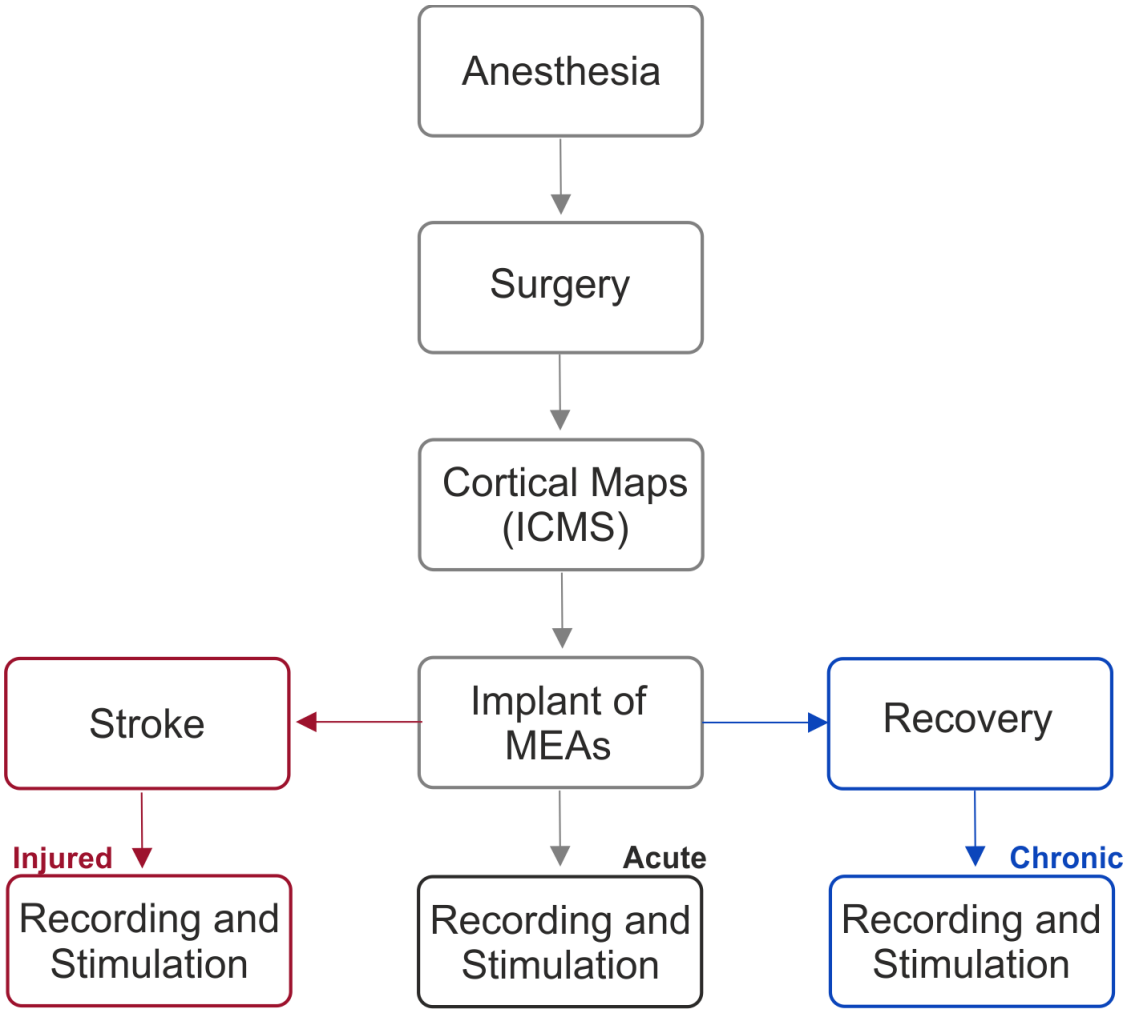

Figure 3.1.1: Scheme of the experimental procedure workflow. Colors identify the experimental groups: Healthy Anaesthetized (Black), Injured Anaesthetized (Red) and Healthy Awake (Blue). Gray denotes the common procedures.

All animals were anesthetized prior to each surgical operation. The cortical maps allow for the identification of the brain regions involved in this study. The animals belonging to the Injured anesthetized group follow the red-line flow, which includes a model of focal brain injury (stroke) and the implantation of MEAs for the recording and stimulation of neurons. The blue flow was applied to the Healthy Awake group, and after the cortical implantation of MEAs, each animal was allowed to rest and recover from surgery for 5 days before starting the recording and stimulation protocol. The Healthy Anesthetized group follows the black flow.

3.1.1. Anesthesia and Surgery

Prior to surgery, the rats were initially induced with gaseous isoflurane within a sealed vaporizer chamber and then anesthetized with injections of ketamine (80-100 mg/kg ip) and xylazine (5-10 mg/kg). Anesthesia was maintained throughout the procedure with repeated bolus injections of ketamine (10-100 mg/kg/hr ip or im) as needed. While this range is broad, we found large differences in the appropriate dose of ketamine in these experiments.

Each rat was secured in a stereotaxic frame, and either lidocaine/prilocaine cream or bupivacaine was applied to the scalp/incision area; in the case of the Healthy Awake animals, a subcutaneous injection of penicillin (G benzathine and G procaine 45,000 IU or 0.1 5 ml, SC) was administered. Then, an anal temperature probe was used to monitor the rat's temperature throughout the experiment. Ophthalmic ointment was applied to the eyes. Using aseptic techniques, the scalp was incised down the midline across the length of the skull. In procedures requiring cortical exposure that may result in edema, the incision may have been extended approximately 1 cm down the neck to facilitate access to the cisterna magna or upper spinal vertebrae. To control brain edema after craniectomy, the muscles of the neck overlying the cisterna magna or between the upper vertebrae were reflected, and a small puncture was made in the spinal dura (foramen magnum or between the atlas and axis vertebrae) to allow for CSF drainage. This drainage is necessary as we found that mannitol is largely ineffective in controlling cortical edema in rats. The temporalis muscle was retracted, and a craniectomy was performed over the primary motor CFA and premotor RFA cortical areas. The dura was removed to facilitate the electrophysiological procedures, and the cortex was covered with sterile silicone oil.

In the Healthy Anesthetized and Injured Anesthetized animals, euthanasia was performed at the end of each experiment by administering a lethal dose of pentobarbital (390 mg ip), and subsequently, cervical spinal cord transection was performed. All surgeries were performed in a facility accredited by the Association for

Assessment and Accreditation of Laboratory Animal Care. The Healthy Awake animals required postoperative care for up to 5 days after surgery before starting the experimental protocol.

All procedures conformed to the Guide for the Care and Use of Laboratory Animals published by the United States Department of Health and Human Services and the National Institutes of Health.

3.1.2. Cortical Maps

The stimulation and recording areas were localized in the S1 and RFA, respectively, and the intracortical microstimulation (ICMS) technique was applied (Kleim *et al.*, 1998). A tapered glass micropipette with a sharply beveled tip of ~10-25 μm diameter was filled with 3.5 M NaCl and introduced into the cortex. An image of the surface vasculature was obtained and displayed on a computer monitor. A fine grid pattern was superimposed over the surface vasculature image, which served as a reference for the site of the micropipette insertion points. The micropipettes were advanced perpendicular to the cortical surface to a depth of ~1750 μm to maximally stimulate the descending pyramidal cells in cortical Layer V. The stimulation pulses included 50 ms trains of 200 μs monophasic cathodal pulses delivered at 350 Hz and were generated and delivered through the micropipettes. Identification of the motor field boundaries was performed by observing the movements evoked by electrical stimulation up to 80 μA. The RFA and CFA were localized with wrist extension, elbow flexion, and occasionally digit movements. The neck and face movement separated the RFA and CFA.

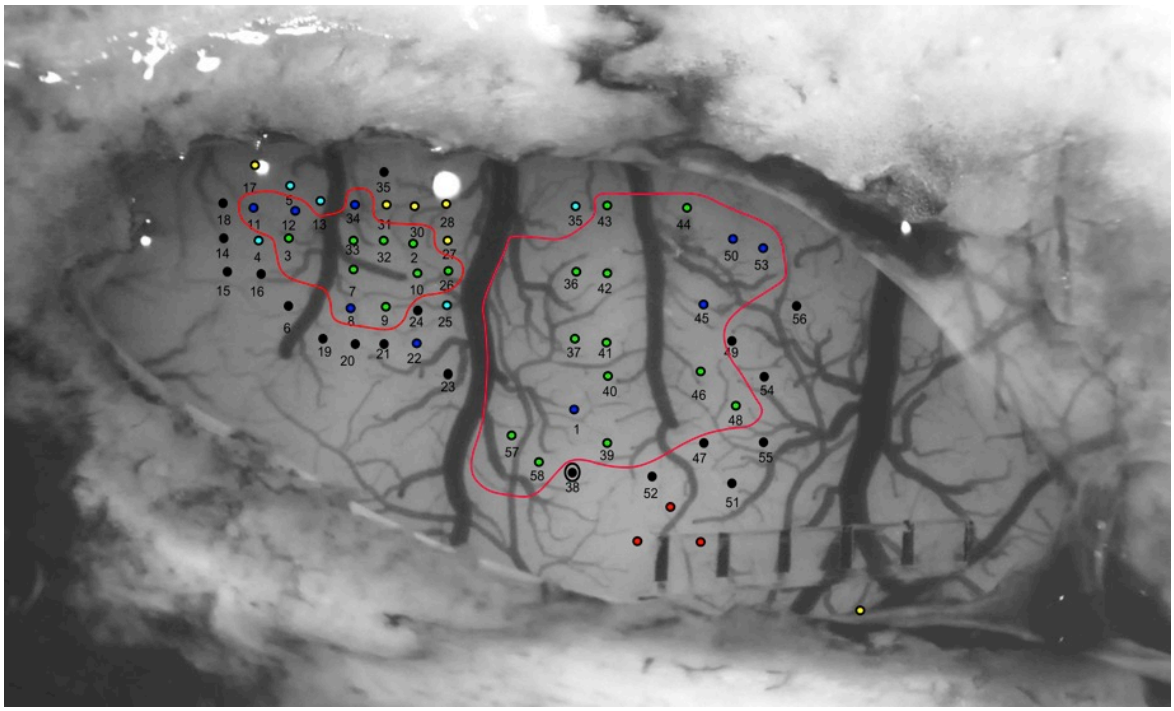

Figure 3.1.2: Color-coded maps of movements evoked by ICMS in the RFA (identified by the left red contour) and CFA (right red contour) brain regions. Circles represent the locations of the microelectrode penetrations, and the colors represent the movement evoked (green: wrist, blue: trunk, light blue: neck, yellow: face, red: whiskers and black: no response) by the near-threshold stimulation (<80 μA). The yellow dot on the bottom right corresponds to the site identified as the forelimb sensory field.

The forelimb sensory fields in S1 were identified with multi-unit recordings. A single-shank Michigan style electrode with sixteen recording sites (NeuroNexus, Ann Arbor, MI) was advanced into the sensory cortex to span across cortical layers II-V. The evoked sensory activity was monitored through a loudspeaker during the procedure. Further characterization of the spikes was performed by amplifying, digitizing, filtering, and displaying the recorded neural activity on a screen (TDT, Alchulta, FL). Two observers correlated the tapping and touching of both the evoked activity output on the speaker and the bursting activity observed on the screen. In the forelimb S1, the evoked activity was required to be localized to a small receptive field; otherwise, the activity was excluded. In the S1 barrel fields (BF), the evoked activity was required to be localized to one or a few adjacent whiskers.

3.1.3. Implantation of MEAs

In both the Healthy Anesthetized and Injured Anesthetized groups, a four-shank, sixteen-contact site electrode with 1-1.5 MΩ impedance at each site (A4x4-5mm-100-125-703-A16, NeuroNexus) was placed within the RFA at a depth of 1600 μm, and a single contact on a single-shank, sixteen-contact electrode with an impedance of ~ 200 kΩ (contact 6, activated A1x16-5mm-100-703-A16, NeuroNexus) was positioned at 1600 μm and used to deliver the stimulation.

In the Healthy Awake animals, six holes were created for the skull screws and anchoring rod using a small drill bit. The skull screws were implanted into the parietal bones, and an anchoring rod was implanted into the intraparietal bone. The screws and rod were further secured with dental acrylic. A four-shank, sixteen-contact site electrode with 1-1.5 MΩ impedance at each site (A4x4-3mm-100-125-177-CM16LP, NeuroNexus) optimized for chronic recordings was chronically implanted into the RFA using a micropositioner at a maximum depth of 1600 μm. Then, the probe and burr hole opening were sealed with a silicone polymer (Kwik-Cast, WPI). The base of the probe connector was lowered onto the dental acrylic and fixed in place. A second four-shank, sixteen-contact electrode (A4x4-3mm-100-125-177-CM16LP, NeuroNexus) optimized for stimulation was chronically implanted into the S1 forepaw field and fixed in the same manner. Any remaining exposed areas were covered with the silicone polymer before suturing the incision.

3.1.4. Model of Brain Injury (Stroke)

The injured anaesthetized procedure follows the healthy protocol reported above, but instead of performing craniectomy over the whole area covering the CFA, RFA and S1, six 0.7-mm diameter holes were drilled into the skull over the dominant hemisphere (contralateral to the preferred forelimb) as follows: anteroposterior 1.5, 0.5, and -0.5 and mediolateral 2.5 and 3.5 from bregma, corresponding to the caudal forelimb area of the motor cortex. Endothelin-1 (ET-1; 0.3 μg ET-1 dissolved in 1 μl

saline or 1 mg ET-1 dissolved in 3.33 ml saline; Bachem Americas, USA), which is a venous and arterial vasoconstrictor, was injected ~ 1.5 mm below the pial surface (Gilmour *et al.*, 2005). The stereotaxic coordinates (Paxinos & Watson, 1998) were used to determine where to administer the ET-1 injections. A borehole was created through the skull, and 0.33 μl ET-1 were injected at a rate of 3 nl/sec via a 160 μm pipette (o.d.) attached to a 1 μl Hamilton syringe. Then, the opening of the skull was closed, and the skin was sutured. Using this procedure, the spread of ET-1 is usually confined to an area of 0.5 mm diameter; therefore, the injections were delivered to produce a continuous infarct without exposing the cortex (Fang *et al.*, 2010). Once the brain lesion was performed, a small craniectomy of 0.3 mm was performed over the RFA and S1 using stereotaxic coordinates, and then, the procedure followed the same steps described above for the healthy group.

3.1.5. Recording and Stimulation Protocols

To obtain a better understanding of the effects of intracortical microstimulation on the electrophysiological activity in distant cortical brain regions, an appropriate analytical investigation should be performed before and after the stimulation. Thus, three different experimental models involving both healthy and injured cortical networks and both anesthetized and awake rodents were properly established.

Healthy Anesthetized Protocol

The aim of this experimental procedure was to investigate the electrophysiological effect of the repeated administration of two different types of ICMS, i.e., ADS in a closed-loop system and RS in an open-loop system in healthy anaesthetized rats. In these experiments, three one-hour stimulation sessions were interleaved with four ten-minute periods of no stimulation for a total of approximately three hours and forty minutes of recorded data (Figure 3.1.3).

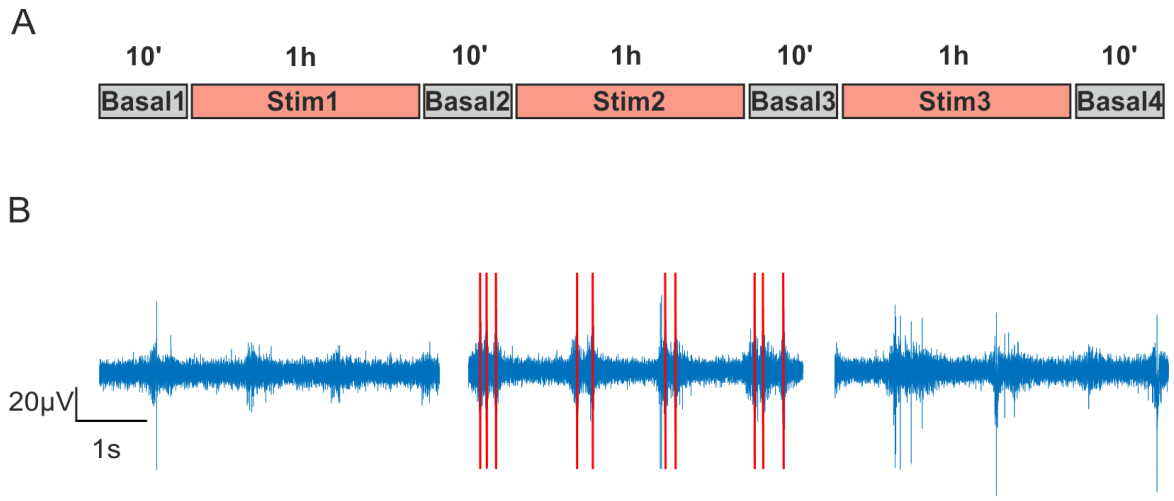

Figure 3.1.3: A) Recording sessions in Healthy Anaesthetized rats consisted of three one-hour intermittent periods of stimulation using either ADS or RS in either S1BF or S1FL; each period was separated by ten-minute periods of no stimulation. B) Example traces of extracellular recordings in a representative experiment during the first basal period (Basal1), the first stimulation session (Stim1) and the second basal period after the stimulation (Basal2). Red lines represent the electrical stimulation artifacts.

In the Control experiments, the same protocol as that used for ADS was followed, but the stimulation was set at 0 μA for the entire recording session.

In this study, I used 25 adult male Long-Evans rats (weight: 350-400 g, age: 4 mo). These animals were assigned to five different groups as reported in Table 3.1.1.

Table 3.1.1: Healthy Anaesthetized dataset.

	Area		**Stimulation Type**		
	BF	**FL**	**RS**	**ADS**	**CTRL**
# Rats	11	10	5 BF, 5 FL	6 BF, 5 FL	4
Total	**11**	**10**	**10**	**11**	**4**

Injured Anesthetized Protocol

This experimental protocol was designed to obtain a better understanding of the effects of localized brain injury on cortical activity and functional connections among involved cortical regions and characterize the role of intracortical microstimulation in

exploiting neuroplasticity processes to guide recovery. However, the effects of the lesion on the dynamics of the involved network, the neural correlates before and after brain injury or the consequent recovery guided by the stimulation are not evident.

In this case, the experimental protocol begun one hour after the ET-1 injections, and during this period, no electrophysiological data were recorded; then, three experimental phases were performed (Figure 3.1.4), including the first 30 minutes of recording with no stimulation (Basal1), one stimulation treatment for one hour using ADS (Stim1) and a second recording of basal activity (Basal2).

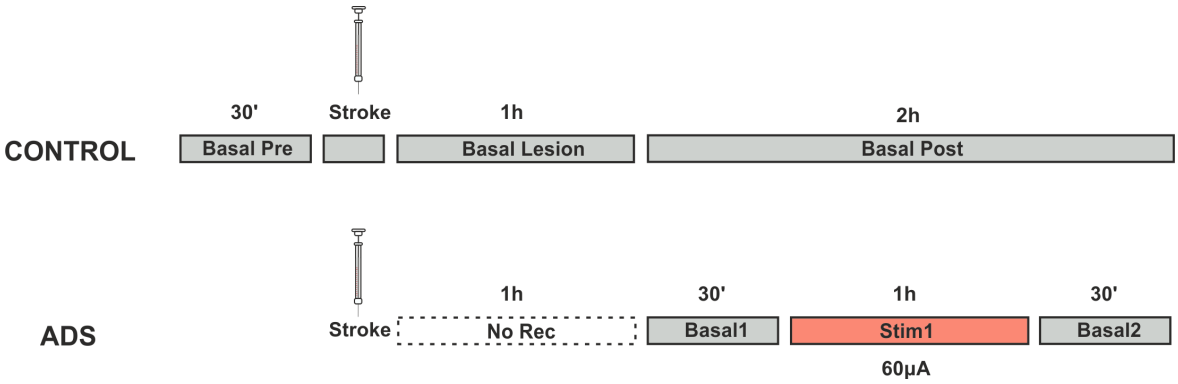

Figure 3.1.4: The experimental timeline of the CONTROL experiments consisted of four phases of spontaneous recordings before, during and after the stimulation, and the timeline of the ADS experiments consisted of two 30-minute basal phases and one 1-hour stimulation session.

In the Control experiments, the same protocol performed in the ADS experiment was conducted, and spontaneous activity was recorded before, during and after the ET-1 injection, but the stimulation was set at 0 μA for the entire recording session (two hours).

The injured anaesthetized dataset consists of twelve experiments divided into two groups as shown in Table 3.1.2.

Table 3.1.2: Injured Anaesthetized dataset.

	Stimulation Type	
	ADS	**CONTROL**
# Rats	7	5
Total	**12**	

Healthy Awake Protocol

To characterize the persistence (long term effect) of the electrophysiological alterations induced by the stimulation and highlight the possible differences with the anesthetized model, an in vivo model must also be exploited in awake animals.

The experimental protocol included two recordings of basal activity (at 30 minutes and 1 h, each for 30 minutes) and one stimulation treatment of 1 hour and 20 minutes for a total of approximately 3 hours and 20 minutes of recordings. Then, the procedure was repeated for 21 consecutive days, and each rat was subjected to only one type of stimulation (either ADS or RS) for the entire duration of the protocol (Figure 3.1.5A).

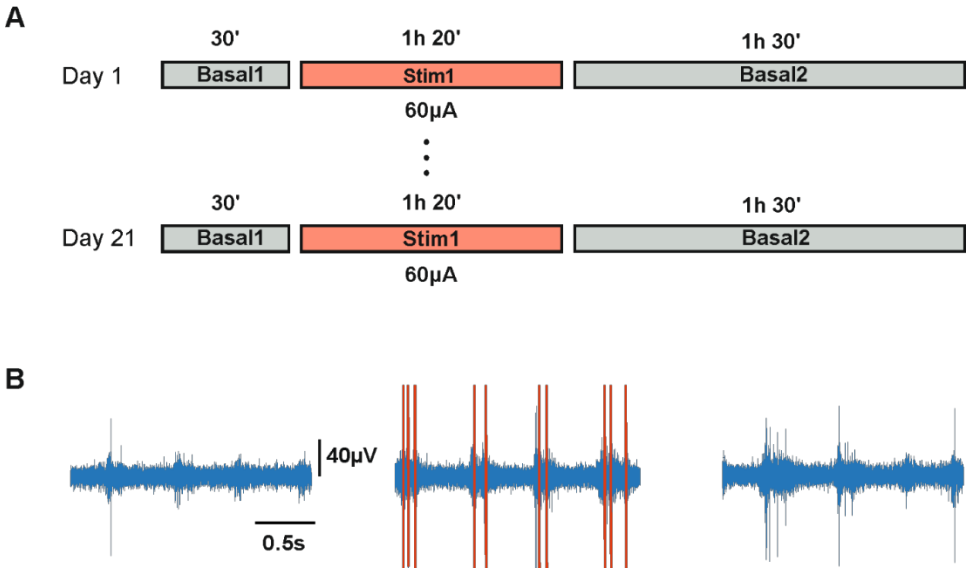

Figure 3.1.5: Experimental protocol. A) Timeline of the protocol. Each rat was treated for 21 consecutive days, and the protocol included two recordings of basal activity (30 minutes and 1 h and 30 minutes) and one stimulation

session of 1 h and 20 minutes. B) A sample trace (2 s) recorded during the three experimental phases (red lines represent the deleted stimulation artifacts).

In the Control experiments, the same protocol as that used for the ADS was followed for all 21 consecutive days, but the stimulation was set at 0 μA during the entire recording session.

In the healthy survival experiments, twelve adult male Long Evans rats weighing 350-400 g at 4 months of age were used.

Table 3.1.3. Grouping of Rats into the Activity-Dependent Stimulation (ADS) or Open-Loop Stimulation (RS) groups.

Table 1.1.3: Healthy Awake dataset.

	Stimulation Type		
	ADS	**RS**	**CONTROL**
# Rats	5	5	2
Total	**12**		

Ethical Statement

The University of Kansas Medical Center Institutional Animal Care and Use Committee (IACUC) approved the animal protocols, which adhered to the Guide for the Care and Use of Laboratory Animals (Council, 2011). During the first month after arrival, the rats were handled daily to acclimate them to human touch and habituate them to the cage environment. Each rat was singly housed in a transparent cage and provided food and water ad libitum. The room was maintained on a 12 h:12 h light:dark cycle, and the ambient temperature was maintained at 22°C.

3.2. Data Recording and Processing

3.2.1. Acquisition system

As previously documented, the MEA technology used for the in vivo applications has had great success in the neuroscience field. Twenty years ago, only prototypes of microelectrode arrays and custom-made acquisition systems were available; however, currently, different commercial systems complete with both hardware and software components exist.

For my PhD study, I used two different commercially available acquisition systems. The Tucker-Davis Technologies (TDT) system has been used for both Healthy Anesthetized and Healthy Awake protocols at the Kansas University Medical Center (KUMED, Dr. Nudo's Cortical Plasticity Laboratory), while the Intan Technologies system has been employed in Injured Anesthetized experiments at the Italian Institute of Technology (IIT, Dr. Chiappalone's Laboratory). The specific components of both systems used are listed below.

Tucker Davis System (TDT)

The whole acquisition system used for the Healthy Awake and Healthy Anaesthetized experiments consists of i) one active headstage and one passive headstage designed for direct connection to acute NeuroNexus probes, ii) a Medusa preamplifier for the recorded signals, iii) a stimulus isolator, iv) a processor base station for the on-line processing and acquisition of the signals and v) software for extracellular neurophysiology (Figure 3.2.1).

A. TDT's high impedance headstages designed for extracellular neurophysiology using NeuroNexus probes were used. Each headstage offers a signal-to-noise with ~ 5 uV rms noise floor and connects directly to a Medusa preamplifier using a standard 25-pin connector.

B. The Medusa Preamplifiers are low-noise digital bioamplifiers. The system amplifies and digitizes up to 16-channels of analog signals at a 24.414 kHz sampling rate. The amplified digital signal is sent to the RZ5 base station via a noiseless fiber optic connector.
C. The MS16 Stimulus Isolator converts the digital waveforms into analog current waveforms as a part of a computer controlled neural microstimulator system that delivers user-defined current waveforms through multichannel electrodes.
D. RZ5 acquires and processes up to 32 channels of neurophysiological signals in real-time. The data can be inputted from Medusa preamplifiers at a sampling rate of ~25 kHz. RZ5 also supports microstimulation applications. RZ5 can be used with one of TDT's stimulus isolators (MS16) to comprise a complete microstimulation system.
E. OpenEx Software Suite is a core group of programs used for configuration, control, display and analysis; these programs are combined under a seamless project interface. Built on a distributed client/server architecture, all OpenEx applications can run in parallel. Software control is implemented with circuit files developed using TDT's RP Visual Design Studio (RPvdsEx). The circuits are loaded to the processor through TDT run-time applications or custom applications. This software package allows the processing of data in Real-Time with TTank Engine, enabling the user to change the system configuration with OpenWorkbench and control the parameters for on-line spike detection and sorting using OpenController.

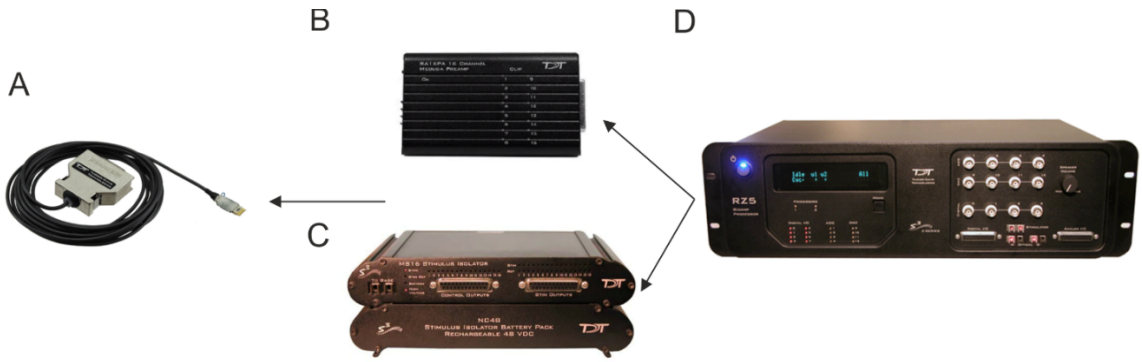

Figure 3.2.1: TDT setup used in the Healthy Anesthetized and Healthy Awake experiments. A) headstage, B) Medusa pre-amplifier, C) MS16 Stimulus isolator and D) the RZ5 base station.

In the Healthy Awake experiments, a motorized commutator directly attached to the headstages was used to prevent the twisting or binding of the cables.

Intan System

In the Injured Anesthetized experiment, I used the Intan Stimulation/Recording System. This system comprises a modular family of components that allows users to record biopotential signals from up to 128 low-noise amplifier channels and generate independent or coordinated constant-current stimulation pulses on any or all channels.

The Intan RHS2000 Stimulation/Recording Controller connects to a host computer via a standard USB cable. Small stimulation/recording headstages are connected to the Controller via digital cables. An open-source multi-platform GUI controls the operation of the headstages, configures the stimulation parameters, and streams data to the screen and disk in real time at user-selected sampling rates of 20, 25, or 30 kS/s. Two stimulation/recording headstages were used in this study, and each headstage included one Intan RHS2116 stimulator/amplifier chip for a total of 16 channels each. The chips have software-reconfigurable bandwidths that can be changed as needed through the GUI. Any set of channels on the headstage can generate constant-current stimulation pulses from 10 nA to 2.55 mA in magnitude, triggered by digital inputs to

the Controller or keypresses on the host computer. The system also supports electrode impedance measurements at arbitrary frequencies.

Figure 3.2.2: INTAN setup used in the Injured Anesthetized experiments. A) RHS2116 16-channel stimulation/recording headstage. B) Intan RHS2000 Stimulation/Recording Controller front panel.

The Intan Stimulation/Recording System is controlled by software written in C++ using multi-platform Qt libraries. The software is open source and may be compiled on Windows, Mac, or Linux systems. A pre-compiled Windows executable is available on the Intan Technologies website along with the latest source code and USB driver files.

3.2.2. Data Analysis

The typical extracellularly acquired signals from a local network of neurons are Local Field Potentials (LFPs) and Single-Unit Activity (SUA). The LFPs, which are believed to be generated by neuronal currents in the local neighborhood of the recording probe, constitute the low-frequency components (< 300 Hz) of the raw signal. Fluctuations in the membrane potential reflect input from a specific cortical area and the activity of excitatory and inhibitory interneurons (Logothetis, 2003). Here, the following 5 frequency bands were typically considered: delta or sharp waves (δ, 1-4 Hz), theta (θ, 4-11 Hz), beta (β, 11-30 Hz), low-gamma (γ_L, 30-55 Hz), and high-gamma (γ_H, 55-130 Hz) (Colgin & Moser, 2010).

SUA, which constitutes the high-frequency portion (>300 Hz) of the raw signal, represents the spiking of local neurons near the recording electrode (Burns *et al.*, 2010; Buzsaki *et al.*, 2012). In most experiments with single unit recording, the output of the cortical area recorded is represented by the activity of large pyramidal cells

(Logothetis, 2003). Their activity can be evaluated after the detection of the spiking waveforms through a spike detection algorithm and the effective isolation and identification of the single units' activity through a spike sorting algorithm (Buzsaki & Draguhn, 2004). In this study, I analyzed the electrophysiological signals by exploiting both temporal scales of the recorded signals (i.e., LFPs and SUA). The different steps performed to obtain the LFP and SUA are briefly described in Figure 3.2.3.

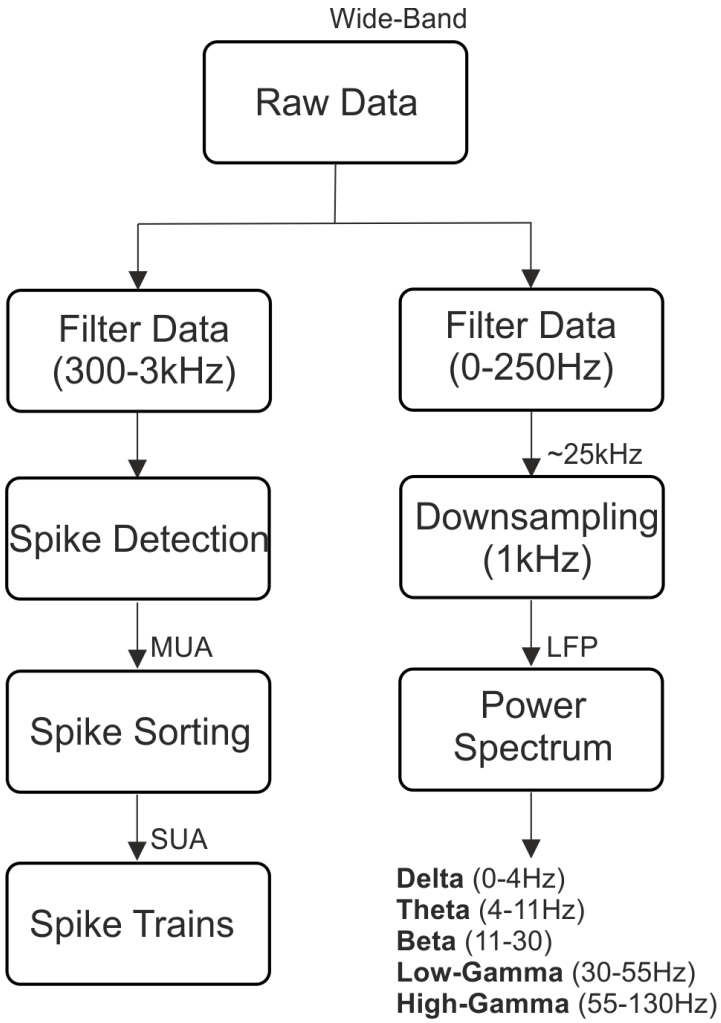

Figure 3.2.3: Scheme of the data pre-processing workflow used to obtain the LFP and SUA.

Analysis of SUA

To collect and analyze the single units' spike trains, the acquired wide-band raw data were bandpass filtered (elliptic filter) based on the frequencies of the spikes (300-3 kHz).

First, information regarding the spike instant was extracted from the filtered data. Extracellularly recorded signals are embedded in biological and thermal noise, and spikes can be detected by means of threshold-based spike detection algorithms (Maeda *et al.*, 1995). A spike train is the sequence of times at which a cell spikes and consists of a punctual process (ST) as follows:

$$ST(t) = \sum_{s=1}^{N} \delta\,(t - t_s)$$

Where t_s is the spike instant, N is the number of detected spikes and $\delta(t)$ is the Dirac-delta function.

In general, a spike train can be detected by applying different types of Spike Detection algorithms to the raw data (Chapin *et al.*, 1999; Wessberg *et al.*, 2000; DeMarse *et al.*, 2001; Marom & Shahaf, 2002).

In this study, we developed and increasingly optimized different methods to maintain the use of state-of-the-art Spike Detection methods under each experimental condition. In the Healthy Anaesthetized group, a custom spike detection algorithm, i.e., Precise Timing Spike Detection (PTSD), which was originally developed for in vitro data, was applied to in vivo data and used to discriminate spike events (Maccione *et al.*, 2009). In the Healthy Awake and Injured Anesthetized groups, a custom MATLAB script was used to identify the peaks in the extracellular electrical fields that corresponded to action potentials from nearby neurons.

Once the spikes were detected, a spike sorting procedure was used to group the detected spikes into clusters based on the similarity of their shapes using superparamagnetic clustering (SPC) with Waveclus (Quiroga *et al.*, 2004) in the

Healthy Anesthetized group and an adapted version of such algorithm in the Healthy Awake and Injured Anesthetized groups.

The resulting output of the final step is a set of single-unit spike trains that can be easily manipulated and analyzed.

To determine whether activity-dependent stimulation (ADS) could induce changes in the intra-cortical spiking activity under the described experimental frameworks, a MATLAB-based graphical user interface was developed to evaluate both the direct effect of the stimulation (Stim periods) and its effect on the periods of quiescence surrounding the stimulation (Basal periods). An existing open-source software package mainly developed for in vitro neural signals and analysis was used (Bologna *et al.*, 2010). Then, I collected and adapted a rich repertoire of standard and advanced signal analysis tools, including some recently published novel analysis tools used for in vivo extracellular neural signals, to evaluate any potential change in the firing activity. This attempt aimed to highlight the most pronounced differences induced by the electrical stimulation by quantifying the first-order statistics of sorted neurons using several different metrics as follows:

- *Firing Rate (MFR):* the average firing rate is expressed as the number of spikes per second. We excluded neurons with an MFR less than 0.01 spikes/s from further analyses.
- *Local Variation with Refractoriness constant (LvR):* the LvR is a measure of the local variation in the inter-spike intervals that is not confounded by firing rate fluctuations (Shinomoto *et al.*, 2009). This measure produces a value that can be used to classify individual activity as *regular* (0.5±0.25), *random* (1±0.25) and *bursty* (1.5±0.25) firing patterns as depicted in figure 3.2.4.

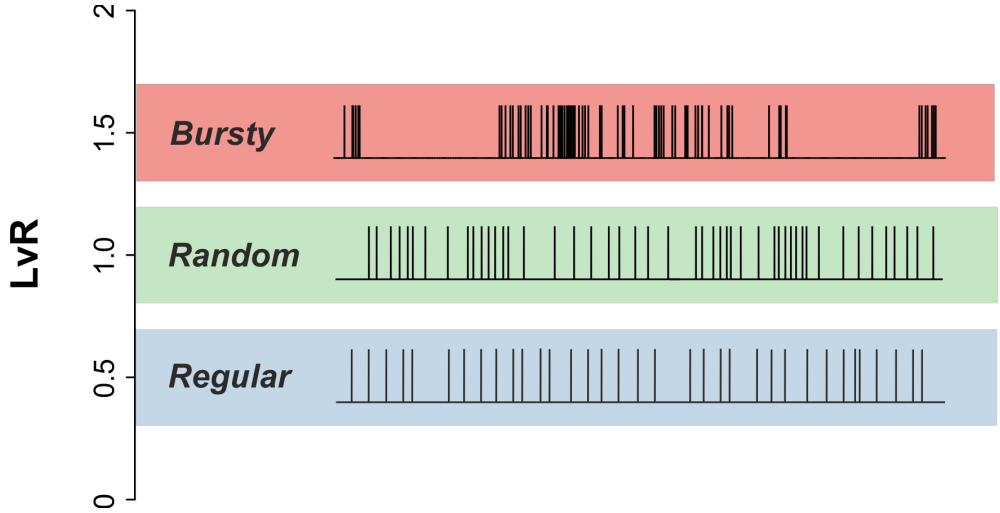

Figure 3.2.4: LvR value description. Regular firing patterns are grouped in a range of 0.5±0.25 (blue), random 1±0.25 (green) and bursty 1.5±0.25 (red).

- *I/O pairwise correlation:* the goal of this analysis is to quantify the correlation between the stimulation paradigms (ADS and RS) and the consequent evoked spiking activity of the detected single units. Each single unit's firing rate and the stimulation train delivered during each experimental session were binned at a 1-ms time resolution. The resulting signal was low-pass filtered to obtain the instantaneous firing rate of single units (IFR) and instantaneous stimulus rate of ICMS (ISR). As shown in Figure 3.2.5, a cross-correlation analysis (I/O correlation, i.e. cross-correlation between ISR and IFR) was performed to evaluate the effect of the local stimulation on the evoked spiking activity of each single unit (Scarsi *et al.*, 2017). A slight variant of Pearson's coefficient was used to evaluate the I/O correlation (MX). Since the response delay to stimulation was unknown, we considered MX the maximum value of the normalized cross-correlation in a 30-s window across its 0-lag point instead of the 0-lag value as per the standard definition. As the ISR of ADS is intrinsically more correlated with neuronal activity than the ISR of RS, a particular compensation factor was envisioned. In the ADS groups, the procedure described above was performed during the first period of basal recording (pre-stimulation, Basal1), and the

stimulation train in this case was chosen as the firing of the single unit selected to trigger the stimulation, which was 10-ms shifted ahead to replicate the stimulation effect during the basal period. Thus, the compensation factor MX^{B1} was subtracted from each MX^{S} calculation during the stimulation. Finally, a population of 100 surrogate MX^{S}_{Surr} calculated by randomly shuffling the time stamps (null-distribution) was produced per single unit during the stimulation phase (Stim). If the maximum correlation (MXc^{S} compensated for ADS or MX^{S} without compensation for RS) fell outside of the 95% confidence interval of the null-distribution (MX of surrogates), the value was considered significant.

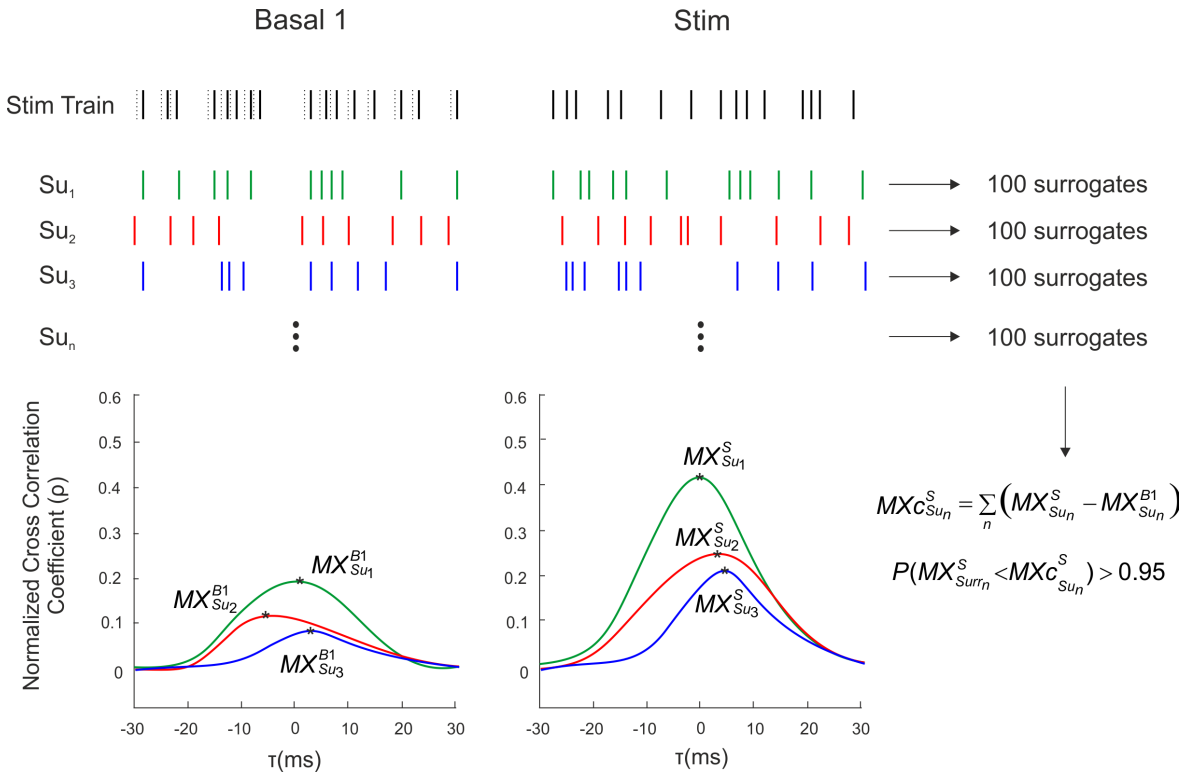

Figure 3.2.5: I/O pairwise correlation algorithm. Cross-correlation analysis was used to determine the effect induced by the stimulation train on the single units' trains. In the ADS group, each MX^{S} calculation during the stimulation period (Stim) was compensated for by the values calculated during Basal1 (MX^{B1}). The maximum value of the correlation (MXc) is considered significant if it is greater than the 95th percentile of the distribution of the maximum values of the surrogates (100 per unit, MX^{S}_{Surr}).

- *Population Coupling (PC):* PC is a measure used to characterize the relationship (correlation) between each neuron and a larger population (population rate)

and was calculated as the summed activity of all neurons in the recorded area at any moment (Renart *et al.*, 2010; Tkačik *et al.*, 2014). This metric estimates the overall synaptic connectivity of each neuron with the cortical network and allows for each unit to be described as a Chorister (i.e., a neuron mostly firing with the population) or a Soloist (i.e., a neuron that is mostly not synchronized with the population, Figure 3.2.6) (Okun *et al.*, 2015). The two categories were defined by selecting the top five scoring neurons as Choristers and the lowest five scoring neuron as Soloists.

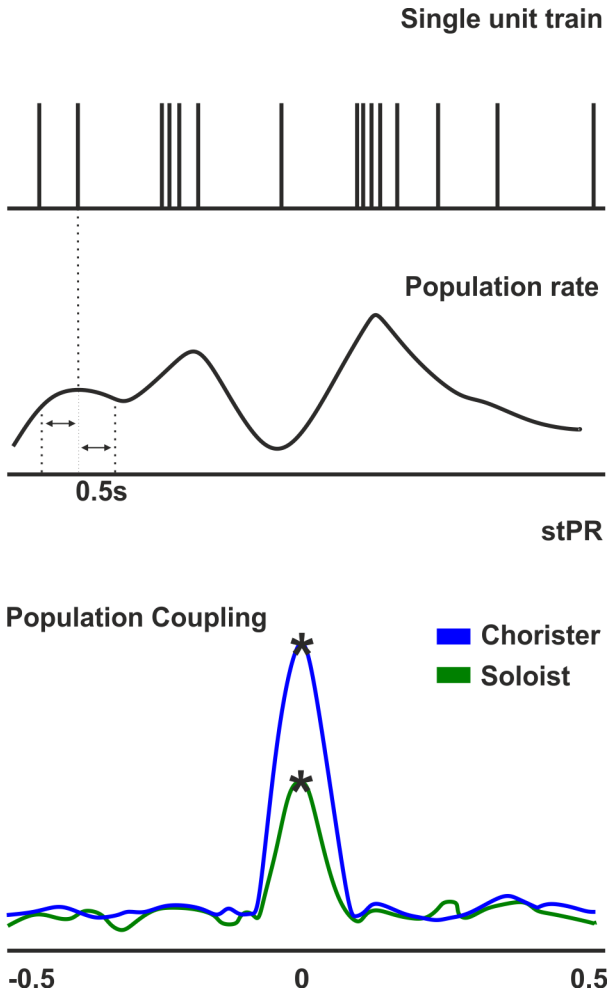

Figure 3.2.6: Population Coupling. The correlation between each single units' firing and the population rate allows the neurons to be divided into the following two categories: Choristers and Soloists.

- *Post-Stimulus Time Histogram (PSTH*): To evaluate the effect of a series of stimuli delivered to a neuronal culture, the so-called PSTH was computed (Kass *et al.*, 2005; Baljon *et al.*, 2009). The spike trains evoked by the repeated delivery of the same stimulus are not identical; thus, the PSTH represents the mean response of one or more cells evoked by a specific stimulation pattern, i.e., the PSTH reports the firing probability as a function of time starting from the stimulation. This measure is equivalent to a cross-correlation between the stimuli trains and the spike trains and is mathematically defined as follows:

$$PSTH(t) = \frac{1}{N}\sum_{i=1}^{N} ST\left(t - t_{stim_i}\right)$$

  Where N is the total number of delivered stimuli, t_{stim_i} is the i^{th} stimulus' instant and ST is the spike train. The temporal axis is usually subdivided into bins of duration Δt; thus, if the histogram is normalized with respect to both the stimuli number and Δt, the PSTH reports the instantaneous firing rate or firing probability per temporal unit if each bin contains at least one spike.

Analysis of LFPs

First, the wide-band signals were down-sampled to 1 kHz after low-pass filtering below 500 Hz to prevent aliasing. Then, I computed the power spectral density of the decimated signal (dB/Hz) using the Welch method [Windows = 5 s, overlap = 50%; DFT (Discrete Fourier Transform) points = 8192; df (frequency resolution) = 0.12 Hz; dt (temporal resolution) = 8.19 s]. In the Healthy Awake experiments, I only considered the lower frequency bands of the signal, particularly the delta (0–4 Hz), theta (4–11 Hz), beta (11–30 Hz), low gamma (30–55 Hz) and high gamma (55-130 Hz) bands. In the Injured Anesthetized experiments, the delta (0–4 Hz), theta (4–8 Hz), alpha (8-13), beta (13–30 Hz), low gamma (30–55 Hz) and high gamma (55-130 Hz) bands were considered.

- *LFP Power*: To characterize the LFP power during each specific experimental phase, the wide-band signals were first down-sampled to 1 kHz after low-pass

filtering below 500 Hz to prevent aliasing. The power noise in the LFP signals was attenuated using a notch filter centered at 60 Hz. Then, the power spectral density of the decimated signal (dB/Hz) was computed using the Welch method [Windows = 5 s, overlap = 50%; DFT (Discrete Fourier Transform) points = 8192; df (frequency resolution) = 0.12 Hz; dt (temporal resolution) = 8.19 s]. The power spectral density (PSD) of each of the described frequency bands was obtained, and their changes were evaluated at different time points.

- *LFP Functional Connectivity*: To measure the functional connectivity between sources *i* and *j*, we applied the method proposed and described by Hipp *et al*. (Hipp *et al.*, 2012). This method provides a calculation of the estimated pairwise correlations between the log-transformed power spectra of sources *i* and *j*. It provides a reliable estimation of the connectivity between long-distance areas. Prior to calculating the Pearson correlation coefficients between the power spectra of the sources, the signals were orthogonalized. Spurious instantaneous correlations were removed, allowing for the emergence of real correlation patterns (for further details see (Hipp *et al.*, 2012; Siems *et al.*, 2016)); then, the power spectra were calculated, log-transformed to work with Gaussian distributions, and correlated in both orthogonalization directions. Thus, adjacency matrix $ADJij\ (f)$ was obtained for each frequency f, bin (1 Hz) in the range (1-130) Hz. The correlation values of the typical LFP frequency bands were obtained by averaging the adjacency matrices of the bands described above.

References

Baljon, P.L., Chiappalone, M. & Martinoia, S. (2009) Interaction of electrically evoked responses in networks of dissociated cortical neurons. *Physical Review E*, **80**, 031906.

Bologna, L.L., Pasquale, V., Garofalo, M., Gandolfo, M., Baljon, P.L., Maccione, A., Martinoia, S. & Chiappalone, M. (2010) Investigating neuronal activity by SPYCODE multi-channel data analyzer. *Neural Networks*, **23**, 685-697.

Burns, S.P., Xing, D. & Shapley, R.M. (2010) Comparisons of the dynamics of local field potential and multiunit activity signals in macaque visual cortex. *J Neurosci*, **30**, 13739-13749.

Buzsaki, G., Anastassiou, C.A. & Koch, C. (2012) The origin of extracellular fields and currents - EEG, ECoG, LFP and spikes. *Nat Rev Neurosci*, **13**, 407-420.

Buzsaki, G. & Draguhn, A. (2004) Neuronal oscillations in cortical networks. *Science*, **304**, 1926-1929.

Chapin, J.K., Moxon, K.A., Markowitz, R.S. & Nicolelis, M.A. (1999) Real-time control of a robot arm using simultaneously recorded neurons in the motor cortex. *Nat Neurosci*, **2**, 664.

Colgin, L.L. & Moser, E.I. (2010) Gamma oscillations in the hippocampus. *Physiology*, **25**, 319-329.

Council, N.R. (2011) Guide for the care and use of laboratory animals, National Academies Press. *Washington, DC*.

DeMarse, T.B., Wagenaar, D.A., Blau, A.W. & Potter, S.M. (2001) The neurally controlled animat: biological brains acting with simulated bodies. *Autonomous robots*, **11**, 305-310.

Fang, P.-c., Barbay, S., Plautz, E.J., Hoover, E., Strittmatter, S.M. & Nudo, R.J. (2010) Combination of NEP 1-40 treatment and motor training enhances behavioral recovery after a focal cortical infarct in rats. *Stroke*, **41**, 544-549.

Gilmour, G., Iversen, S.D., O'Neill, M.F., O'Neill, M.J., Ward, M.A. & Bannerman, D.M. (2005) Amphetamine promotes task-dependent recovery following focal cortical ischaemic lesions in the rat. *Behavioural brain research*, **165**, 98-109.

Hipp, J.F., Hawellek, D.J., Corbetta, M., Siegel, M. & Engel, A.K. (2012) Large-scale cortical correlation structure of spontaneous oscillatory activity. *Nat Neurosci*, **15**, 884.

Kass, R.E., Ventura, V. & Brown, E.N. (2005) Statistical issues in the analysis of neuronal data. *J Neurophysiol*, **94**, 8-25.

Kleim, J.A., Barbay, S. & Nudo, R.J. (1998) Functional reorganization of the rat motor cortex following motor skill learning. *J Neurophysiol*, **80**, 3321-3325.

Logothetis, N.K. (2003) The underpinnings of the BOLD functional magnetic resonance imaging signal. *Journal of Neuroscience*, **23**, 3963-3971.

Maccione, A., Gandolfo, M., Massobrio, P., Novellino, A., Martinoia, S. & Chiappalone, M. (2009) A novel algorithm for precise identification of spikes in extracellularly recorded neuronal signals. *J Neurosci Methods*, **177**, 241-249.

Maeda, E., Robinson, H. & Kawana, A. (1995) The mechanisms of generation and propagation of synchronized bursting in developing networks of cortical neurons. *Journal of Neuroscience*, **15**, 6834-6845.

Marom, S. & Shahaf, G. (2002) Development, learning and memory in large random networks of cortical neurons: lessons beyond anatomy. *Quarterly reviews of biophysics*, **35**, 63-87.

Okun, M., Steinmetz, N.A., Cossell, L., Iacaruso, M.F., Ko, H., Bartho, P., Moore, T., Hofer, S.B., Mrsic-Flogel, T.D., Carandini, M. & Harris, K.D. (2015) Diverse coupling of neurons to populations in sensory cortex. *Nature*, **521**, 511-515.

Paxinos, G. & Watson, C. (1998) The rat brain in stereotaxic coordinates. Vol. Academic Press, San Diego.

Quiroga, R.Q., Nadasdy, Z. & Ben-Shaul, Y. (2004) Unsupervised spike detection and sorting with wavelets and superparamagnetic clustering. *Neural Comput*, **16**, 1661-1687.

Renart, A., De La Rocha, J., Bartho, P., Hollender, L., Parga, N., Reyes, A. & Harris, K.D. (2010) The asynchronous state in cortical circuits. *science*, **327**, 587-590.

Scarsi, F., Tessadori, J., Chiappalone, M. & Pasquale, V. (2017) Investigating the impact of electrical stimulation temporal distribution on cortical network responses. *BMC neuroscience*, **18**, 49.

Shinomoto, S., Kim, H., Shimokawa, T., Matsuno, N., Funahashi, S., Shima, K., Fujita, I., Tamura, H., Doi, T., Kawano, K., Inaba, N., Fukushima, K., Kurkin, S., Kurata, K., Taira, M., Tsutsui, K., Komatsu, H., Ogawa, T., Koida, K., Tanji, J. & Toyama, K. (2009) Relating neuronal firing patterns to functional differentiation of cerebral cortex. *PLoS Comput Biol*, **5**, e1000433.

Siems, M., Pape, A.-A., Hipp, J.F. & Siegel, M. (2016) Measuring the cortical correlation structure of spontaneous oscillatory activity with EEG and MEG. *Neuroimage*, **129**, 345-355.

Tkačik, G., Marre, O., Amodei, D., Schneidman, E., Bialek, W. & Berry II, M.J. (2014) Searching for collective behavior in a large network of sensory neurons. *PLoS Comput Biol*, **10**, e1003408.

Wessberg, J., Stambaugh, C.R., Kralik, J.D., Beck, P.D., Laubach, M., Chapin, J.K., Kim, J., Biggs, S.J., Srinivasan, M.A. & Nicolelis, M.A. (2000) Real-time prediction of hand trajectory by ensembles of cortical neurons in primates. *Nature*, **408**, 361.

Chapter 4 Effect of ICMS on healthy anaesthetized animals

This chapter describes the main results obtained in the first set of experiments performed at Kansas University in 2015. In particular, the characterization of the changes in intra-cortical neuronal activity induced by the ADS treatment using Healthy Anesthetized procedures within a single four-hour experiment involving healthy brains is discussed. These results are a part of a scientific journal publication (Averna *et al.*, 2018; Averna *et al.*, 2019).

4.1. Introduction

Focal, invasive electrical stimulation techniques such as intracortical microstimulation (ICMS) and deep brain stimulation (DBS) have the ability to target and directly activate a relatively small population of neurons compared to non-invasive techniques such as transcranial magnetic stimulation (TMS) or transcranial direct current stimulation (tDCS). While ICMS is typically employed in invasive animal studies, focal properties of invasive electrical stimulation have made DBS advantageous for implementation into clinical tools for treating a variety of neurological conditions such as epileptic seizures (Kerrigan *et al.*, 2004; Lee *et al.*, 2006; Fisher *et al.*, 2010; Morrell, 2011) and Parkinson's disease (Anderson *et al.*, 2005; Deuschl *et al.*, 2006; Bronstein *et al.*, 2011; Weaver *et al.*, 2012; Little *et al.*, 2013). ICMS, specifically, is also being investigated for the direct treatment of conditions such as pain and depression among others, and in brain-computer interfaces to augment or restore lost function after injury, such as for visual (Dobelle & Mladejovsky, 1974; Schmidt *et al.*, 1996; Bradley *et al.*, 2005; Torab *et al.*, 2011; Davis *et al.*, 2012) or somatosensory (Berg *et al.*, 2013; Tabot *et al.*, 2013; Thomson *et al.*, 2013) neuroprosthetic devices. While the local physical and neurophysiological effects of this type of stimulation have been described in detail (Ranck Jr, 1975; Cohen & Newsome, 2004; Tehovnik *et al.*, 2006; Histed *et al.*, 2013; Tehovnik & Slocum, 2013), there is much less information on how focal stimulation impacts areas distant from the immediate spread of the electrical current or across multi-synaptic pathways. This is

an important consideration, as these stimulated regions are not isolated (Fox *et al.*, 2014) but have anatomical connections with several other regions within the brain. The effectiveness of treatments that rely on focal electrical stimulation are likely dependent on the modulation of these pathways but there are still open questions about how this stimulation affects the firing patterns within these distant regions.

The impact of focal electrical stimulation on distant brain regions may be even more pertinent in "closed-loop" designs, in which intrinsic neural activity drives stimulation protocols. One such design, named activity-dependent stimulation (ADS), uses the occurrence of action potentials (spikes) in one neuron to trigger stimulation at another location or electrode site. ADS relies on the concept of Hebbian plasticity, in which repeated concomitant firing of two neurons will strengthen the connection between them. In closed-loop systems, secondary neuronal firing is induced via the stimulation. By artificially pairing spike-firing in one populations of neurons with focal electrical stimulation of a second population of neurons, it may be possible to shape the efficacy of specific neural pathways *in vivo* (Jackson *et al.*, 2006; Rebesco *et al.*, 2010; Rebesco & Miller, 2011; Guggenmos *et al.*, 2013; Nishimura *et al.*, 2013a).

The purpose of the present study was to determine if neural firing patterns in distant regions are altered in response to short-duration stimulation sessions in anesthetized rats. To model a relevant system *in vivo*, the rostral forelimb area (RFA), a premotor area, was used for neural recordings while either closed-loop ADS or random stimulation (RS) was delivered to somatosensory cortex (S1), either in the S1 forelimb area (S1FL) or the S1 barrel field (S1BF). These areas share reciprocal neuroanatomical connections, providing an anatomical framework for changing synaptic efficacy (Mohammed & Jain, 2016). In a previous study, we found that an ADS protocol in a chronic injury model, i.e., pairing the occurrence of spikes in RFA with ICMS applied to S1, led to increased firing within RFA over a period of several days (Guggenmos *et al.*, 2013). In the present study, we investigated ADS effects under the more controlled conditions of an anesthetized preparation, enabling us to assess

alterations in RFA spike firing patterns over single stimulation sessions. This preparation allowed us to more readily test various parameters such stimulation condition (ADS or RS) and stimulation location (S1FL or S1BF). Because these regions are functionally and anatomically connected, the results may be generalizable to other, similarly interconnected regions. Understanding changes in neuronal activity in distant areas in response to focal closed-loop and random ICMS may lead to more effective brain stimulation protocols that target functional connectivity within specific brain pathways, and thus, to improve current therapeutic devices for neurological disorders.

4.2. Methods

4.2.1. Animals

All experiments were approved by the University of Kansas Medical Center Institutional Animal Care and Use Committee. A total of 23 adult, male Long-Evans rats (weight: 350-400 g, age: 4-5 months; Charles River Laboratories, Wilmington, MA, USA) were used in this study. These animals were assigned to five different groups as reported in Table 4.2.1.

Table 2.2.1 Total number of animals and number of units examined per experimental condition.

Location of the stim electrode	Stimulation Type			Total
	RS	ADS	CTRL	
S1 BF	4 / 113	6 / 180	-	10 / 293
S1 FL	4 / 103	5 / 114	4 / 81	13 / 298
Total	8 / 216	11 / 294	4 / 81	23 / 591

4.2.2. Surgical Procedures

Prior to surgery, anesthesia was induced with gaseous isoflurane within a sealed vaporizer chamber followed by bolus injections of ketamine (80-100 mg/kg IP) and xylazine (5-10 mg/kg). Anesthesia was maintained throughout the procedure with repeated bolus injections of ketamine (10-100 mg/kg/hr IP or IM) as needed. A midline incision was made to expose the skull. A laminectomy was performed at the cisterna magna to drain cerebrospinal fluid, thus controlling brain edema. A craniectomy was made over the extent of the location of pre-motor cortex (PM or RFA), primary motor

cortex (M1 or CFA) and primary somatosensory cortex (S1) using a drill with a burr bit. Saline was applied periodically to avoid heat generation by the drill. The dura was resected over the extent of the opening. Silicone oil (dimethylpolysiloxane) was applied to the cortical surface to avoid desiccation and facilitate electrophysiological procedures. Following the experiment, rats were humanely euthanized using pentobarbital (390 mg IP).

4.2.3. Mapping Cortical Areas

Upon completion of the surgical procedure, a picture of the vascular pattern of the cortical surface was taken and uploaded to a graphics program (Canvas GFX, Inc., Plantation, FL, USA) where a 250 μm virtual grid was overlaid onto the image. The location of RFA was determined using standard ICMS protocols (Kleim, 2003). Briefly, a glass microelectrode (10-25 μm diameter) filled with saline was inserted into the cortex at a depth of ~1700 μm (impedance at 1,000 Hz = ~ 500kΩ). Stimulus trains of 13-200μs pulses at 333 Hz were applied at 1 Hz intervals using a stimulus isolator (BAK Electronics, Umatilla FL, USA). Current was increased until a visible movement about a joint was observed, up to a maximum current of 80μA. Sites were sampled at a resolution of 250μm between locations. RFA was defined as the region in the frontal cortex where ICMS evoked forelimb movements. RFA was bordered caudally by a region where ICMS evoked neck and trunk movements, and medially by face and jaw movements (Kleim *et al.*, 1998). RFA was easily distinguished from the caudal forelimb area (CFA) based on its relatively smaller size.

Somatosensory areas were identified by correlating neural responses evoked by slight indentation of the skin or vibrissae brushing. A single-shank, sixteen-channel Michigan style electrode (A1x16-5mm-100-703-A16, NeuroNexus, Ann Arbor, MI, USA) was lowered to a maximum depth of ~1700 μm and attached to a unity gain headstage connected to a digitizing pre-amplifier and piped to a processing unit (Tucker-Davis Technologies, Alachua, FL, USA). Activity of all 16 channels was

displayed in real time on a computer screen for visual discrimination of spikes, and a user selected channel was sent to a speaker for auditory discrimination of spikes. S1FL was defined as the region where a consistent, short-latency spike discharge was evoked in response to light stimulation of a small receptive field on the wrist, paw or digits. S1BF was defined by a constant short-latency spike discharge evoked by deflection a single or small number of the mystacial vibrissae. For each sensory area, multiple cortical sites were characterized to ensure reliability of the target location.

4.2.4. Experimental Protocol

Following identification of RFA and S1 FL/BF, a four-shank, sixteen-contact site microelectrode probe (A4x4-5mm-100-125-703-A16, NeuroNexus, Ann Arbor, MI, USA) was placed within RFA at a depth of ~1600 μm for recording purposes (Figure 4.2.1A). An active unity gain connector was attached to the probe and connected through a preamplifier for recording (Tucker-Davis Technologies - TDT, Alachua, FL, USA). Passband filtered data (300-5000Hz) underwent online spike detection using a principal component sorting algorithm through which neural data could be sorted from non-cellular data online. An activated single-shank, sixteen-contact microelectrode probe with an impedance of 100-300kΩ (A1x16-5mm-100-703-A16, NeuroNexus, Ann Arbor, MI, USA), was inserted into the somatosensory area to a depth of ~1500 μm for stimulation purposes (Figure 4.2.1A). For all experimental conditions, a single 60 μA balanced biphasic, cathodal-leading stimulation pulse (200 μs positive, 200 μs negative) was delivered into S1 through a single contact site on the electrode (site 6, corresponding to the tip of the electrode) on each stimulation trigger. The decision to limit stimulation amplitude to 60 μA (12nC/phase and charge density of 1.7 mC/cm^2) was motivated by the finding that stimulation <= 60 μA has been shown to have a negligible effect on the electrode-tissue interface (Chen *et al.*, 2014) and on the neuronal tissue itself (Rajan *et al.*, 2015). Stimulation pulses were delivered using a stimulus isolator and a passive headstage (MS16 Stimulus Isolator, Tucker-Davis Technologies - TDT, Alachua, FL, USA).

Rats were randomly assigned to one of four experimental groups based on stimulation condition (activity-dependent stimulation, ADS or random stimulation, RS) and stimulation location (S1 forelimb area, FL or S1 barrel field, BF). Thus, each rat was subjected to only one set of experimental parameters. An additional control group (CTRL) received no stimulation (see Table 4.2.1 for group assignments). For all groups, the experimental protocol consisted of four 10-minute periods where the stimulator was set to deliver 0 μA (i.e. Basal0, Basal1, Basal2 and Basal3), interspersed with three one-hour periods where stimulation was delivered at 60 μA (Stim1, Stim 2, Stim3), for a total of approximately three hours and forty minutes of recorded data for a single experimental session (Figure 4.2.1B). Based on group assignment, rats received either random stimulation (RS) pulses (Poisson distribution, mean stimulation interval of 7Hz) or activity-dependent stimulation (ADS, mean stimulation interval of 7Hz), which was triggered on a single spike profile of a channel in RFA with a moderate rate of firing (4-10Hz). For ADS there was a 10ms delay between spike detection and stimulation. There was also an 18ms "blanking" period immediately following the stimulation pulse where stimulation could not be triggered to eliminate any direct stimulation feedback loop.

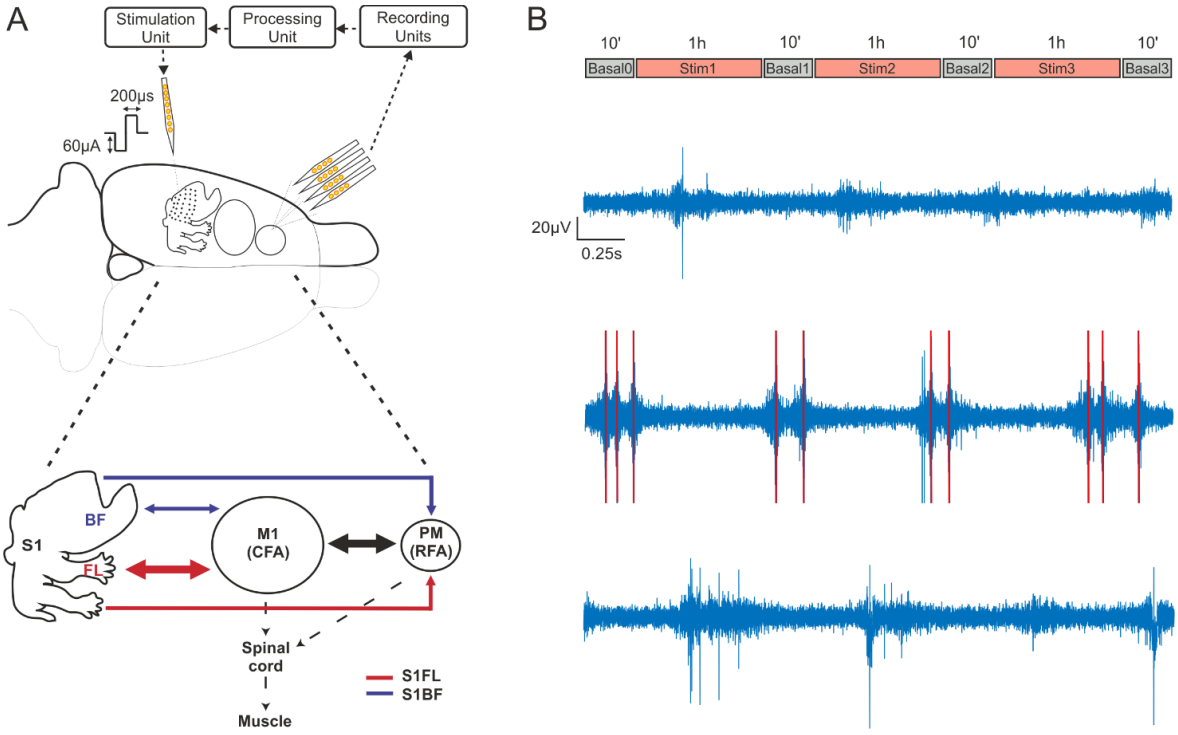

Figure 4.2.1: Recording and stimulation experimental paradigm. (A) Extracellular recordings were performed through a four-shank, 16-contact microelectrode array. Signals were acquired (Recording Unit) and processed to detect the single-unit activity (Processing Unit) selected by the user and employed as a reference neuron to trigger a stimulus pulse to the channel of the single-shank microelectrode (Stimulation Unit). A summary diagram showing all cortico-cortical connections considered in our experiments is shown at the bottom. Arrow thickness corresponds to the amount of labeling (medium or high) suggested by Zakiewicz (Zakiewicz et al., 2014). (B) Recording sessions of the RFA consisted of three one-hour intermittent periods of stimulation using either ADS or RS to either S1BF or S1FL, each separated by ten-minute periods of no stimulation. Example traces from a representative experiment of extracellular recording during the first basal period (Basal1) (C), the first stimulation session (Stim1, D) and the second basal period after the stimulation (Basal2, D). Red lines represent the electrical stimulation artifacts.

In four rats (1 ADSBF, 2 ADSFL, 1 RSBF) from the total of 23, recording sessions were truncated after the first two hour-long stimulation periods (after Basal2), due to either a substantial decrease in neural activity, presumably due to the anesthetic protocol, or due to technical issues related to environmental noise, but unrelated to the stimulation protocol. However, data from these rats up to the time that the protocol was terminated were considered to be valid and have been included in the analyses. Control experiments underwent the same protocol as ADS, but the stimulator was set at 0 µA for the entire recording session.

4.2.5. Data Processing

Bandpass-filtered neural data (~ 300 Hz to 3 kHz) were recorded (Tucker-Davis Technologies - TDT, Alchulta, FL, USA) at ~25 kHz per channel and processed using custom MATLAB (The Mathworks, Natick, MA, USA) scripts. A custom offline spike detection algorithm, Precise Timing Spike Detection (Maccione *et al.*), was used to discriminate spikes (Maccione *et al.*, 2009) followed by superparamagnetic clustering (Blatt *et al.*, 1996; Quiroga *et al.*, 2004) to sort the detected spikes. A supervised discrimination method was used to singularly validate the spike profiles.

Mean Firing Rate (MFR)

The neuronal firing rates were evaluated before and after the stimulation by calculating the mean firing rate in each period. Neurons whose firing rate was less than 0.01 spikes/s were discarded. Determination of whether the difference in firing rates between two time-points for a given unit significantly deviated from a null (zero centered) distribution was calculated using a bootstrapping method (Slomowitz *et al.*, 2015). The two time segments to be compared ($Basal_i$, $Basal_{i+1}$; i=1:3) were divided into 1 min bins, and then randomly shuffled 10,000 times into two groups. The differences between the means of the two randomly shuffled groups produced a null-distribution. The real difference was significant if it fell outside of the 95% confidence interval of the null-distribution.

Local Variation compensate for Refractoriness

The temporal patterns of spike activity exhibited in RFA was evaluated using a revised version of Lv parameter, namely LvR (Local Variation compensate for Refractoriness), as proposed in (Shinomoto *et al.*, 2009). LvR measures the local variation of the ISI and describes the intrinsic firing irregularity of individual neurons, not being confounded by firing rate fluctuations (Shinomoto *et al.*, 2009). This metric produces a value, ranging from 0 to more than 2 and can be used to classify the

individual neuron's activity into *Regular* (approx. 0.5±0.25), *Random* (approx. 1±0.25) and *Bursty* (approx. 1.5±0.25) firing patterns (Shinomoto *et al.*, 2009)..

Post-Stimulus Time Histogram

Post-Stimulus Time Histograms – PSTH (Rieke *et al.*; Rieke, 1999) (1 ms bins, normalized over the total number of stimulation pulses) of stimulus-associated action potentials of each sorted unit were calculated during the 28ms following stimulus pulses delivered from either S1FL or S1BF. The area under the normalized PSTH curve was used to quantify the total amount of stimulation-evoked neural activity during each stimulation phase.

Statistical Model

Statistical analysis was performed by applying a general linear mixed effects model for repeated measures analysis and SAS/STAT® software (Version 9.2 of the SAS System for Windows, SAS Institute Inc., Cary, NC, USA). This model was utilized as it allows more flexibility than traditional multivariate regression analysis. It permits modeling of not only the means of the data (as in the standard linear model) but also their variances as well as within-subject covariances (i.e., the model allows subjects with missing outcomes -unbalanced data- to be included in the analysis).

In this model, the subjects were the recorded neurons from each rat $\left(neuron\ (rat)\right)$. The model included two fixed between-subject factors: the stimulation condition (with three levels for factor $StimCond$: RS, ADS and CRTL) and the stimulation location or $Area$ (with two levels for factor $Area$: S1FL and S1BF). The outcome was a variable measured at four fixed time points (within-subject factor $Time$). The model also included the interactions of second and third order among the factors ($StimCond * Area$, $StimCond * Time$, $Area * Time$ and $StimCond * Area * Time$).

The rat was considered a random factor and implied a different intercept for each rat. The variance-covariance matrix for errors was considered unstructured, as it was

different for each subject. The MIXED procedure of SAS, by default, fits the structure of the covariance matrix by using the method of restricted maximum likelihood (REML) (Harville, 1977), also known as residual maximum likelihood. Finally, the fixed part of the expected values of the basal period recorded at the time t, with the stimulus s applied to the area a, was: $\mu + \tau_t + \alpha_a + \sigma_s + \delta_{t,a} + \gamma_{t,s} + \varepsilon_{a,s} + \gamma_{t,a,s}$, where the parameters τ_t, with $t \in \{1, 2, 3, 4\}$, referred to factor $Time$, the parameters α_a, with $a \in \{FL, BF\}$, referred to factor $Area$, the parameters σ_s, with $s \in \{ADS, RS, CTRL\}$, referred to factor $StimCond$ and the parameter $\delta_{t,a}$, $\gamma_{t,s}$, $\varepsilon_{a,s}$ and $\gamma_{t,a,s}$ referred to second and third order interactions of. The reference level of the factor *StimCond* was set to be CTRL first, then to be RS, in order to easily compare the three levels. P values < 0.05 were considered significant.

4.3. Results

We investigated the capability of two ICMS stimulation conditions to affect spike rate and temporal patterns of firing in a distant but interconnected cortical region. In healthy, ketamine-anesthetized rats, multi-site microelectrode probes were used to determine the effects of ICMS delivered to somatosensory cortical areas (FL and BF) on spontaneous spike firing rates, regularity of firing patterns, and stimulus-evoked spike firing in RFA.

4.3.1. ICMS results in increased firing rate in a distant cortical area

First, mean firing rate (MFR) was compared between the initial basal period (Basal0) and subsequent basal periods (Basal1, Basal2, and Basal3) following each one-hour period of RS or ADS ICMS. Figure 4.3.1A illustrates spike firing rates in a representative animal (ICMS in BF, ADS condition) demonstrating an overall increase of firing from Basal0 (top, left) to Basal3 (top, right). The increase in MFR occurred in each of the experimental conditions (ADSBF, ADSFL, RSBF, RSFL) but not in control experiments (CTRL) (Figure 4.3.1B).

Table 4.3.1 contains the global results of hypothesis tests for the considered fixed effects. Main effects and third-order interactions of the effects are described in Table 4.3.2.

Due to firing rate variability typically observed among different animals, as well as temporal fluctuations in firing rates in anaesthetized preparations, it was important to examine multiple post-stimulation basal periods in each animal. This approach provided not only greater statistical power, but allowed us to examine cumulative changes in firing rate in successive basal periods. In control (CTRL) experiments, no significant differences were found in MFR between any of the basal periods (Figure 4.3.1B and Table 4.3.2). In contrast, MFR was significantly increased in 5 of 6 RS, and 6

of 6 ADS basal period comparisons. The only exception was the Basal3 vs. Basal0 comparison for RS in BF.

It is important to note that both ADS and RS generally induced a significant increase in firing rate in subsequent basal periods with respect to control experiments, regardless of any observed differences. As reported in Table 4.3.2 (see Table 4.3.2, *StimCond*Area*Time*, *ADS/RS vs CTRL*), in the ADSBF group, MFR was significantly lower than in the CTRL group during Basal 0, but showed significantly higher MFR compared with CTRL in Basal3. For the ADSFL group, there were no significant differences with the CTRL group in Basal 0 but a significantly higher MFR in each of the subsequent basal phases. For the RSBF group, MFR was higher than the CTRL group for each the basal periods, while RSFL demonstrated a comparable MFR with respect to CTRL in Basal 0, but showed significant greater values for each of the subsequent phases. When considering the Effect *Area*, the stimulation of BF was more effective in increasing firing rate than the FL (see Table 4.3.2, *Area*, *BF vs FL*).

A table containing all the combinations of the third-order interaction *StimCond*Area*Time* is reported in the Supplementary Material section (see Table A1).

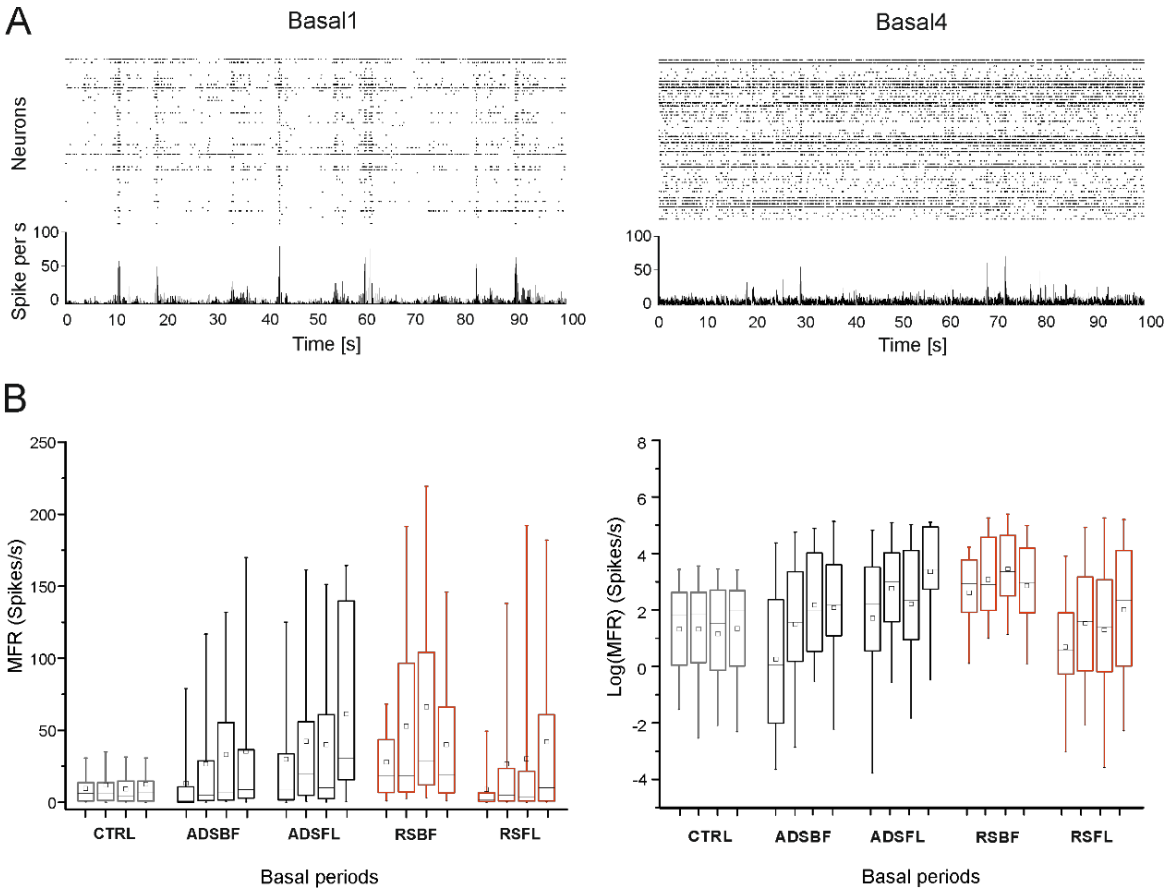

Figure 4.3.1: Firing rate analysis. (A) Spike rasters (dotted graphs, one row per neuron) and corresponding array-wide firing rates (line graphs) measured by summing all spikes detected on the entire array in a 1-ms window during the 100-ms time frame of Basal1 (left) and Basal4 (right) in a single animal that was subjected to the ADS protocol in the BF. (B) Left: Quantitative representation of the Mean Firing Rate (MFR) distributions in each experimental group (CTRL, light gray; ADSBF, black; ADSFL, black; RSBF, red; RSFL, red) during each Basal phase (1 to 4). Right: Representations of the Log(MFR) distributions in each experimental group during all Basal phases. The data are summarized in box plots, where the horizontal lines denote the 25th, the median and the 75th percentile values and the whiskers denote the 5th and the 95th percentile values; the square inside the box indicates the mean of each dataset. The statistical analysis is reported in Tables 4.3.1 and 4.3.2.

Table 4.3.1: Results of the MIXED procedure test on the logarithmic firing rate log(MFR): hypothesis tests for the significance of each of the fixed effects considered. Type 3 Tests of Fixed Effects

Effect	Num DF	Den DF	F Value	Pr>F
Area	1	560	0.21	0.6460
StimCond	2	560	10.19	**<.0001**
StimCond*Area	1	560	33.86	**<.0001**
Time	3	560	34.91	**<.0001**
StimCond*Time	6	560	23.68	**<.0001**
Area*Time	3	560	9.51	**<.0001**
StimCond*Area*Time	3	560	9.74	**<.0001**

Table 4.3.2: Results of the MIXED procedure analysis of the logarithmic firing rate log(MFR): differences in the Least Squares Means (the marginal means are estimated across a balanced population). Significant p-values are highlighted in bold. Notably, in the control experiments (CTRL), we implanted a stimulating electrode in FL, but no stimulation was delivered.

Effect	Stim	Area	Time	Estimate	StdError	p-value
StimCond	RS vs ADS			0.56	0.18	**0.0019**
Area		BF vs FL		1.80	0.33	**<.0001**
StimCond*Area*Time	CTRL	FL	1 vs 0	-0.12	0.20	0.542
			2 vs 0	-0.18	0.21	0.394
			3 vs 0	-0.10	0.22	0.638
	ADS	BF	1 vs 0	1.23	0.11	**<.0001**
			2 vs 0	1.39	0.13	**<.0001**
			3 vs 0	1.97	0.14	**<.0001**
		FL	1 vs 0	1.05	0.16	**<.0001**
			2 vs 0	0.51	0.16	**0.002**
			3 vs 0	1.05	0.19	**<.0001**
	RS	BF	1 vs 0	0.47	0.18	**0.0097**
			2 vs 0	0.84	0.19	**<.0001**
			3 vs 0	0.25	0.20	0.2169
		FL	1 vs 0	1.61	0.15	**<.0001**
			2 vs 0	1.49	0.16	**<.0001**
			3 vs 0	1.20	0.17	**<.0001**
	ADS vs CTRL	BF	0	-1.11	0.33	**0.0007**
		FL		034	0.36	0.3464
		BF	1	0.24	0.28	0.3868
		FL		1.51	0.30	**<.0001**
		BF	2	0.45	0.29	0.1177
		FL		1.02	0.31	**0.0010**
		BF	3	0.96	0.30	**0.0013**
		FL		1.49	0.33	**<.0001**
	RS vs CTRL	BF	0	1.24	0.38	**0.0011**
		FL		-0.57	0.35	0.1095
		BF	1	1.82	0.32	**<.0001**
		FL		1.17	0.30	**0.0001**
		BF	2	2.26	0.33	**<.0001**
		FL		1.10	0.31	**0.0004**
		BF	3	1.59	0.34	**<.0001**
		FL		0.74	0.32	**0.0214**
	RS vs ADS	BF	0	2.35	0.30	**<.0001**
		FL		-0.90	0.31	**0.0036**

We also calculated the proportion of units (i.e., neurons) whose firing rates significantly increased, decreased or remained constant after the stimulation protocol (i.e., Basal1, Basal2, Basal3) with respect to the initial basal period of recordings (i.e., Basal0, Figure 4.3.2A, 4.3.2B). Both stimulation conditions induced a significantly greater proportion of units that showed increased firing rates across basal periods (Figure 4.3.2C) compared to the control group. No differences were observed in the proportion of units showing a decrease in MFR in the stimulation (Figure 4.3.2D) vs the control experiments.

Overall these results demonstrate that, notwithstanding possible initial differences in MFR among groups, both RS and ADS stimulation conditions significantly increased the MFR of neurons recorded from RFA in the post-ICMS basal periods with respect to the initial basal period. ADS consistently showed an increase in MFR over time, in contrast to RS which showed an increase in MFR, but not for all of the experimental conditions and in sharp contrast to CTRL which never exhibited an increase in MFR. Increased MFR was accompanied by an increase in the proportion of units with increased firing rates in both RS and ADS stimulation conditions.

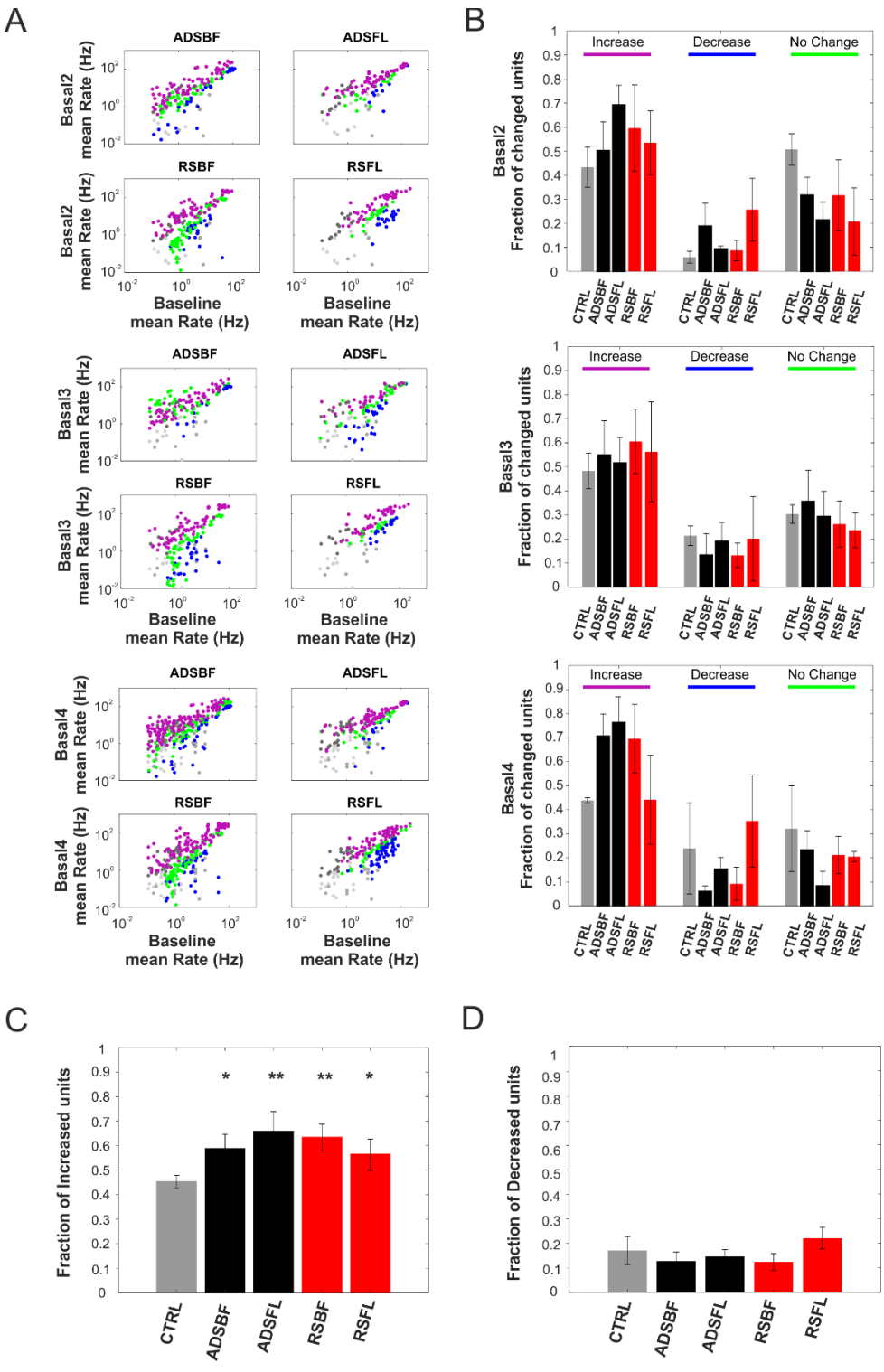

Figure 4.3.2: A) Per unit correlation between the baseline firing rates (x-axis, Basal1) and the firing rates after each stimulation session (y-axis, Basal2, Basal3, and Basal4) calculated per group (ADSBF, ADSFL, RSBF, and RSFL). Colors represent units that significantly increased (magenta), decreased (blue) or remained stable (green). Gray

dots represent the correlation of the control group (CTRL). (B) Average fraction of units that significantly changed their firing with respect to the baseline period of recording (Basal1) calculated in all five experimental groups (i.e., CTRL-light gray; ADSBF and ADSBF black; RSBF and RSFL red). (C) Average fraction of neurons that increased their firing rate across the five experimental groups. (D) Total fraction of neurons that changed their firing rate (Increase + Decrease) (*p < 0.05, relative to the CTRL; one-way ANOVA with Dunnett's multiple comparison test. Error bars represent the SEM). The data are reported as the mean ± SEM (standard error of the mean).

4.3.2. ICMS modulates neuronal firing patterns in a distant cortical area

We used the LvR coefficient (Figure 4.3.3A, cf. Materials and Methods), a metric of local variation of the inter-spike interval (ISI), to 'classify' the type of spike-firing pattern (e.g., '*Bursty*', '*Random'* and *'Regular'*) of the recorded neurons in RFA during spontaneous activity. The purpose of this analysis was to understand whether the different ICMS stimulation conditions in the two areas affected spike-firing patterns. LvR distribution of neurons exhibited stable baseline firing patterns, with LvR values between *'Random'* and *'Bursty'* states (see Figure 4.3.3B, ADSBF in Basal0, dotted line: LvR = 1.27±0.24, mean±SD).

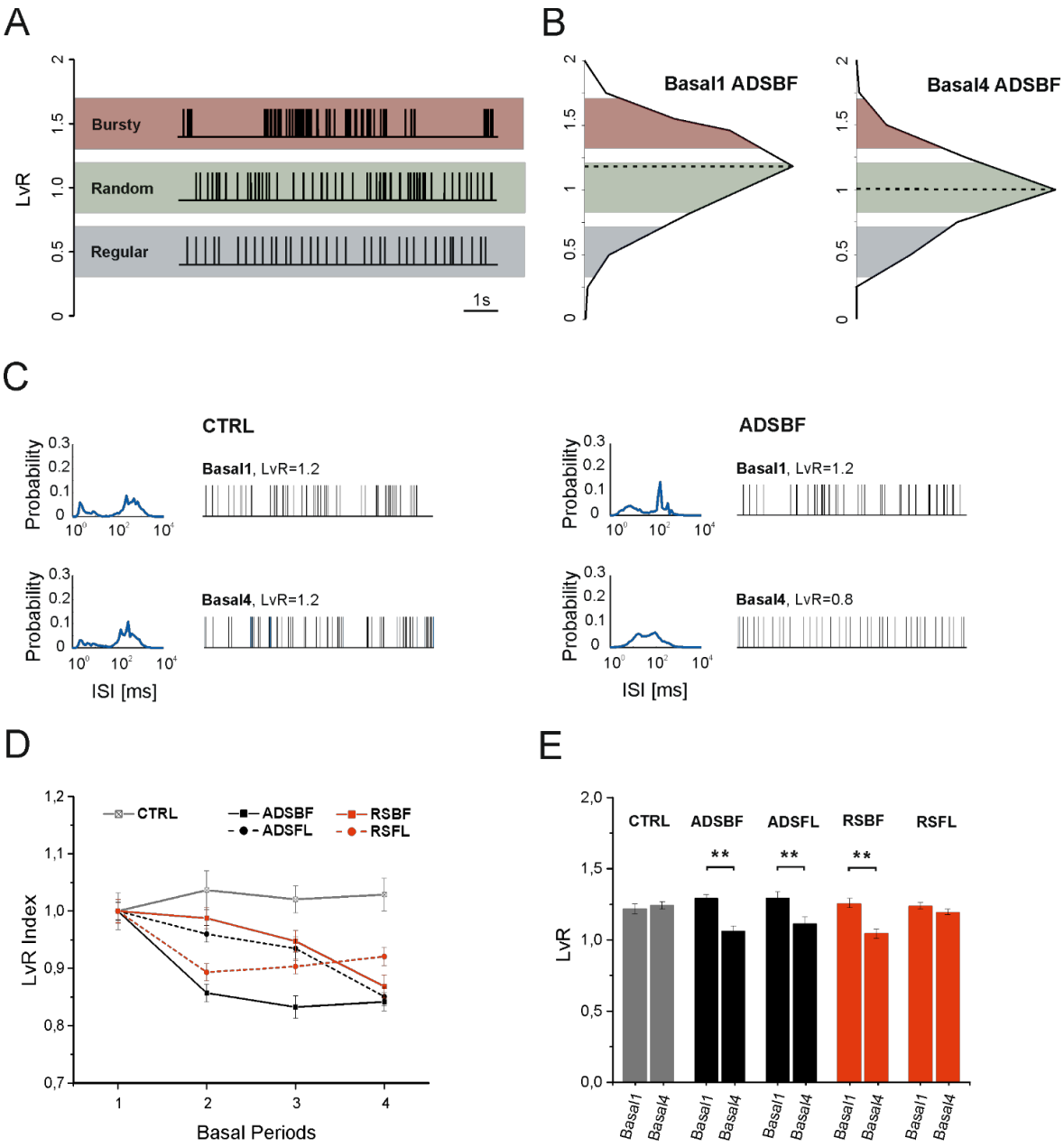

Figure 4.3.3: (A) Example spike sequences of representative neurons with LvR of 0.5 (Regular, red), 1 (Random, green) and 1.5 (Bursty, blue) in the dataset ADSBF. (B) LvR distributions shown as histograms with a common bin size of 0.25 determined across all subjects belonging to ADSBF during the first (Basal1, left) and last (Basal4, right) period of quiescence. Black dotted lines represent the median of the LvR distributions. (C) Distributions of representative neurons' interspike interval (ISI) and sample firing pattern consisting of 100 consecutive ISIs belonging to the CTRL group (Left) and ADSBF group (right) during Basal1 (top) and Basal4 (bottom). (D) Mean ± SEM trend of normalized LvR under each experimental condition. Each subject's LvR value was normalized to the mean LvR value calculated during Basal1; the statistical analysis is reported in Tables 4 and 5. (E) Mean ± SEM LvR comparison between Basal1 and Basal4 under all experimental conditions (CTRL, gray; ADSBF and ADSFL, black; RSBF and RSFL, red). **$p < 0.01$; unpaired two-tailed Student's t-test.

Table 4.3.3 contains results of hypothesis tests for each of the considered fixed effects. It shows that the effect *StimCond* and the combinations *StimCond*Area* and *StimCond*Area*Time* were not significant. The global effect *Area* reached significance (p=0.0497), while *Time* and the other interactions were clearly significant.

No statistical difference was found for LvR values comparing the two stimulation conditions (see Table 4.3.4, Effect *StimCond*, ADS vs RS). The contrast between FL and BF indicates that there were no significant differences between the two stimulated somatosensory areas (Table 4.3.4, Effect *Area*, BF vs FL). Table 4.3.4 also reports how both ADS and RS altered the firing patterns across time. As expected, LvR was not affected in the CTRL experiments (Figure 4.3.3C-E and Table 4.3.4, *StimCond*Area*Time* CTRL). The main result is that ICMS, either RS or ADS, generally induced a strong *decrease* in LvR, moving activity from the '*Bursty*' condition during Basal 0 towards the *'Random'* state of firing in the last basal period (Figure 4.3.3B, ADSBF in Basal3, dotted line: LvR = 1.07±0.02, mean±SD and Figure 4.3.3D-E, Table 4.3.4). This effect was observed in 5 of 6 basal period comparisons using RS and 6 of 6 basal period comparisons using ADS. The one exception was that no change in LvR was observed between Basal3 and Basal0 in the RSFL group (Table 4.3.4).

As was observed for MFR, there were differences between groups in LvR even during the initial basal period (Basal0). However, the significant changes that occurred in LvR in the post-ICMS basal periods invariably were decreases. For example, ADSBF LvR was significantly higher than CTRL during Basal 0, but this difference disappeared in Basal1. ADSBF showed a significantly lower LvR than the CTRL in Basal2 and Basal3, indicating an overall decrease of LvR for ADSBF group with respect to CTRL. LvR in the ADSFL group was significantly higher than the CTRL in Basal0, but the difference disappeared in all subsequent basal phases. The RSBF group was higher than the CTRL in Basal0, but the difference disappeared in Basal1 and Basal2. Finally, RSBF was significantly lower than CTRL during Basal3. RSFL was found to be not statistically different from CTRL in any of the basal periods. A table containing all of the

combinations of the effect *StimCond*Area*Time* is reported in the Supplementary Material section (see Table A2).

Table 4.3.3: Results of the MIXED procedure on LvR: hypothesis tests for the significance of each of the fixed effects considered. Type 3 Tests of Fixed Effects.

Effect	Num DF	Den DF	F Value	Pr>F
Area	1	497	3.87	**0.0497**
StimCond	2	497	0.39	0.6798
StimCond*Area	1	497	0.63	0.4295
Time	3	497	20.51	**<.0001**
StimCond*Time	6	497	3.91	**0.0008**
Area*Time	3	497	7.19	**<.0001**
StimCond*Area*Time	3	497	2.05	0.1057

Table 4.3.4: Results of the MIXED procedure used to analyze the LvR: differences in the Least Squares Means (the marginal means are estimated across a balanced population). Significant p-values are highlighted in bold.

Effect	StimCond	Area	Time	Estimate	StdError	p-value
StimCond	ADS vs RS			0.02	0.02	0.3819
Area		BF		0.01	0.04	0.7259
StimCond*Area*Time	CTRL	FL	1 vs 0	0.02	0.03	0.550
			2 vs 0	0.03	0.03	0.377
			3 vs 0	0.07	0.03	0.054
	ADS	BF	1 vs 0	-0.14	0.02	**<.0001**
			2 vs 0	-0.18	0.03	**<.0001**
			3 vs 0	-0.20	0.24	**<.0001**
		FL	1 vs 0	-0.08	0.03	**0.003**
			2 vs 0	-0.12	0.03	**0.0001**
			3 vs 0	-0.11	0.03	**0.0003**
	RS	BF	1 vs 0	-0.14	0.28	**<.0001**
			2 vs 0	-0.15	0.03	**<.0001**
			3 vs 0	-0.19	0.03	**<.0001**
		FL	1 vs 0	-0.14	0.03	**<.0001**
			2 vs 0	-0.12	0.03	**0.0001**
			3 vs 0	-0.06	0.03	0.051
	ADS vs CTRL	BF	0	0.12	0.04	**0.0045**
		FL		0.12	0.04	**0.0063**
		BF	1	-0.04	0.35	0.2511
		FL		0.02	0.04	0.5923
		BF	2	-0.09	0.04	**0.0113**
		FL		-0.03	0.04	0.4936
		BF	3	-0.15	0.33	**<.0001**
		FL		-0.06	0.04	0.1100
	RS vs CTRL	BF	0	0.10	0.04	**0.0183**
		FL		0.09	0.05	0.0504
		BF	1	-0.06	0.04	0.1343
		FL		-0.07	0.04	0.0989
		BF	2	-0.07	0.04	0.0588
		FL		-0.07	0.04	0.0912
		BF	3	-0.15	0.04	**<.0001**
		FL		-0.04	0.04	0.3115
	RS vs ADS	BF	0	-0.01	0.04	0.7400
		FL		-0.17	0.04	**<.0001**

4.3.3. ADS and RS exhibit different effects on stimulus-associated action potentials in a distant cortical area

Evoked action potentials (in RFA) in response to ICMS were analyzed by discriminating the spiking activity in the 28ms after each S1FL or S1BF stimulus pulse (Figure 4.3.4C) using post-stimulus time histograms (PSTH, cf. Materials and Methods). Due to differences in the dynamics of the evoked electrical artifacts in different animals, we used an adaptive-length blanking window (from 4 to 6ms, Figure 4.3.4A). As shown in Figure 4.3.4B, the interstimulus intervals (ISIs) used for the RS groups comprised a range of values comparable to those of the ADS groups. Interestingly, the ISI distributions for ADS was stable over repeated stimulation trials (see Figure 4.3.4B, left). There was, however, a bias toward ~200ms interstimulus intervals in the ADS group, whereas the RS intervals exponentially decreased across the range (Figure 4.3.4B).

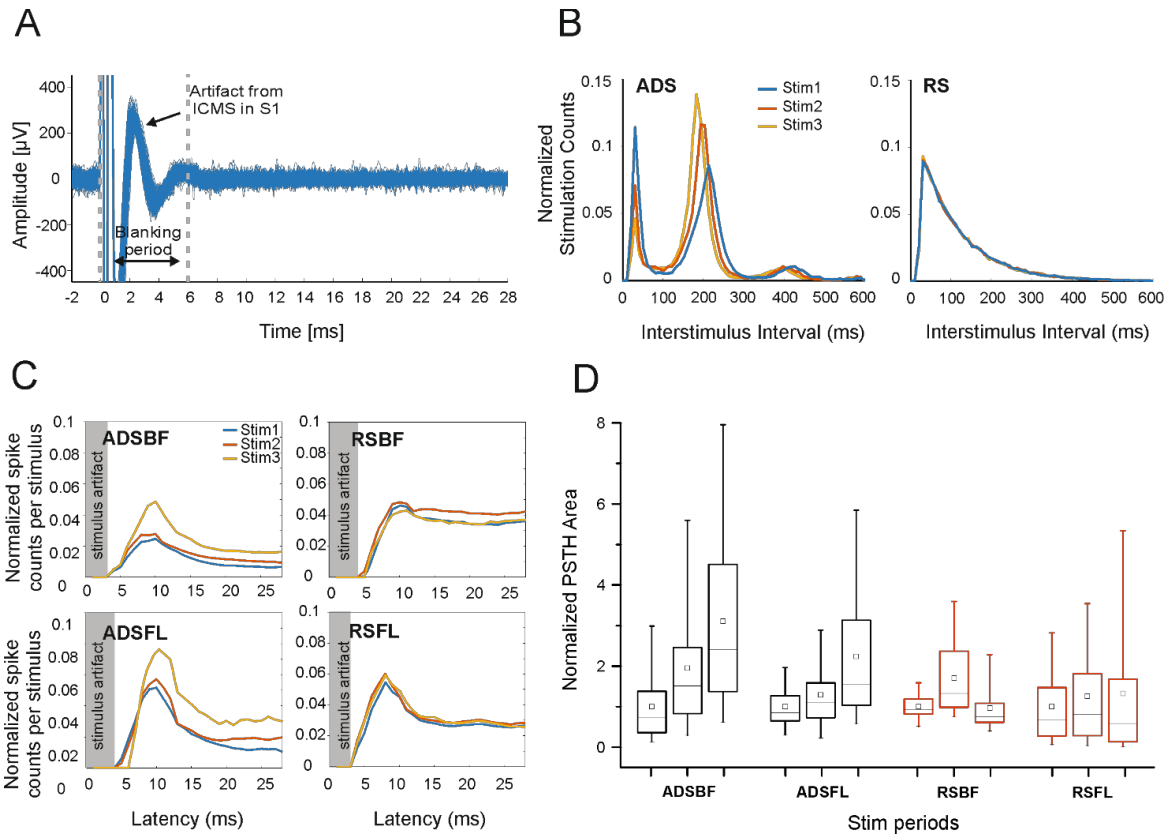

Figure 4.3.4: (A) Sample trace of recordings from the RFA showing stimulus artifacts from ICMS delivered to S1BF. Blanking period used for the analysis is delimited by the gray dotted lines. In total, 100 superimposed traces are shown. (B) Stimulation interval distribution (Interstimulus intervals, 600-ms) in representative ADS and RS subjects during the three stimulation sessions (Stim1, Stim2 and Stim3). Stimulation counts were normalized to the session length. (C) Post-stimulus spiking histograms derived from neural recordings in the RFA during three stimulation sessions in the four ICMS groups (ADSBF, ADSFL, RSBF, and RSFL). Histograms portray the average number of action potentials discriminated from the neural recordings within 1-ms bins. The data were pooled across subjects per group and normalized to the total number of either ADS or RS specific events. (D) Normalized PSTH areas in the four groups (ADSBF and ADSFL, black; RSBF and RSFL, red) of ICMS during the three stimulation phases (Stim1, Stim2, and Stim3). Each subject's PSTH area was normalized to the mean area calculated in Basal1 to show the data trends over time. The statistical analysis is reported in Tables 4.3.5 and 4.3.6.

Table 4.3.5 contains results of hypothesis tests for each of the considered fixed effects. It indicates that the effects *Area, Time* and their interactions induced significant changes in the evoked activity. However, the fixed effect *StimCond* was not significant (see Table 4.3.5, Effect *StimCond*).

Our analysis indicated that ICMS in BF was significantly more effective in evoking short-latency spikes (<28 ms) than in FL (Table 4.3.6, Effect *Area*, BF vs FL). Examining differences between the two stimulation conditions, it appeared that ADS

had a more consistent, cumulative effect in eliciting evoked spikes over time (see Table 4.3.6, Effect *StimCond*Area*Time*, ADS, both BF and FL). This is evident in Figure 4.3.4C and D, showing a progressive increase in short-latency spike counts and PSTH area, respectively in ADS. Changes in evoked spike activity with RS were smaller and inconsistent. Statistically significant differences between RS and ADS were found in 3 of 3 of the FL stim period comparisons and 2 of 3 BF stim period comparisons (Table 4.3.6).

Regarding the stimulus location, we observed that ADSFL consistently evoked more post-stimulus spikes than RSFL. A table containing all the combinations of the effect *StimCond*Area*Time* is reported in the Supplementary Material section (see Table A3).

Table 4.3.5: Results of the MIXED procedure on PSTH: hypothesis tests for the significance of each of the fixed effects considered. Type 3 Tests of Fixed Effects.

Effect	Num DF	Den DF	F Value	Pr>F
Area	1	299	16.71	**<.0001**
StimCond	1	299	0.10	0.7469
StimCond*Area	1	299	45.42	**<.0001**
Time	2	299	30.73	**<.0001**
StimCond*Time	2	299	17.58	**0.0008**
Area*Time	2	299	16.55	**<.0001**
StimCond*Area*Time	2	299	3.32	**0.0375**

Table 4.3.6: Results of the MIXED procedure on PSTH: differences of Least Squares Means (the marginal means are estimated over a balanced population). Significant p-values are highlighted in bold.

Effect	StimCond	Area	Time	Estimate	StdError	p-value
StimCond	RS vs ADS			0.01	0.05	0.7469
Area		BF vs		0.19	0.05	**<.0001**
StimCond*Area*Time	ADS	BF	2 vs 1	0.19	0.03	**<.0001**
			3 vs 1	0.38	0.05	**<.0001**
			3 vs 2	0.18	0.03	**<.0001**
		FL	2 vs 1	0.06	0.03	**0.0263**
			3 vs 1	0.26	0.06	**0.0001**
			3 vs 2	0.21	0.04	**<0.0001**
	RS	BF	2 vs 1	0.16	0.04	**<.0001**
			3 vs 1	0.03	0.06	0.6663
			3 vs 2	0.14	0.04	**0.0009**
		FL	2 vs 1	0.03	0.03	0.3777
			3 vs 1	0.11	0.05	**0.0358**
			3 vs 2	0.08	0.04	**0.0231**
	RS vs ADS	BF	1	0.45	0.07	**<.0001**
		FL		-0.23	0.07	**0.0005**
		BF	2	0.42	0.06	**<.0001**
		FL		-0.26	0.06	**<.0001**
		BF	3	0.10	0.09	0.2527
		FL		-0.39	0.09	**<.0001**

4.4. Discussion

For several decades, electrical microstimulation has been an important tool for investigating neural circuits, demonstrating evidence of cortical map plasticity, and for therapeutic neuromodulation (Buonomano & Merzenich, 1998; Benali *et al.*, 2008; De Hemptinne *et al.*, 2015). Despite its widespread use, our understanding of its effects beyond local depolarization of neuronal membranes remains limited. While the behavioral outcomes of microstimulation in sensory and motor regions of the brain have been characterized extensively (Cheney *et al.*, 2013; Overstreet *et al.*, 2013), few studies have examined the long-term effects of repetitive microstimulation on neuronal activity in the broader network of interconnected brain regions (Nudo *et al.*, 1990). Those that have examined distant effects of microstimulation have focused primarily on the alteration in neuronal activity in primary motor cortex (M1) induced by the stimulation of the subthalamic nucleus (STN) as a model to understand the effects of DBS therapy in Parkinson's disease (Kuriakose *et al.*, 2009; Li *et al.*, 2012; De Hemptinne *et al.*, 2013; De Hemptinne *et al.*, 2015; McCairn & Turner, 2015). As adaptive, or closed-loop, microstimulation modalities are increasingly being explored as potential options for therapeutic applications (Guggenmos *et al.*, 2013; Meidahl *et al.*, 2017), it is important to understand how various stimulation patterns differentially alter both spontaneous and stimulus-evoked neuronal activity in interconnected regions of the brain. The specific aim of the present work was to characterize the neurophysiological effects of random and activity-dependent ICMS on healthy cortical networks. Indeed, our study indicates ICMS is able to alter, within hours, the firing characteristics within a distant, but connected, cortical area (RFA).

To determine the impact of focal electrical microstimulation on distant cortical regions in healthy anesthetized rats within single recording sessions, we applied either randomized ICMS (i.e., open-loop) or activity-triggered ICMS (i.e., closed-loop) to one of two somatosensory cortical areas (forelimb or barrel field) while recording resultant neuronal activity in the RFA, a premotor cortical area. These regions were

chosen due to their known intracortical connections and our ability to alter synaptic efficacy in the target pathways in a previous study (Guggenmos *et al.*, 2013). We found that ICMS in somatosensory areas induced an increase in spontaneous firing rates in RFA when compared to non-stimulated controls (Figure 4.3.1 and Figure 4.3.2, Table 4.3.2). Further, we observed a reduction in the LvR values, indicating a shift towards more random interspike intervals of recorded units within RFA (Figure 4.3.3E, Table 4.3.4). Finally, we found an increase in the stimulus-evoked activity in RFA (Figure 4.3.4, Table 4.3.5, 4.3.6). While both forms of stimulation induced increases in spontaneous firing rates and decreases in LvR, effects were marginally more consistent with ADS. A more pronounced difference between the two stimulation conditions was found in the ability to evoke short-latency spikes (<=28 ms) in RFA. Increases in evoked spikes as a result of ADS were progressive over multiple stimulation periods, and significantly different from results of RS.

Both RS and ADS modulated spontaneous firing rates and patterns within RFA in a similar manner. Both resulted in decreased LvR which was initially associated with a mixed '*Random*'-'*Bursty*' intrinsic firing pattern, indicating a shift towards a '*Random*' state of firing at the end of the treatment (see Figure 4.3.3E). Regarding the role of the stimulus location, we found that stimulation from BF was more effective than FL in increasing the spontaneous firing rate in RFA (see Table 4.3.2, effect *Area*, BF vs FL). Examining the evoked response, stimulation from BF was also more effective in directly evoking action potentials in RFA (see Figure 4.3.4C, D and Table 4.3.6, effect *Area*, BF vs FL).

Given the reciprocal cortico-cortical connections between RFA and the two somatosensory areas, these results were unexpected (Zakiewicz *et al.*, 2014).Other cortical (and subcortical) structures undoubtedly play a role in these distant effects of repetitive microstimulation (cf. Figure 4.2.1). The primary motor cortex (caudal forelimb area or CFA in rats), has dense reciprocal connections with RFA as well as the somatosensory areas. However, if CFA activity was modulated in the present paradigm,

one would expect that the influence would be greater with S1FL stimulation compared to S1BF stimulation, due to the important role in sensorimotor integration mediated by CFA-S1FL connections. This hypothesis will need to be verified by simultaneously measuring spike activity from CFA.

Both ICMS protocols were able to induce changes in firing rate with respect to non-stimulated animals (CTRL) where no changes were observed. Interestingly, even if there was an initial difference between ADS and RS groups during the baseline period of recording, ADS was invariably able to increase firing rates over time, compared with RS. No differences were found in the LvR analysis (Table 4.3.4, Effect *StimCond*, RS vs ADS) but ADS more reliably displayed lowered LvR over time (c.f. Table 4.3.4, Effect *StimCond*Area*Time*, Time 4 vs 1 for all the groups).

More interestingly, ADS, and not RS, facilitated progressive increases of stimulus-associated activity over time (see Effect *StimCond*Area*Time* for ADS and RS in Table 4.3.6) suggesting that the pairing of neural activity and stimulation may lead to stronger associations over prolonged stimulation sessions. This may result from a number of factors. One potential mechanism that allows ADS to be more effective than RS is that ADS is thought to utilize a Hebbian-based spike-timing method similar to the nervous system's natural mechanism to promote learning and memory which is typically effective in inducing long term plasticity (Jackson *et al.*, 2006; Guggenmos *et al.*, 2013).

While these studies provide important evidence for the effects of electrical microstimulation on the broader neuronal network, it is important to consider the limitations imposed by the ketamine-anesthetized preparation. An anesthetized preparation has numerous advantages for the present investigation, since the state of the animal and the associated neurophysiological set-up is relatively stable over several hours. While it is technically feasible to conduct these studies in awake, ambulatory animals, substantial variability in spike activity is introduced by the sensorimotor activities of the animals. However, ketamine is widely known as a

noncompetitive N-methyl d-aspartate receptor antagonist, and can modulate other receptors or channels such as the GABAa receptor. As a result, ketamine has diverse and temporally complex effects on neuronal activity (Homayoun & Moghaddam, 2007; Brown *et al.*, 2010; Brown *et al.*, 2011). For example, under ketamine anesthesia, different cell types in the hippocampus show differential effects in firing rate and synchrony (Kuang *et al.*, 2010). Ketamine causes enhanced gamma oscillations acutely, but decreased network gamma oscillations with chronic (Ahnaou *et al.*, 2017) administration. Thus, while ketamine anesthesia undoubtedly had some effect on neuronal firing in the present study, the changes in MFR, LvR and evoked spikes are thought to be largely independent of the anesthetic state. This hypothesis will need to be verified in awake, ambulatory animals.

In summary, RS and ADS protocols both induce changes in the recorded activity in RFA. It is clear that focal electrical stimulation has the ability to alter activity in remote brain regions not directly influenced by the current spread from the electrode. The closed-loop condition (ADS) can effectively be considered as more reliable in its ability to alter evoked responses and thus in modulating cortico-cortical connectivity in the rat brain within a single recording period. Closed-loop stimulation for therapeutic applications in the human brain is still uncommon. However, many similar approaches are already being tested for epilepsy, in Parkinson disease and in animal models of spinal cord injury (Skarpaas & Morrell, 2009; Santos *et al.*, 2011; Jackson & Zimmermann, 2012; Nishimura *et al.*, 2013b). Other potential clinical applications based on closed-loop ICMS treatments include stroke, focal TBI, and surgical resections. Although the beneficial effect of these approaches in humans is still not clear, we propose that ADS could be used to modulate cortical state and connectivity by steering neuroplasticity after injury. Additional studies need to be performed to determine the precise parameters and characteristics related to these alterations.

List of Selected pubblications

Journal Papers

Averna A, Pasquale V, Murphy M, Rogantin MP, Vank Acker G, Nudo R.J, Chiappalone M. and Guggenmos D. *Differential effects of open- and closed-loop intracortical microstimulation on firing patterns of neurons in distant cortical areas*. 2019, bioRxiv doi: 10.1101/534032

Peer-reviewed conference papers

Averna A, Guggenmos D, Pasquale V, Semprini M, Nudo RJ and Chiappalone M. *Neuroengineering Tools for Studying the Effect of Intracortical Microstimulation in Rodent Models*. IEEE Engineering in Medicine and Biology Society – July 17-21, 2018. Honolulu (HI), USA. **Oral Presentation**. doi: 10.1109/EMBC.2018.8512915, 3076-3079.

Presentations at international conferences

Averna A, Bisio M, Pruzzo G, Chiappalone M, Bonifazi P. and Difato F. *Neurophysiology guided single cell optical surgery.* 4th Joint Workshop on Computer/Robot Assisted Surgery. Hotel Melià, Genoa, Italy. October 14-16, 2014. **Oral Presentation**.

Averna A, Guggenmos D, Van Acker G, Difato F, Pasquale V, Bisio M, Tessadori J, Nudo R.J. and Chiappalone M. *In vitro and in vivo neurotechnological approaches for brain repair*. Workshop on Robotic and Interactive Technologies for Neuroscience and Neurorehabilitation, RIC-IIT, Arenzano, August 31- Semptember 02, 2015. **Oral Presentation**.

Averna A, Guggenmos D, Pasquale V, Dunham C, Chiappalone M, Nudo R.J. *Effects of intracortical microstimulationon functional connectivity implications for*

neurorehabilitation studies. European Medical and Biological Engineering Conference (EMBEC) and the Nordic-Baltic Conference on Biomedical Engineering and Medical Physics (NBC) – Tampere (Finland) June 11-15 2017. **Oral Presentation**

Awards

The first prize **best paper award** is presented to: **Alberto Averna**, Marta Bisio, Giacomo Pruzzo, Michela Chiappalone, Paolo Bonifazi and Francesco Difato, for the outstanding paper entitled: "*Neurophysiology guided single cell optical surgery*". 4th Joint Workshop on Computer/Robot Assisted Surgery. 14-16 October 2014 - Genoa, Italy.

Best Poster Certificate awarded to **Alberto Averna** for the poster titled "*Evaluation of the effects of intra-cortical microstimulation on distant cortical brain regions: implications for neuro-rehabilitation studies*". 7th Summer School of Neuroengineering. 18-22 June 2018 - Genoa, Italy.

References

Ahnaou, A., Huysmans, H., Biermans, R., Manyakov, N. & Drinkenburg, W. (2017) Ketamine: differential neurophysiological dynamics in functional networks in the rat brain. *Translational psychiatry*, **7**, e1237.

Anderson, V.C., Burchiel, K.J., Hogarth, P., Favre, J. & Hammerstad, J.P. (2005) Pallidal vs subthalamic nucleus deep brain stimulation in Parkinson disease. *Archives of neurology*, **62**, 554-560.

Averna, A., Guggenmos, D., Pasquale, V., Semprini, M., Nudo, R. & Chiappalone, M. (Year) Neuroengineering Tools For Studying The Effect Of Intracortical Microstimulation In Rodent Models. 2018 40th Annual International Conference of the IEEE Engineering in Medicine and Biology Society (EMBC). IEEE, City. p. 3076-3079.

Averna, A., Pasquale, V., Murphy, M., Rogantin, M.P., Van Acker, G., Nudo, R., Chiappalone, M. & Guggenmos, D. (2019) Differential effects of open- and closed-loop intracortical microstimulation on firing patterns of neurons in distant cortical areas. *bioRxiv*, 534032.

Benali, A., Weiler, E., Benali, Y., Dinse, H.R. & Eysel, U.T. (2008) Excitation and inhibition jointly regulate cortical reorganization in adult rats. *Journal of Neuroscience*, **28**, 12284-12293.

Berg, J., Dammann III, J., Tenore, F., Tabot, G., Boback, J., Manfredi, L., Peterson, M., Katyal, K., Johannes, M. & Makhlin, A. (2013) Behavioral demonstration of a somatosensory neuroprosthesis. *IEEE Transactions on Neural Systems and Rehabilitation Engineering*, **21**, 500-507.

Blatt, M., Wiseman, S. & Domany, E. (1996) Superparamagnetic clustering of data. *Physical review letters*, **76**, 3251.

Bradley, D.C., Troyk, P.R., Berg, J.A., Bak, M., Cogan, S., Erickson, R., Kufta, C., Mascaro, M., McCreery, D. & Schmidt, E.M. (2005) Visuotopic mapping through a multichannel stimulating implant in primate V1. *J Neurophysiol*, **93**, 1659-1670.

Bronstein, J.M., Tagliati, M., Alterman, R.L., Lozano, A.M., Volkmann, J., Stefani, A., Horak, F.B., Okun, M.S., Foote, K.D. & Krack, P. (2011) Deep brain stimulation for Parkinson disease: an expert consensus and review of key issues. *Archives of neurology*, **68**, 165-165.

Brown, E.N., Lydic, R. & Schiff, N.D. (2010) General anesthesia, sleep, and coma. *New England Journal of Medicine*, **363**, 2638-2650.

Brown, E.N., Purdon, P.L. & Van Dort, C.J. (2011) General anesthesia and altered states of arousal: a systems neuroscience analysis. *Annual review of neuroscience*, **34**, 601-628.

Buonomano, D.V. & Merzenich, M.M. (1998) Cortical plasticity: from synapses to maps. *Annual review of neuroscience*, **21**, 149-186.

Chen, K.H., Dammann, J.F., Boback, J.L., Tenore, F.V., Otto, K.J., Gaunt, R.A. & Bensmaia, S.J. (2014) The effect of chronic intracortical microstimulation on the electrode–tissue interface. *J Neural Eng*, **11**, 026004.

Cheney, P., Griffin, D. & Van Acker III, G. (2013) Neural hijacking: action of high-frequency electrical stimulation on cortical circuits. *The Neuroscientist*, **19**, 434-441.

Cohen, M.R. & Newsome, W.T. (2004) What electrical microstimulation has revealed about the neural basis of cognition. *Curr Opin Neurobiol*, **14**, 169-177.

Davis, T., Parker, R., House, P., Bagley, E., Wendelken, S., Normann, R. & Greger, B. (2012) Spatial and temporal characteristics of V1 microstimulation during chronic implantation of a microelectrode array in a behaving macaque. *J Neural Eng*, **9**, 065003.

De Hemptinne, C., Ryapolova-Webb, E.S., Air, E.L., Garcia, P.A., Miller, K.J., Ojemann, J.G., Ostrem, J.L., Galifianakis, N.B. & Starr, P.A. (2013) Exaggerated phase–amplitude coupling in the primary motor cortex in Parkinson disease. *Proceedings of the National Academy of Sciences*, 201214546.

De Hemptinne, C., Swann, N.C., Ostrem, J.L., Ryapolova-Webb, E.S., San Luciano, M., Galifianakis, N.B. & Starr, P.A. (2015) Therapeutic deep brain stimulation reduces cortical phase-amplitude coupling in Parkinson's disease. *Nat Neurosci*, **18**, 779.

Deuschl, G., Schade-Brittinger, C., Krack, P., Volkmann, J., Schäfer, H., Bötzel, K., Daniels, C., Deutschländer, A., Dillmann, U. & Eisner, W. (2006) A randomized trial of deep-brain stimulation for Parkinson's disease. *New England Journal of Medicine*, **355**, 896-908.

Dobelle, W. & Mladejovsky, M. (1974) Phosphenes produced by electrical stimulation of human occipital cortex, and their application to the development of a prosthesis for the blind. *The Journal of physiology*, **243**, 553-576.

Fisher, R., Salanova, V., Witt, T., Worth, R., Henry, T., Gross, R., Oommen, K., Osorio, I., Nazzaro, J. & Labar, D. (2010) Electrical stimulation of the anterior nucleus of thalamus for treatment of refractory epilepsy. *Epilepsia*, **51**, 899-908.

Fox, M.D., Buckner, R.L., Liu, H., Chakravarty, M.M., Lozano, A.M. & Pascual-Leone, A. (2014) Resting-state networks link invasive and noninvasive brain stimulation across diverse psychiatric and neurological diseases. *Proceedings of the National Academy of Sciences*, **111**, E4367-E4375.

Guggenmos, D.J., Azin, M., Barbay, S., Mahnken, J.D., Dunham, C., Mohseni, P. & Nudo, R.J. (2013) Restoration of function after brain damage using a neural prosthesis. *Proceedings of the National Academy of Sciences of the United States of America*, **110**, 21177-21182.

Harville, D.A. (1977) Maximum likelihood approaches to variance component estimation and to related problems. *Journal of the American Statistical Association*, **72**, 320-338.

Histed, M.H., Ni, A.M. & Maunsell, J.H. (2013) Insights into cortical mechanisms of behavior from microstimulation experiments. *Progress in neurobiology*, **103**, 115-130.

Homayoun, H. & Moghaddam, B. (2007) NMDA receptor hypofunction produces opposite effects on prefrontal cortex interneurons and pyramidal neurons. *Journal of Neuroscience*, **27**, 11496-11500.

Jackson, A., Mavoori, J. & Fetz, E.E. (2006) Long-term motor cortex plasticity induced by an electronic neural implant. *Nature*, **444**, 56-60.

Jackson, A. & Zimmermann, J.B. (2012) Neural interfaces for the brain and spinal cord—restoring motor function. *Nature Reviews Neurology*, **8**, 690.

Kerrigan, J.F., Litt, B., Fisher, R.S., Cranstoun, S., French, J.A., Blum, D.E., Dichter, M., Shetter, A., Baltuch, G. & Jaggi, J. (2004) Electrical stimulation of the anterior nucleus of the thalamus for the treatment of intractable epilepsy. *Epilepsia*, **45**, 346-354.

Kleim, J.A., Barbay, S. & Nudo, R.J. (1998) Functional reorganization of the rat motor cortex following motor skill learning. *J Neurophysiol*, **80**, 3321-3325.

Kleim, J.A., Bruneau, R., VandenBerg, P., MacDonald, E. (2003) Motor cortex stimulation enhances motor recovery and reduces peri-infarct dysfunction following ischemic insult. *Neurological Research*, **25**, 789-793.

Kuang, H., Lin, L. & Tsien, J.Z. (2010) Temporal dynamics of distinct CA1 cell populations during unconscious state induced by ketamine. *PloS one*, **5**, e15209.

Kuriakose, R., Saha, U., Castillo, G., Udupa, K., Ni, Z., Gunraj, C., Mazzella, F., Hamani, C., Lang, A.E. & Moro, E. (2009) The nature and time course of cortical activation following subthalamic stimulation in Parkinson's disease. *Cerebral cortex*, **20**, 1926-1936.

Lee, K., Jang, K. & Shon, Y. (2006) Chronic deep brain stimulation of subthalamic and anterior thalamic nuclei for controlling refractory partial epilepsy *Advances in functional and reparative neurosurgery*. Springer, pp. 87-91.

Li, Q., Ke, Y., Chan, D.C., Qian, Z.-M., Yung, K.K., Ko, H., Arbuthnott, G.W. & Yung, W.-H. (2012) Therapeutic deep brain stimulation in Parkinsonian rats directly influences motor cortex. *Neuron*, **76**, 1030-1041.

Little, S., Pogosyan, A., Neal, S., Zavala, B., Zrinzo, L., Hariz, M., Foltynie, T., Limousin, P., Ashkan, K. & FitzGerald, J. (2013) Adaptive deep brain stimulation in advanced Parkinson disease. *Annals of neurology*, **74**, 449-457.

Maccione, A., Gandolfo, M., Massobrio, P., Novellino, A., Martinoia, S. & Chiappalone, M. (2009) A novel algorithm for precise identification of spikes in extracellularly recorded neuronal signals. *J Neurosci Methods*, **177**, 241-249.

McCairn, K.W. & Turner, R.S. (2015) Pallidal stimulation suppresses pathological dysrhythmia in the parkinsonian motor cortex. *J Neurophysiol*, **113**, 2537-2548.

Meidahl, A.C., Tinkhauser, G., Herz, D.M., Cagnan, H., Debarros, J. & Brown, P. (2017) Adaptive deep brain stimulation for movement disorders: the long road to clinical therapy. *Movement disorders*, **32**, 810-819.

Mohammed, H. & Jain, N. (2016) Ipsilateral cortical inputs to the rostral and caudal motor areas in rats. *Journal of Comparative Neurology*, **524**, 3104-3123.

Morrell, M.J. (2011) Responsive cortical stimulation for the treatment of medically intractable partial epilepsy. *Neurology*, **77**, 1295-1304.

Nishimura, Y., Perlmutter, S.I., Eaton, R.W. & Fetz, E.E. (2013a) Spike-timing-dependent plasticity in primate corticospinal connections induced during free behavior. *Neuron*, **80**, 1301-1309.

Nishimura, Y., Perlmutter, S.I. & Fetz, E.E. (2013b) Restoration of upper limb movement via artificial corticospinal and musculospinal connections in a monkey with spinal cord injury. *Frontiers in neural circuits*, **7**, 57.

Nudo, R., Jenkins, W. & Merzenieh, M. (1990) Repetitive microstimulation alters the cortical representation of movements in adult rats. *Somatosensory & motor research*, **7**, 463-483.

Overstreet, C., Klein, J. & Tillery, S.H. (2013) Computational modeling of direct neuronal recruitment during intracortical microstimulation in somatosensory cortex. *J Neural Eng*, **10**, 066016.

Quiroga, R.Q., Nadasdy, Z. & Ben-Shaul, Y. (2004) Unsupervised spike detection and sorting with wavelets and superparamagnetic clustering. *Neural Comput*, **16**, 1661-1687.

Rajan, A.T., Boback, J.L., Dammann, J.F., Tenore, F.V., Wester, B.A., Otto, K.J., Gaunt, R.A. & Bensmaia, S.J. (2015) The effects of chronic intracortical microstimulation on neural tissue and fine motor behavior. *J Neural Eng*, **12**, 066018.

Ranck Jr, J.B. (1975) Which elements are excited in electrical stimulation of mammalian central nervous system: a review. *Brain research*, **98**, 417-440.

Rebesco, J.M. & Miller, L.E. (2011) Enhanced detection threshold for in vivo cortical stimulation produced by Hebbian conditioning. *J Neural Eng*, **8**, 016011.

Rebesco, J.M., Stevenson, I.H., Koerding, K., Solla, S.A. & Miller, L.E. (2010) Rewiring neural interactions by micro-stimulation. *Frontiers in systems neuroscience*, **4**, 39.

Rieke, F. (1999) *Spikes: exploring the neural code*. MIT press.

Rieke, F., Warland, D. & de Ruyter, v.S. R., & Bialek, W.(1997). Spikes: Exploring the neural code. *MITpress, Cambridge, Massachusetts*.

Santos, F.J., Costa, R.M. & Tecuapetla, F. (2011) Stimulation on demand: closing the loop on deep brain stimulation. *Neuron*, **72**, 197-198.

Schmidt, E., Bak, M., Hambrecht, F., Kufta, C., O'rourke, D. & Vallabhanath, P. (1996) Feasibility of a visual prosthesis for the blind based on intracortical micro stimulation of the visual cortex. *Brain*, **119**, 507-522.

Shinomoto, S., Kim, H., Shimokawa, T., Matsuno, N., Funahashi, S., Shima, K., Fujita, I., Tamura, H., Doi, T., Kawano, K., Inaba, N., Fukushima, K., Kurkin, S., Kurata, K., Taira, M., Tsutsui, K., Komatsu, H., Ogawa, T., Koida, K., Tanji, J. & Toyama, K. (2009) Relating neuronal firing patterns to functional differentiation of cerebral cortex. *PLoS Comput Biol*, **5**, e1000433.

Skarpaas, T.L. & Morrell, M.J. (2009) Intracranial stimulation therapy for epilepsy. *Neurotherapeutics*, **6**, 238-243.

Slomowitz, E., Styr, B., Vertkin, I., Milshtein-Parush, H., Nelken, I., Slutsky, M. & Slutsky, I. (2015) Interplay between population firing stability and single neuron dynamics in hippocampal networks. *Elife*, **4**.

Tabot, G.A., Dammann, J.F., Berg, J.A., Tenore, F.V., Boback, J.L., Vogelstein, R.J. & Bensmaia, S.J. (2013) Restoring the sense of touch with a prosthetic hand through a brain interface. *Proceedings of the National Academy of Sciences*, **110**, 18279-18284.

Tehovnik, E., Tolias, A., Sultan, F., Slocum, W. & Logothetis, N. (2006) Direct and indirect activation of cortical neurons by electrical microstimulation. *J Neurophysiol*, **96**, 512-521.

Tehovnik, E.J. & Slocum, W.M. (2013) Electrical induction of vision. *Neuroscience & Biobehavioral Reviews*, **37**, 803-818.

Thomson, E.E., Carra, R. & Nicolelis, M.A. (2013) Perceiving invisible light through a somatosensory cortical prosthesis. *Nature communications*, **4**, 1482.

Torab, K., Davis, T., Warren, D., House, P., Normann, R. & Greger, B. (2011) Multiple factors may influence the performance of a visual prosthesis based on intracortical microstimulation: nonhuman primate behavioural experimentation. *J Neural Eng*, **8**, 035001.

Weaver, F.M., Follett, K.A., Stern, M., Luo, P., Harris, C.L., Hur, K., Marks, W.J., Rothlind, J., Sagher, O. & Moy, C. (2012) Randomized trial of deep brain stimulation for Parkinson disease Thirty-six-month outcomes. *Neurology*, **79**, 55-65.

Zakiewicz, I.M., Bjaalie, J.G. & Leergaard, T.B. (2014) Brain-wide map of efferent projections from rat barrel cortex. *Front Neuroinform*, **8**, 5.

Chapter 5 Effect of ICMS on stroke injured anesthetized animals

This chapter describes the main results obtained in the second set of experiments performed at both IIT and the Kansas University between 2017 and 2018. In particular, the characterization of the changes in intra-cortical neuronal activity induced by the ADS treatment and the electrophysiological effect of a focal model of stroke using the Injury Anesthetized procedure in which a potent vasoconstrictor was injected to induce a focal lesion are discussed.

5.1. Introduction

Advances in brain-computer interfaces have provided a promising vector for neurorepair and the restoration of lost function (Greenwald *et al.*, 2016). In this study, we examined the effects of a brain-machine-brain interface (BMBI) designed to facilitate motor function recovery after stroke or TBI.

As its name entails, the BMBI first discriminates neural activity from the brain and then processes that information in a machine or prosthesis. The final B in the acronym implies that feedback is supplied to the brain, creating a loop of information exchange between the brain and machine. The feedback can be partially provided by visual cues or peripheral stimulation, but the BMBI used in this study provides feedback by electrically stimulating the brain through an implanted electrode. When the recording and stimulating electrodes are implanted distantly from each other, BMBIs can function as artificial communication links between separate regions of the brain. This unique function of BMBIs can be exploited for activity-dependent stimulation (ADS); discriminated action potentials (spikes) are recorded in one brain location and used to directly trigger stimulation in another brain location. A landmark study performed by Jackson *et al*. utilized recording and stimulating electrodes implanted separately in the primate primary motor cortex (M1) (Jackson *et al.*, 2006). Within a couple of days of activity-dependent stimulation, the output properties of the recording site began to resemble the output properties of the stimulation site. Augmenting corticocortical

interconnections in this manner drives specific neurophysiological changes specific to the targeted regions (Jackson *et al.*, 2006). A study conducted by Song *et al*. applied ADS to two sites in the primate S1, and strengthened connections were observed between the recording and stimulation sites as measured by an increased number of matched activity pairs (Song *et al.*, 2013). The altered network connections observed in these experiments provide evidence that Hebbian synaptic plasticity is involved in the impact of ADS in the neocortex (Jackson *et al.*, 2006; Guggenmos *et al.*, 2013; Song *et al.*, 2013).

A relatively new application of BMBIs is the promotion of brain repair after TBI (Guggenmos *et al.*, 2013). In the previous study, adult rats received a traumatic brain injury in their primary motor cortex (M1). One group of rats was treated with an ADS protocol that triggered stimulation in the somatosensory cortex (S1) based on spikes recorded in the premotor cortex (PM). The rational was to reestablish the connections between S1 and PM that were attenuated by the damage to M1. In the same study, a second group of rats was treated with random, open-loop stimulation (RS) in the somatosensory cortex. The ADS-treated rats recovered fine motor control more quickly than the RS-treated rats; however, both treatments were superior to the non-stimulated control rats. The behavioral recovery was empirically remarkable; however, the underlying electrophysiological change responsible for the electrophysiological effect induced by ADS remains unclear (Averna *et al.*, 2018; Averna *et al.*, 2019). Our aim in this study was to elucidate those mechanisms.

In this study, two groups of injured animals were used. One group (ADS) received activity-dependent stimulation treatment after a focal infarct to evaluate any electrophysiological changes induced by the stimulation. The second set of experiments (Control) was conducted to characterize the electrophysiological effect of this type of brain injury, and in these experiments, the stimulation was turned off for the entire duration of the recordings.

5.2. Methods

5.2.1. Animals

All experiments were approved by the University of Kansas Medical Center Institutional Animal Care and Use Committee. In total, 12 adult male Long-Evans rats (weight: 350-400 g, age: 4-5 months; Charles River Laboratories, Wilmington, MA, USA) were used in this study. The injured anaesthetized dataset comprised twelve experiments divided into two groups as shown in Table 5.2.1.

Table 5.2.1: Injured Anaesthetized dataset.

	Stimulation Type	
	ADS	**CTRL**
# Rats	7	5
Total	**12**	

5.2.2. Surgical Procedures

In the Injured Anesthetized procedure, the rats were induced with gaseous isoflurane prior to surgery within a sealed vaporizer chamber. The anesthetization was followed by injections of ketamine (80-100 mg/kg IP) and xylazine (5-10 mg/kg). Maintenance boluses of ketamine (10-100 mg/kg/h ip or im) were repeatedly injected as needed throughout the procedure. A stereotaxic frame was used to secure the rats' heads, and an anal temperature probe was used to monitor the rats' temperature. The rats' eyes were protected with ophthalmic ointment. Either Lidocaine/Prilocaine cream or bupivacaine was applied to the scalp prior to performing a skin incision spanning rostro-caudally between ~6 mm rostral to bregma and ~5 mm distal to the

atlanto-occipital junction. The cisterna magna or upper vertebrae were exposed by reflecting the overlaying neck muscles. The spinal dura located in the foramen magnum was slightly punctured to control brain edema by allowing CSF drainage.

Six 0.7-mm diameter holes were drilled into the skull over the dominant hemisphere (contralateral to the preferred forelimb) as follows: anteroposterior 1.5, 0.5, and -0.5 and mediolateral 2.5 and 3.5 from bregma, corresponding to the caudal forelimb area (CFA) of the motor cortex. Endothelin-1 (ET-1; 0.3 μg ET-1 dissolved in 1 μl saline or 1 mg ET-1 dissolved in 3.33 ml saline; Bachem Americas, USA), which is a venous and arterial vasoconstrictor, was injected ~ 1.5 mm below the pial surface (Gilmour *et al.*, 2005). Stereotaxic coordinates (Paxinos & Watson, 1998) were used to determine where to administer the ET-1 injections. A borehole was created through the skull, and 0.33 μl ET-1 were injected at a rate of 3 nl/sec via a 160 μm pipette (o.d.) attached to a 1 μl Hamilton syringe. The spread of ET-1 with this procedure is usually confined to an area of 0.5 mm diameter; therefore, the injections were placed to produce a continuous infarct without exposing the cortex (Fang *et al.*, 2010). Once the brain lesion was performed, a small craniectomy 0.3 mm was performed over the RFA and S1 using stereotaxic coordinates, and then, the procedure followed the same steps described in the Healthy protocol.

5.2.3. Mapping Cortical Areas

The RFA and S1 FL were identified using electrophysiological recording and stimulation techniques. The RFA was identified using methods similar to those previously described (Kleim *et al.*, 1998; Nishibe *et al.*, 2010). Stimulation was applied at each cortical site through a pulled glass electrode with a beveled 15-25 μm tip filled with 3.5 M saline and conducted through a platinum wire to which a flexible stimulating wire was connected. Ground was achieved by attaching a return lead to a moistened gauze wrapped around the tail. Stimulus trains of 13-pulses at 333 Hz (40

ms in duration) were applied to layer V at 1 Hz intervals using a stimulus isolator (BAK Electronics, Umatilla FL, USA).

Associated movements occurring below a maximum stimulus intensity of 80 μA were characterized. Muscle twitches associated with the forelimb were noted, and those associated with the trunk caudal to the RFA border were identified as the boundary between the RFA and CFA. Once the RFA was mapped, S1 FL was identified for the stimulation site using a single shank, 16-channel Michigan style array (NeuroNexus, Ann Arbor, MI, USA) coupled to a recording system (TDT). The identification of the forelimb-responsive sites in S1 was achieved by evoking audible and visible spiking neural activity concurrent with forepaw palpation.

5.2.4. Experimental Protocol

As depicted in Figure 5.2.1A, a four-shank, sixteen-contact site electrode with 1-1.5 MΩ impedance at each site (A4x4-5mm-100-125-703-A16, NeuroNexus) was placed within the RFA at a depth of 1700 μm. The cell activity was detected in real-time using a user-selected voltage threshold. Based on this data, a contact site yielding neural spiking data at a moderate rate of spontaneous activity (4-10 Hz) was identified and used as a trigger channel for stimulating a cortical site in the forelimb-responsive S1 FL. The stimulation was applied through a single contact on a four-shank, sixteen-contact electrode with an impedance of ~ 200 kΩ (contact 6, activated A4x4-5mm-100-703-A16, NeuroNexus). The continuous extracellular signal recorded from each electrode was amplified, digitized and stored for offline analysis at a sampling rate of 30 kHz using INTAN RHD2000 hardware and acquisition software (http://www.intantech.com). The stimulation pulse was designed using the INTAN controller software. A single 60 μA biphasic, cathodal-leading stimulus pulse (200 μs positive, 200 μs negative) was triggered each time a user-selected neuronal spike profile was recorded from a single recording site in the RFA. The latency between the spike detection in the RFA and delivery of a stimulus pulse in the FL or BF was set at

10 ms (2.5 ms spike processing time, 7.5 ms imposed delay). To prohibit stimulus-activated RFA spikes and stimulus artifacts from triggering stimulation, a short blanking period (28 ms) followed each stimulus.

In this case, the experimental protocol began one hour after the ET-1 injections, which is a period during which no electrophysiological data were recorded, and the experiment consisted of three experimental phases (Figure 5.2.1B). First, no stimulation was applied during the first 30 minutes of recording (Basal1); then, one 1-hour stimulation treatment was applied via ADS (Stim1), followed by a second recording of basal activity (Basal2).

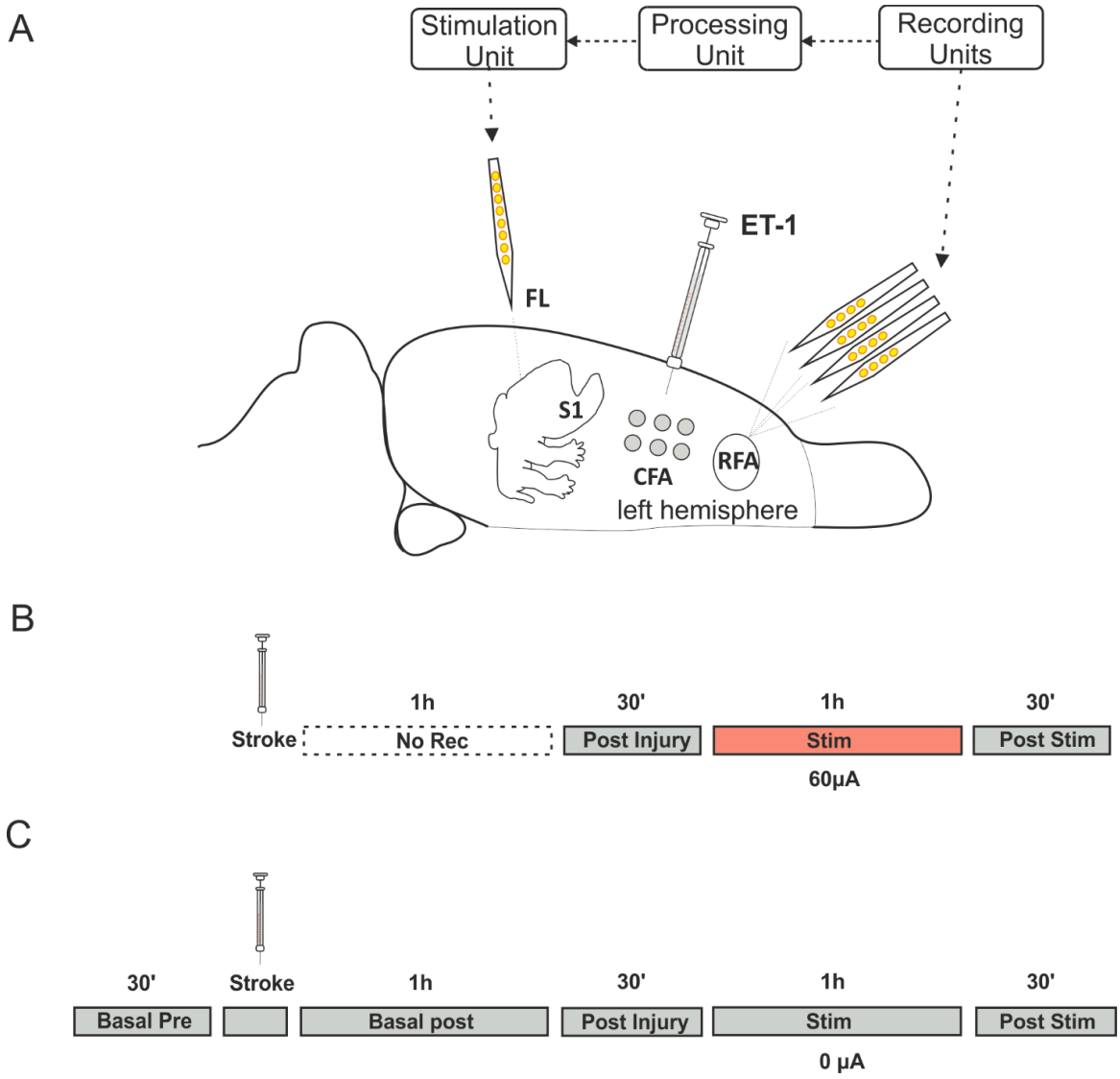

Figure 5.2.1: Experimental scheme. A) Cell activity was recorded using a commercial data acquisition system, which was programmed to detect the data recorded from the RFA in real-time and use such information to trigger stimulation in a cortical site in S1 FL. B) The experimental timeline of the ADS consisted of two 30-minutes basal phase and 1 stimulation sessions of 1 hour. C) The CONTROL experiment consisted of four phases of spontaneous recordings before, during and after the stimulation.

In the Control experiments (Figure 5.2.1C), the same protocol used in the ADS experiment was used, and spontaneous activity was recorded before, during and after the ET-1 injection, but the stimulation was set at 0 µA for the entire recording session (two hours).

5.2.5. Data Processing

In these experiments, the wide-band neural data were recorded (INTAN Technologies, Los Angeles, CA, USA) at ~ 30 kHz per channel.

I analyzed the electrophysiological signals by investigating the LFP temporal scale of the recorded signals (see Chapter3- Materials and Methods).

The wide-band signals were first down-sampled to 1 kHz, followed by low pass filtering below 500 Hz to prevent aliasing. To evaluate the effect of both the brain injury and ADS on the recorded brain areas, power and connectivity analyses were performed.

- *LPF Power:* I computed the power spectral density of the decimated signal (dB/Hz) using the Welch method [Windows = 5 s, overlap = 50%; DFT (Discrete Fourier Transform) points = 8192; df (frequency resolution) = 0.12 Hz; dt (temporal resolution) = 8.19 s]. I only considered the lower frequency bands of the signal, which are of particular interest due to their association with many brain processes; in particular, the delta (δ, 1–4 Hz), theta (θ, 4–8 Hz), alpha (α, 8-11 Hz), beta (β, 11–30 Hz), low-gamma (lowγ, 30–55 Hz) and high-gamma (highγ, 55-130) bands were considered.
- *LFP Connectivity:* To measure the functional connectivity between the LFP sources, we applied the method proposed by Hipp *et al*. (Hipp *et al.*, 2012) (see Chapter 3, Materials and Methods). The pairwise correlation values were considered significant if their values were significantly higher than the average correlation of each LFP source to the rest of the sources (one-sided t-test, $p < 0.001$) (Hipp *et al.*, 2012). Both the average number of functional connections and the value of the correlation were calculated for all pairs of significant LFP sources intra-areas (all pairs of electrodes in the RFA and S1) and inter-areas (all pairs of electrodes between the RFA and S1) for each frequency band.

5.3. Results

5.3.1. LFP power changes after stroke

The LFP power spectra during the baseline period of recording (Basal Pre) were dominated by low temporal frequencies. The LFP fluctuated less quickly 1 hour after the ET-1 injections. Figure 5.3.1A shows a spectrogram calculated for a representative channel in the RFA during Basal Pre (left), immediately after the ET-1 injections (Basal Post, Figure 5.3.1A center) and one hour after stroke (Post Injury, Figure 5.3.1A right). As shown in Figure 5.3.1B. the LFP power was differentially distributed in the two recording regions (RFA red boxes and S1 blue boxes). The changes in power are shown in Figure 5.3.1C, where RFA (red bars, left) showed stable power in all frequency bands immediately after stroke, but a strong decrease in all bands, except for Low γ, was induced after one hour (Figure 5.3.1C, left, RFA Post Injury). A different effect was observed in S1 (blue bars, right), where the power was constant for θ, α and β but increased for δ and High γ. One hour after injury (S1 Post Injury), the power decreased only in θ and High γ (Figure 5.3.1, right, S1 Post Injury).

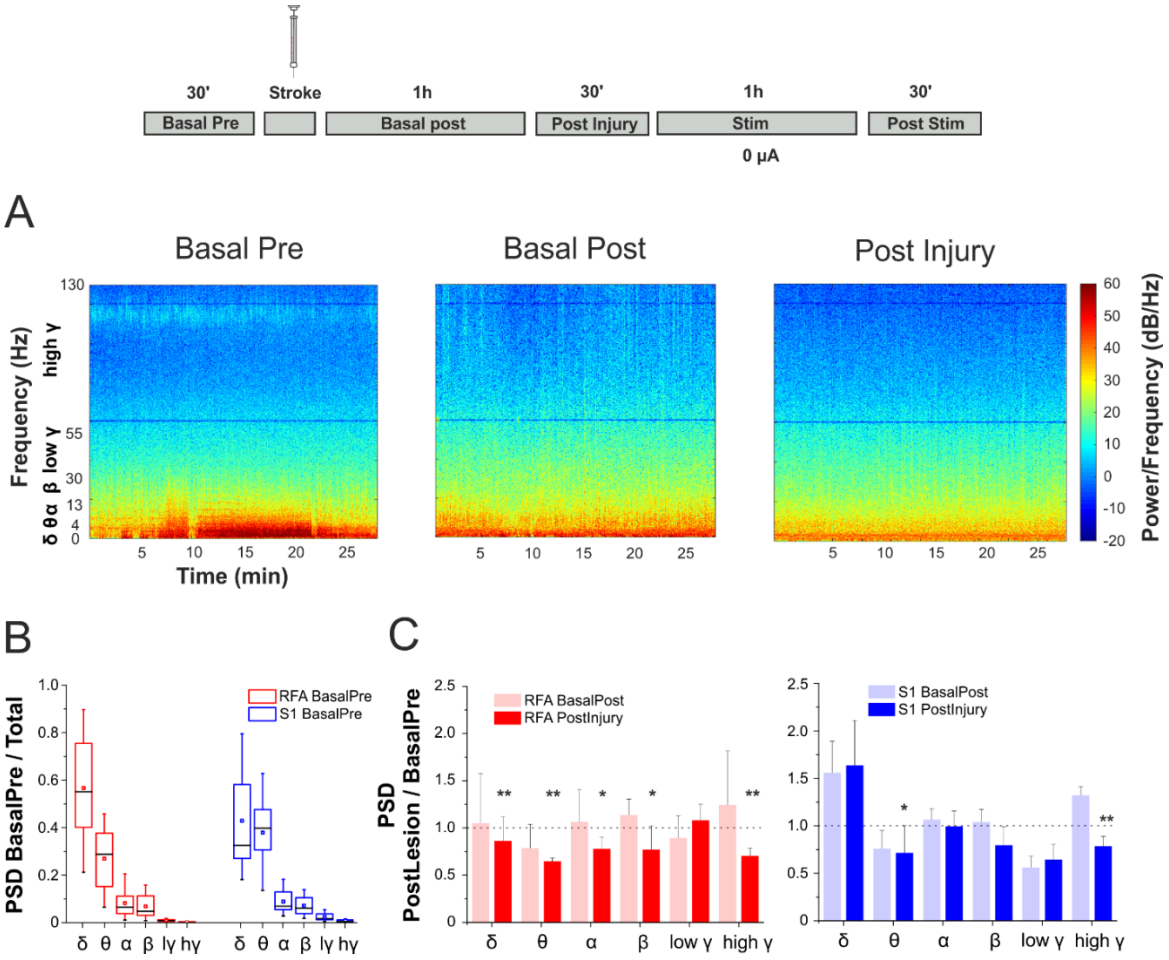

Figure 5.3.1: A) Spectrogram showing the time variation of PSD in the different LFP bands during different experimental phases (Basal Pre, Basal Post, and Post Injury) for a representative electrode in the RFA. B) Box plots representing the integrated normalized (across the total power) PSD per frequency band in the two brain regions recorded (RFA red, S1 blue). C) Column bar representing the integrated normalized (across the mean value calculated in Basal Pre) PSD per frequency band during different experimental phases (Basal, Post and Post Injury) in the two areas (RFA red, S1 blue). *p<0.05, **p < 0.001; Wilcoxon signed-rank test. Error bars represent the SEM. The data are reported as the median ± SEM (standard error of the median).

5.3.2. ADS modulates LFP power

To reveal the effect of ADS after stroke injury, the LFP power was also evaluated before (Post Injury) and after (Post Stim) the stimulation. As depicted in Figure 5.3.2A, the distribution of power among the frequency bands changed after the stimulation (Figure 5.3.2A, Post Injury and Post Stim). The LFP power before the stimulation (Post Injury) was differentially distributed in the two recording regions (RFA red boxes and

S1 blue boxes) but was comparable with that calculated under the control condition (Figure 5.3.2B). ADS induced a significant increase in power (with respect to the Post Injury phase and the Control) in the RFA in the δ, θ, α and β bands, and stable power was observed in both Low and High γ (Figure 5.3.2C, red bars). Moreover, the effect of ADS in S1 was represented by an increase in all LFP bands, except for θ (Figure 5.3.2C, blue bars).

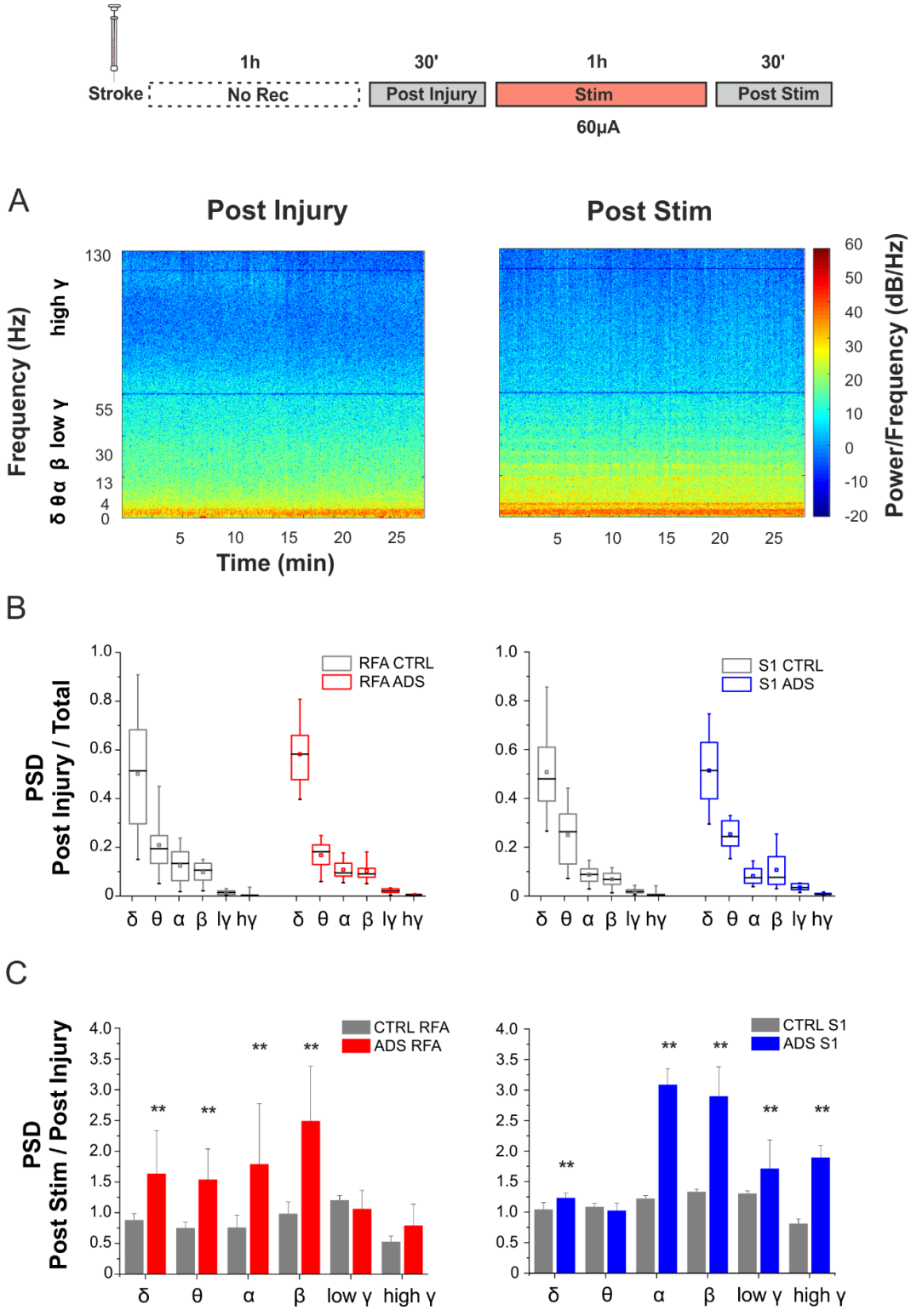

Figure 5.3.2: A) Spectrogram showing the time variation in PSD in the different LFP bands during different experimental phases (Post Injury and Post Stim) in a representative electrode in the RFA. B) Box plots representing

the integrated normalized (across the total power) PSD per frequency band in the two brain regions recorded (RFA red, S1 blue) with respect to the corresponding content calculated under the CTRL condition. C) Column bar representing the integrated normalized (across the mean value calculated in Post Injury) PSD per frequency band during Post Stim in the two areas (RFA red, S1 blue) with respect to the CTRL condition (*p<0.05, **p < 0.001; Wilcoxon signed-rank test). The data are reported as the median ± SEM (standard error of the median).

5.3.3. Stroke manipulates functional connections between S1 and RFA

Functional connectivity in the LFP domain (see Methods, 5.2.5 Data Processing) was evaluated before and after stroke. Figure 5.3.3A shows a representative correlation matrix calculated during each experimental phase of the CONTROL experimental procedure. Although the value of the correlation remained stable in the recorded brain regions (RFA and S1), it varied during the experiment in all pairs of correlation between the S1 and RFA (Inter, Figure 5.3.3B). Figure 5.3.3C shows the average number of significant correlations calculated during each experimental phase. The percentage of connectivity within the RFA and S1 has comparable values of approximately 70 and 60% of the total, respectively, but remains much lower between them (approximately 30%). Finally, the number of significant correlations remained constant within the RFA and S1 during all experimental phases considered but statistically increased between the two areas (inter) after stroke (Figure 5.3.3C).

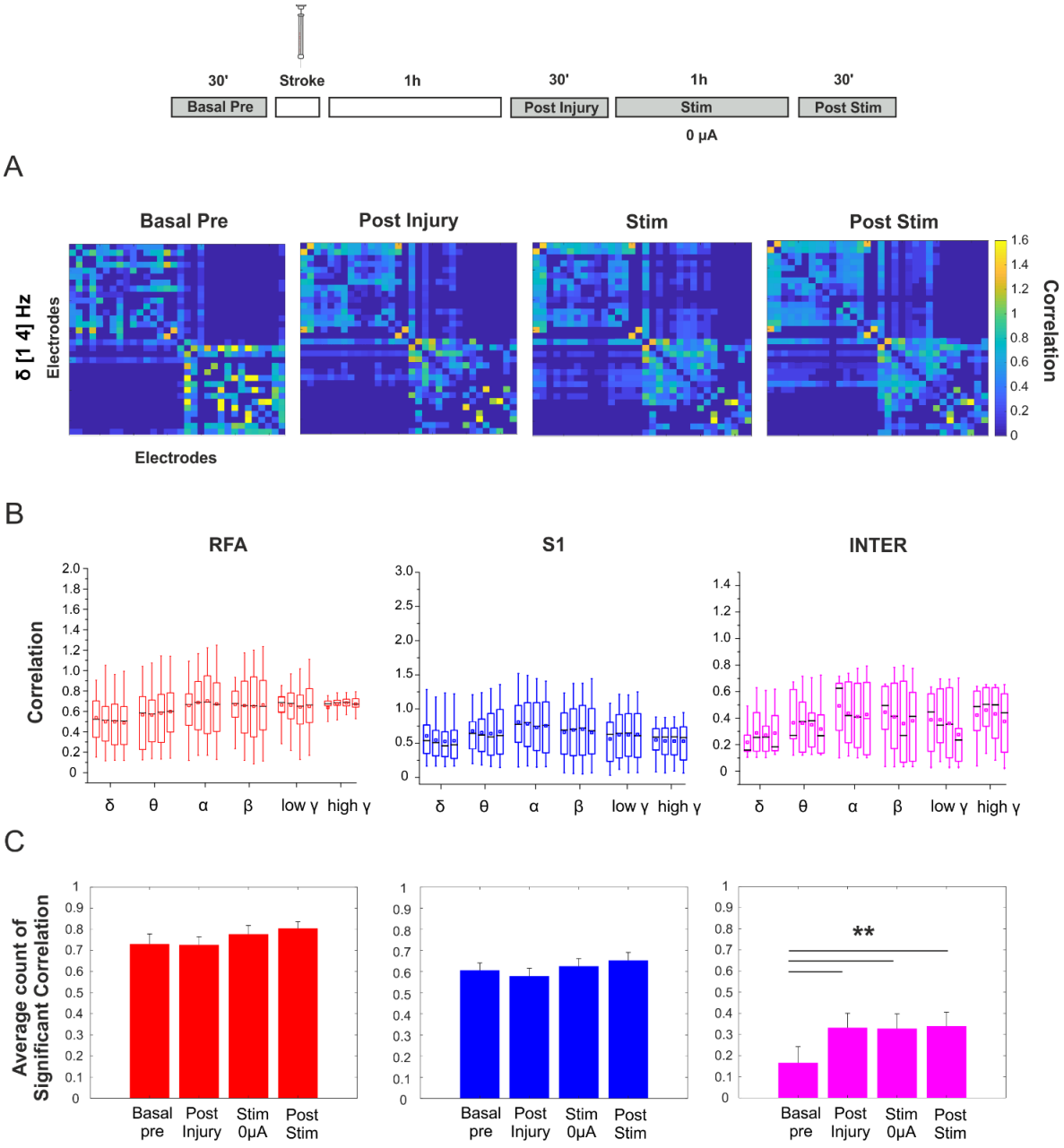

Figure 5.3.3: A) Correlation matrices computed for a representative case (δ band) during each experimental phase shown on the top. B) Box plots of the number of correlations between each frequency bands calculated in the RFA (red boxes), in S1 (blue boxes) and between them (Inter, purple boxes) during each experimental phase. C) Average number of significant correlations calculated both within (RFA red, S1 blue bars) and between (Inter, purple bars) the brain regions studied (**p < 0.001; Friedman repeated measures analysis of variance of ranks). The data are reported as the median ± SEM (standard error of the median).

5.3.4. ADS induces functional connectivity changes both within (RFA, S1) and between areas

Figure 5.3.4 shows the correlation matrices related to the significant functional connections in a representative experiment (ADS group) calculated during each recording phase (Post Injury, Stim, and Post Stim) of all frequency bands studied (δ, θ, α, β, lowγ and highγ).

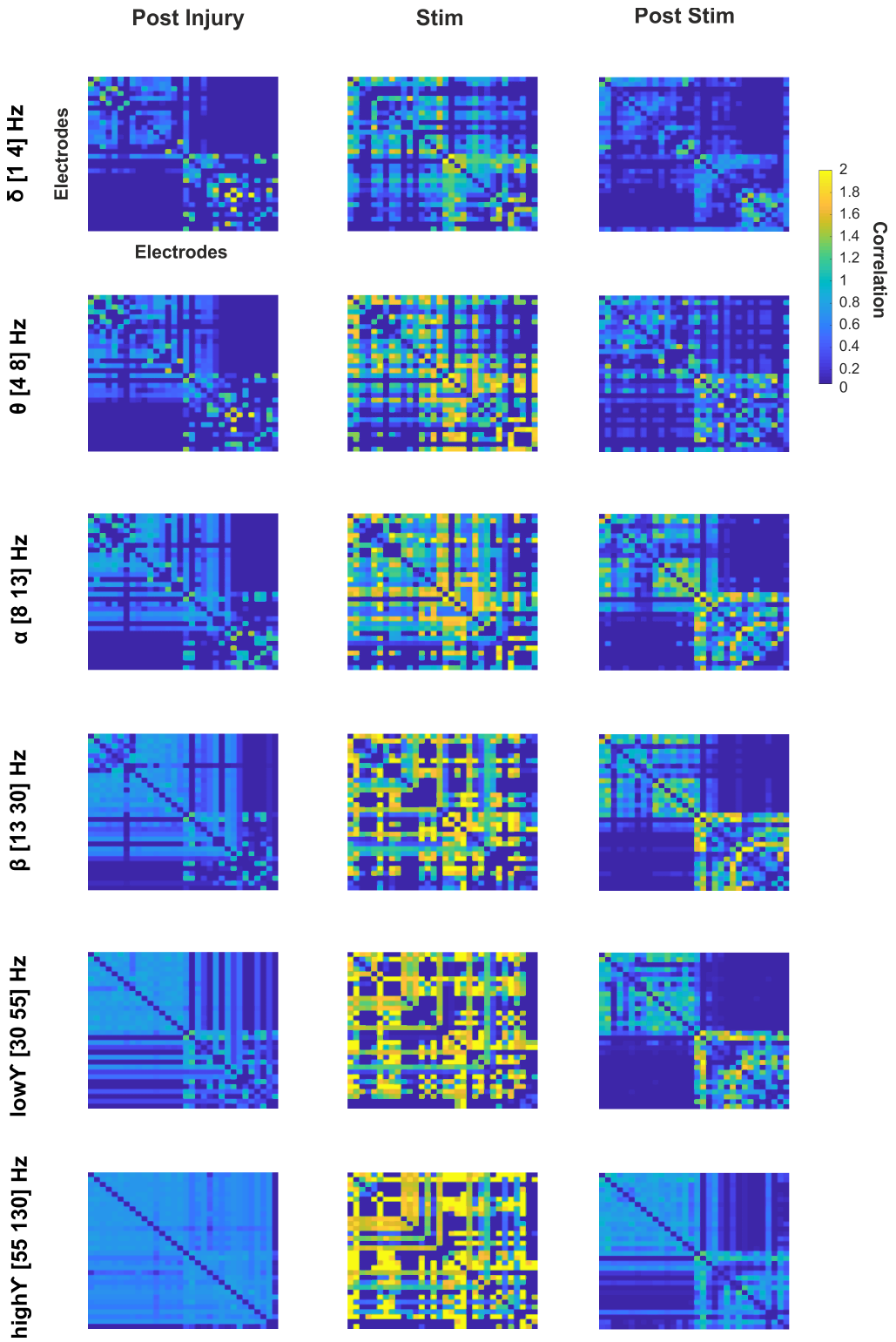

Figure 5.3.4: Correlation matrices computed for all frequency bands (δ, θ, α, β, lowγ and highγ) during each experimental phase in the ADS modality (Post Injury, Stim, and Post Stim).

The changes in the correlation induced by the stimulation were quantified. Figure 5.3.5A provides a histogram of the ratio between the correlations calculated during Post Stim (Post) and Post Injury (Pre) both within (RFA red and S1 blue) and between (Inter purple) the areas. An increase in functional connectivity within S1 was observed in all frequency bands, except for δ (Figure 5.3.5B, blue boxes). The connectivity within the RFA showed comparable values in all frequency bands, except for δ (Figure 5.3.5B, red boxes). The inter connectivity values decreased in α, β, lowγ and highγ and remained constant in the other bands (Figure 5.3.5B, purple boxes).

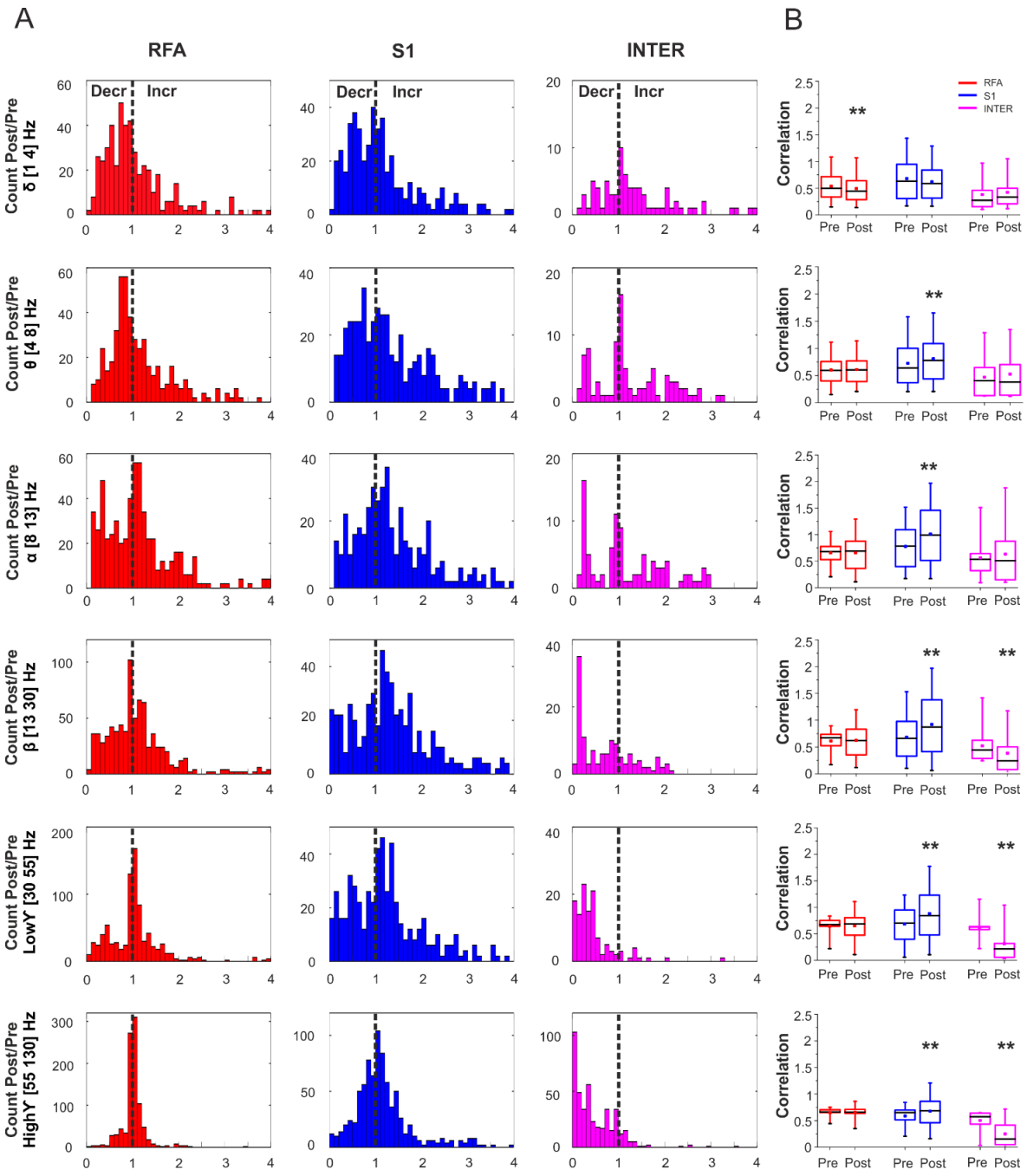

Figure 5.3.5: A) Histogram of the ratio between the Post Stim (Post) and Post Injury (pre) correlations both within (RFA red and S1 blue) and between (Intra, purple) the areas. B) Box plots of the correlations calculated in the three modalities before (Post Injury, Pre) and after (Post Stim, Post) ADS (**p < 0.001; Wilcoxon signed-rank test. Error bars represent the SEM). The data are reported as the median ± SEM (standard error of the median).

Finally, the number of functional connections induced by the ADS treatment were quantified (see Appendix, Figure A2). As shown in Figure 5.3.6A, the neural population

activity recorded in the present experimental modality exhibited both within (RFA and S1) and between functional connections. The number of significant functional inter connections increased and was significantly greater than that in the CONTROL after ADS for θ and α, while similar decreases were observed in lowγ and highγ (Figure 5.3.6B).

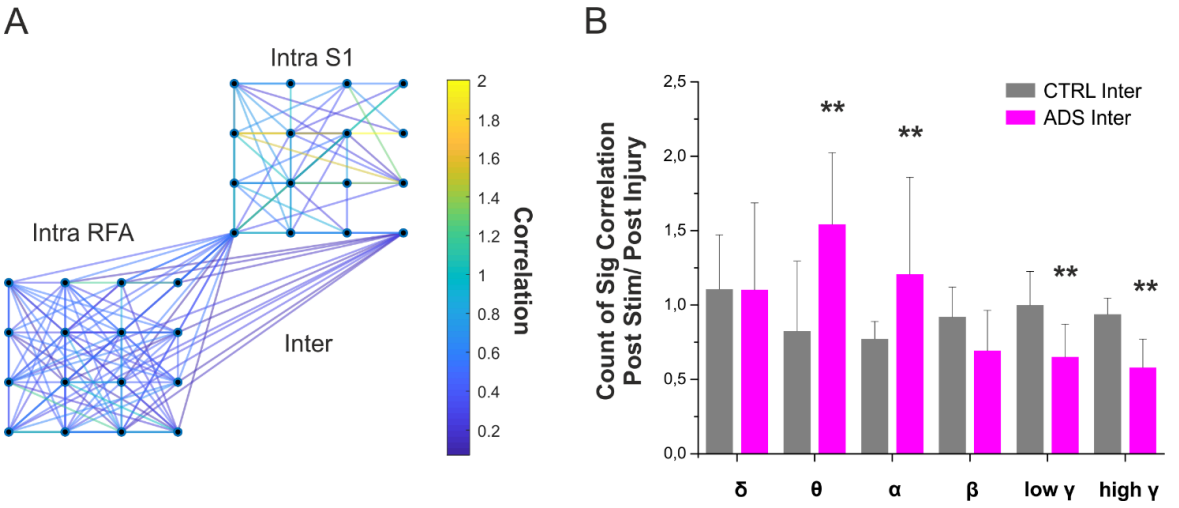

Figure 5.3.6: A) Representative case of significant functional connections within (Intra RFA and Intra S1) and between (Inter) calculated during the Post Injury phase for the δ band. B) Column bar representing the ratio between Post Stim and Post Injury number of Inter connections with respect to the CTRL condition (**p < 0.001; Mann-Whitney U test). The data are reported as the median ± SEM (standard error of the median).

5.4. Discussion

As already demonstrated in Chapter 4, ADS in the somatosensory area (S1) was effective in altering the intracortical activity of the RFA in healthy anesthetized rats during a single recording session (Averna *et al.*, 2018; Averna *et al.*, 2019). In this study, an ischemic lesion in the primary motor cortex equivalent in rats (CFA) was induced, and I tested the ability of ADS to induce electrophysiological changes in both the stimulated brain region (S1) and a distant cortical location (RFA) when the direct communication between the two areas was interrupted by injury. The reciprocal connections between the Pre-Motor (RFA) Somatosensory (S1) and the Primary Motor Cortex (CFA) have been anatomically identified in rodents (Hira *et al.*, 2013; Zakiewicz *et al.*, 2014). Thus, injury to the CFA might influence the neural circuitry in both the ipsilateral RFA and S1.

Although an accurate analysis of the single units' activity (SUA, see Chapter 3, Materials and Methods) has not been implemented, the preliminary results of the LFP are highly encouraging.

The LFP power following the stroke lesion was shown to decrease in almost all frequency bands in the recorded brain regions (Figure 5.3.1A). Interestingly, the ADS treatment induced a significant increase in δ, θ, α and β in the RFA and δ, α, β, lowγ and highγ in S1 (Figure 5.3.2C), thus suggesting the reestablishment of local cortical activity between the two areas.

Stroke also modulates the intracortical connectivity. We found that both the number of correlations and the number of functional connections calculated in all frequency bands remained stable within the RFA and S1 for the entire duration of the experiment (see Figure 5.3.3B, C). The number of correlations between the S1 and RFA (Inter) changed throughout the experimental phases, and the number of significant functional connections during the baseline period (Basal Pre) was much lower than the Intra connectivity (within RFA and S1); interestingly, this number increased following

stroke (Figure 5.3.3C). It has already been shown that Inter correlations decrease between the two hemispheres (Vallone *et al.*, 2016) following stroke, but this study is the first to show an effect in the ipsilateral cortico-cortical Inter-connections.

ADS manipulates both intra-cortical and inter-cortical connectivity. An increase in functional connectivity within the S1 was observed in θ, α, β, lowγ and highγ. In the RFA, the only decrease was found in the δ band (Figure 5.3.5B). The fact that ADS is more effective in manipulating Intra S1 connectivity is well explained by the fact that the direct cortico-cortical communications between the RFA and S1 were disrupted by stroke and that the stimulation involved other subcortical pathways to communicate, thus resulting in a reduced effect in the RFA.

However, both the value and number of the inter-cortical correlation changed following ADS. In particular, the value of the correlation decreased in α, β, lowγ and highγ and remained constant in the other bands, while the number of functional connections significantly increased in the θ and α bands and decreased in the lowγ and highγ bands. These results suggest a reorganization of information flow among the cortical regions after the tentative ADS treatment to reestablish the communication between the two dislocated brain regions (RFA and S1). The functional meaning and the mechanisms underlying the generation of the α and θ band activity are still mostly unknown, but it has been previously demonstrated that interactions between distant cortical areas evolve mainly in the middle (θ, α, 4–12 Hz)-frequency ranges (Von Stein *et al.*, 2000). Thus, an increase in the number of functional connections in the middle-frequency range suggests a greater presence of top-down processes. Indeed, enhanced α and θ interactions have been found in cats during states of intense expectancy (Chatila *et al.*, 1992).

Taken together, these results indicate that activity-dependent stimulation is able to manipulate neuronal activity in the cortex, even in case of an M1 lesion in the rodent, thus evincing the electrophysiological properties that remain beyond the behavioral recovery presented by Guggenoms et al (Guggenmos *et al.*, 2013).

References

Averna, A., Guggenmos, D., Pasquale, V., Semprini, M., Nudo, R. & Chiappalone, M. (Year) Neuroengineering Tools For Studying The Effect Of Intracortical Microstimulation In Rodent Models. 2018 40th Annual International Conference of the IEEE Engineering in Medicine and Biology Society (EMBC). IEEE, City. p. 3076-3079.

Averna, A., Pasquale, V., Murphy, M., Rogantin, M.P., Van Acker, G., Nudo, R., Chiappalone, M. & Guggenmos, D. (2019) Differential effects of open- and closed-loop intracortical microstimulation on firing patterns of neurons in distant cortical areas. *bioRxiv*, 534032.

Chatila, M., Milleret, C., Buser, P. & Rougeul, A. (1992) A 10 Hz "alpha-like" rhythm in the visual cortex of the waking cat. *Clinical Neurophysiology*, **83**, 217-222.

Fang, P.-c., Barbay, S., Plautz, E.J., Hoover, E., Strittmatter, S.M. & Nudo, R.J. (2010) Combination of NEP 1-40 treatment and motor training enhances behavioral recovery after a focal cortical infarct in rats. *Stroke*, **41**, 544-549.

Gilmour, G., Iversen, S.D., O'Neill, M.F., O'Neill, M.J., Ward, M.A. & Bannerman, D.M. (2005) Amphetamine promotes task-dependent recovery following focal cortical ischaemic lesions in the rat. *Behavioural brain research*, **165**, 98-109.

Greenwald, E., Masters, M.R. & Thakor, N.V. (2016) Implantable neurotechnologies: bidirectional neural interfaces—applications and VLSI circuit implementations. *Medical & biological engineering & computing*, **54**, 1-17.

Guggenmos, D.J., Azin, M., Barbay, S., Mahnken, J.D., Dunham, C., Mohseni, P. & Nudo, R.J. (2013) Restoration of function after brain damage using a neural prosthesis. *Proceedings of the National Academy of Sciences of the United States of America*, **110**, 21177-21182.

Hipp, J.F., Hawellek, D.J., Corbetta, M., Siegel, M. & Engel, A.K. (2012) Large-scale cortical correlation structure of spontaneous oscillatory activity. *Nat Neurosci*, **15**, 884.

Hira, R., Ohkubo, F., Tanaka, Y.R., Masamizu, Y., Augustine, G.J., Kasai, H. & Matsuzaki, M. (2013) In vivo optogenetic tracing of functional corticocortical connections between motor forelimb areas. *Frontiers in neural circuits*, **7**, 55.

Jackson, A., Mavoori, J. & Fetz, E.E. (2006) Long-term motor cortex plasticity induced by an electronic neural implant. *Nature*, **444**, 56-60.

Kleim, J.A., Barbay, S. & Nudo, R.J. (1998) Functional reorganization of the rat motor cortex following motor skill learning. *J Neurophysiol*, **80**, 3321-3325.

Nishibe, M., Barbay, S., Guggenmos, D. & Nudo, R.J. (2010) Reorganization of motor cortex after controlled cortical impact in rats and implications for functional recovery. *Journal of neurotrauma*, **27**, 2221-2232.

Paxinos, G. & Watson, C. (1998) The rat brain in stereotaxic coordinates. Vol. Academic Press, San Diego.

Song, W., Kerr, C.C., Lytton, W.W. & Francis, J.T. (2013) Cortical plasticity induced by spike-triggered microstimulation in primate somatosensory cortex. *PloS one*, **8**, e57453.

Vallone, F., Lai, S., Spalletti, C., Panarese, A., Alia, C., Micera, S., Caleo, M. & Di Garbo, A. (2016) Post-stroke longitudinal alterations of inter-hemispheric correlation and hemispheric dominance in mouse pre-motor cortex. *PloS one*, **11**, e0146858.

Von Stein, A., Chiang, C. & König, P. (2000) Top-down processing mediated by interareal synchronization. *Proceedings of the National Academy of Sciences*, **97**, 14748-14753.

Zakiewicz, I.M., Bjaalie, J.G. & Leergaard, T.B. (2014) Brain-wide map of efferent projections from rat barrel cortex. *Front Neuroinform*, **8**, 5.

Chapter 6 Effect of ICMS on healthy behaving animals

This chapter describes the main results obtained in the third set of experiments performed at Kansas University between 2016 and 2017. In particular, the characterization of the changes in intra-cortical neuronal activity induced by the ADS treatment using Chronic procedures while repeating the treatment for 21 consecutive days in healthy rats is described.

6.1. Introduction

As described in Chapter 5, recent studies (Adkins-Miur, 2003; Kleim *et al.*, 2003; Jackson *et al.*, 2006; Guggenmos *et al.*, 2013) have demonstrated that intracortical microstimulation can be successfully used to manipulate neuronal functional connectivity, representing a potentially powerful tool for steering neuroplasticity occurring after brain injury. One technique, i.e., activity-dependent stimulation (ADS), utilizes neural activity recorded at one site as a trigger for electrical stimulation at another site, and as previously described (see Chapter 2 and Chapter 4), ADS has shown success in promoting behavioral recovery by re-establishing an artificial connection between the somatosensory and pre-motor cortex following primary motor cortical injury (Guggenmos *et al.*, 2013).

In the ADS-treated rats in the previous study (Healthy Anesthetized group), neural activity in the RFA was significantly increased during the 28 ms following the stimulation in S1 (see Chapter 4, Healthy Anaesthetized). These results suggest that the network interactions between S1 and the RFA were reinforced by ADS during a single recording session in healthy anesthetized rodents (Averna *et al.*, 2018; Averna *et al.*, 2019).

The aim of the work presented in this chapter was to investigate the ability of ADS to alter the normal neural firing patterns of activity in the RFA and eventually potentiate the functional connectivity between distant cortical locations in awake behaving healthy animals. Thus, we tested the effect of two types of ICMS, i.e., ADS and

RS, on the spiking patterns of neurons recorded in the premotor cortex equivalent in rats, i.e., the rostral forelimb area (RFA), for 21 consecutive days in freely moving rats.

6.2. Methods

6.2.1. Animals

All experiments were approved by the University of Kansas Medical Center Institutional Animal Care and Use Committee. In total, 12 adult male Long-Evans rats (weight: 350-400 g, age: 4-5 months; Charles River Laboratories, Wilmington, MA, USA) were used in this study.

Table 6.2.1: Healthy Awake dataset. Grouping of Rats into Activity-Dependent Stimulation (ADS), Open Loop Stimulation (RS) and Control (CTRL).

	Stimulation Type		
	ADS	**RS**	**CTRL**
# Rats	5	5	2
Total	**12**		

6.2.2. Surgical Procedures

Anesthesia was induced with gaseous isoflurane prior to surgery within a sealed vaporizer chamber, followed by injections of ketamine (80-100 mg/kg IP) and xylazine (5-10 mg/kg). Maintenance boluses of ketamine (10-100 mg/kg/h ip or im) were repeatedly injected as needed throughout the procedure. A stereotaxic frame was used to secure the rat heads, and an anal temperature probe was used to monitor the rats' temperature. The rats' eyes were protected with ophthalmic ointment. Either Lidocaine/Prilocaine cream or bupivacaine was applied to the scalp prior to performing a skin incision spanning rostro-caudally between ~6 mm rostral to bregma and ~5 mm distal to the atlanto-occipital junction. The cisterna magna or upper vertebrae were exposed by reflecting the overlaying neck muscles. The spinal dura

located in the foramen magnum was slightly punctured to control brain edema by allowing CSF drainage. After the retraction of the temporalis muscle, a craniectomy was performed to expose the primary motor (Caudal Forelimb Area: CFA) and premotor (Rostral Forelimb Area: RFA) cortical areas. The electrophysiological procedures were facilitated by the removal of the dura and application of sterile silicone oil to the cortex. Following the craniectomy, six holes were created using a small drill bit for the skull screws and anchoring rod. The skull screws were implanted into the parietal and intraparietal bones and secured with dental acrylic. An additional dose of Penicillin (1.5 cc) was injected subcutaneously at the end of the surgical procedure to prevent bacterial infections.

6.2.3. Mapping Cortical Areas

The location of the RFA was determined using standard ICMS protocols (Kleim, 2003). Briefly, a glass microelectode (10-25 μm diameter) filled with saline was inserted into the cortex at a depth of ~1700 μm. Stimulus trains of 13-200 μs pulses at 333 Hz were applied at 1 Hz intervals using a stimulus isolator (BAK Electronics, Umatilla FL, USA). The current was increased until visible movement around a joint was observed up to 80 μA. The sites were sampled at a resolution of 250 μm. The RFA was defined as forelimb motor responses bordered caudally by neck and trunk responses and medially by face and jaw movements (Kleim *et al.*, 1998). Upon the completion of the surgical procedure, a picture of the vascular pattern of the cortical surface was taken and uploaded to a graphics program (Canvas GFX, Inc., Plantation, FL, USA), and a 250 μm grid was overlaid onto the image.

The somatosensory area was identified by correlating the neural recordings from a penetrating electrode to skin palpations. The micropipettes were advanced perpendicular to the cortical surface to a depth of ~1750 μm to maximally stimulate the descending pyramidal cells in cortical Layer V. Stimulation pulses consisting of 50 ms trains of 200 μs monophasic cathodal pulses were generated and delivered at 350

Hz through micropipettes. The identification of the motor field boundaries was performed by observing the movements evoked by electrical stimulation up to 80 μA. The RFA and CFA were localized with wrist extension, elbow flexion, and, occasionally, digit movements. Neck and face movement separated the RFA and CFA.

The forelimb sensory fields in S1 were identified with multi-unit recordings. A single-shank Michigan style electrode with sixteen recording sites (NeuroNexus, Ann Arbor, MI) was advanced into the sensory cortex to span across cortical layers II-V. The evoked sensory activity was monitored through a loudspeaker during the procedure. Further characterization of the spikes was performed by amplifying, digitizing, filtering, and displaying the recorded neural activity on a screen (TDT, Alchulta, FL). The electrode penetration sites that responded to palpation in the digits, paw and wrist were defined as forelimb sensory fields.

6.2.4. Experimental Protocol

A four-shank, sixteen-contact site electrode with 1-1.5 MΩ impedance at each site (A4x4-3mm-100-125-177-CM16LP, NeuroNexus) was chronically implanted into the RFA at a maximum depth of 1600 μm (Figure 6.2.1A). The probe was coupled to an active unity gain connector that was connected to the recording system (TDT, Alchulta, FL) through an amplifier. The neural data could be sorted based on the activity of near cells in real-time once the neural data acquisition system (TDT, Alchulta, FL) recorded the cell activity. A single contact site that detected the neural spiking data at a moderate rate of spontaneous activity (4-10 Hz) was selected as the trigger channel for stimulating a cortical site in the forelimb-responsive S1.

A second four-shank, sixteen-contact electrode (A4x4-3mm-100-125-177-CM16LP, NeuroNexus) was chronically implanted into S1 and used for stimulation through a single contact with ~200 KΩ impedance (Figure 6.2.1A). A stimulator isolator and passive headstage (MS16 Stimulus Isolator, TDT) delivered the stimulus. Each neuronal spike recorded from a single contact in the RFA triggered a single 60 μA

biphasic, cathodal-leading stimulus pulse (200 μs positive and 200 μs negative) in S1 after a 10 ms delay. In the RS designated rats, randomized stimuli (Gaussian distribution centered approximately 7 Hz) that approximated the observed frequency in the ADS rats (4-10 Hz) were used. Each stimulus was followed by a 28 ms blanking period to prevent stimulus-activated RFA spikes and stimulus artifacts from triggering stimulation. Before starting the protocol, each animal was allowed to recover from surgery for 5 days. Both groups were stimulated and recorded daily for 21 days. Each animal was allowed to move freely inside a self-made plastic cage (50x50x60 cm) for the entire duration of each experimental session (Figure 6.2.1C). The daily recording consisted of 80-minute periods of stimulation flanked by a 30-minute period (before stimulation) and a 90-minute period (after stimulation) of no stimulation for a cumulative 3 hours and 20 minutes of recorded data per day (Figure 6.2.1B).

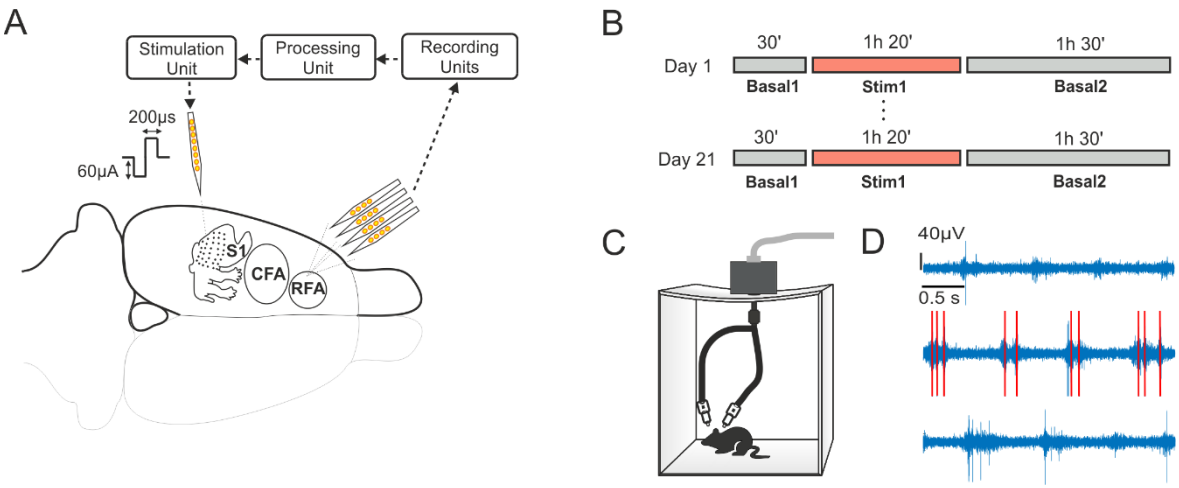

Figure 6.2.1: Experimental scheme in an implanted rat. A) A 4-shank array of recording electrodes is implanted in the left hemisphere; one neuron from the L-RFA is used to trigger stimulation in the somatosensory area (in the case of ADS). B) Timeline of the protocol. Each rat was treated for 21 consecutive days, and the protocol included two recordings of basal activity (30 min and 1 h and 30 min) and one stimulation session (1 h and 20 min). C) Each animal could freely move inside a transparent cage during the experimental session. Right, a sample trace recorded during the three experimental phases (red lines represent the deleted stimulation artifacts).

In the Control experiments, the daily recordings were performed identically, but the stimulation was set to 0 μA for the entire 3 hours and 20 minutes of recording.

6.2.5. Data Processing

In these experiments, wide-band neural data were recorded (Tucker-Davis Technologies - TDT, Alchulta, FL, USA) at ~ 25 kHz per channel. I analyzed the electrophysiological signals by investigating both temporal scales of the recorded signals (i.e., LFPs and SUA, see Chapter 3- Materials and Methods).

SUA

In the Healthy Awake experiments, the neural data were filtered through a band-pass filter (elliptic filter) in the bandwidth of the spikes (300-3000 Hz). A custom MATLAB script was used to identify the peaks in the extracellular electrical fields that corresponded to the action potentials of nearby neurons.

After the spikes were detected, epochs spanning -0.4 ms to +0.8 ms around the peak onset were included to create waveform "snippets" that were used for the feature extraction and unsupervised clustering using SPC (Blatt *et al.*, 1996). To improve the behavior of the decomposition step, the spike waveforms were interpolated to a sampling rate at which 100 samples span that range (the interpolation factor depends on the acquisition sample rate). Wavelets (specifically, MATLAB 'bior1.3' wavelet, with 3 decomposition scales) were used to decompose the spikes. This choice of wavelet was made empirically after observing the clustering results obtained using the following types of wavelets: '*haar*', '*bior1.3*', '*db4*', and *'sym8'* at scales ranging from 2-3. After the decomposition, the top 12 wavelet features were extracted using a heuristic to identify the features that provided good separation in the wavelet feature space. First, any wavelet coefficients that were very close to 0 (< 0.1*number of spikes) were immediately excluded. Then, the remaining coefficients were z-scored across all spikes. Kurtosis was computed for each remaining column of the wavelet coefficients. Because of the interpolation step, some coefficients with high kurtosis could be "near" each other and correspond to features of the spike that had a high correlation with one another; therefore, these coefficients were not useful in discriminating the spikes from

one another. This, MATLAB '*findpeaks*' was used again to identify the peaks in the distribution of kurtosis scores in each wavelet coefficient. Thus, the peaks in kurtosis in the wavelet coefficients along different points of the spike were emphasized and used to select the wavelet coefficients used for SPC for the unsupervised clustering. The procedure described above was then repeated for each recording channel.

Mean Firing Rate (MFR)

I evaluated the neuronal firing rates before and after the stimulation by calculating the average firing rate during each period. Neurons whose firing rate was less than 0.01 spikes/s were discarded. I determined whether the difference in the firing rates of a given unit between two time-points significantly deviated from a null (zero centered) distribution using the bootstrapping method (Slomowitz *et al.*, 2015). The two time segments compared (Basal1 and Basal2) were divided into 1-min bins, which were then randomly shuffled 10,000 times into two groups. The differences between the means of the two randomly shuffled groups produced a null-distribution. The real difference was significant if it fell outside of the 95% confidence interval of the null-distribution.

I/O pairwise correlation

To evaluate the effect of the local stimulation on the evoked spiking activity of each single unit detected, the I/O algorithm (see Chapter 3, Materials and Methods, 3.2.2 Data Analysis) was implemented in MATLAB. Briefly, each single unit's firing rate and stimulation train delivered during each experimental session were binned into a 1-ms time resolution. The resulting signal was low-pass filtered to obtain the instantaneous firing rate of the single units (IFR) and instantaneous stimulus rate (ISR) of the ICMS (Figure 6.3.4A). A cross-correlation was used to analyze each pair of signals. I evaluated the maximum value of the normalized cross-correlation (MX) in a 30-s window across its 0-lag point. Such a value, in the case of the ADS experiments, was compensated for intrinsic correlations (See Chapter 3- Materials and Methods, Figure 3.2.5) and considered significative only when greater than the 95th percentile of the surrogates'

distribution. The identified units with significant correlations and positive lag of MX were considered in computing the number of stimulus-associated responses and the amount of evoked activity (PSTH).

Post-Stimulus Time Histogram

I calculated the Post-Stimulus Time Histograms (PSTH) (Rieke *et al.*; Rieke, 1999) (1 ms bins, normalized across the total number of stimulation pulses) of the stimulus-associated action potentials of each sorted unit during the 28 ms following the stimulus pulses delivered from S1. The area under the normalized PSTH curve was used to quantify the total amount of stimulation-evoked neural activity during each stimulation phase. Only the units with significant responses were considered in this analysis (see Materials and Methods, I/O pairwise correlation).

LFP

The wide-band signals were first down-sampled to 1 kHz, followed by low pass filtering below 500 Hz to prevent aliasing. Then, I computed the power spectral density of the decimated signal (dB/Hz) using the Welch method [Windows = 5 s, overlap = 50%; DFT (Discrete Fourier Transform) points = 8192; df (frequency resolution) = 0.12 Hz; dt (temporal resolution) = 8.19 s]. I only considered the lower frequency bands of the signal, which are of particular interest due to their association with many brain processes; in particular, the delta (1–4 Hz), theta (4–11 Hz), beta (11–30 Hz), low-gamma (30–55 Hz) and high-gamma (55-130) bands were considered. To characterize the LFP, the PSD was calculated for each of these frequency bands and normalized in two different ways to highlight the differences induced by the stimulation. A 10ms blanking window around each stimulation pulse (2ms before and 8ms after) has been considered on the raw data to prevent artifact contamination of the signal. The baseline power spectral densities (during Basal1) were normalized across the total power of the LFP of each specific channel (Figure 6.3.6C, Left) to evaluate the differences among the experimental groups. To quantify the changes induced by the stimulation protocols, the power at each frequency calculated during Stim and Basal2 was normalized to the

average power of that frequency during the baseline period, i.e., Basal1 (Figure 6.3.6C, Center, Right).

6.3. Results

6.3.1. ICMS induces no changes in Firing Rate in awake animals

First, I examined the change in the MFR between the baseline phase and subsequent basal periods following ICMS. Figure 6.3.1 shows a representative experiment in which ICMS (ADS in the figure) did not produce any qualitative change in firing between Basal1 (left) to Basal2 (right) or an alteration in the array-wide spiking activity of the network (Figure 6.3.1, bottom).

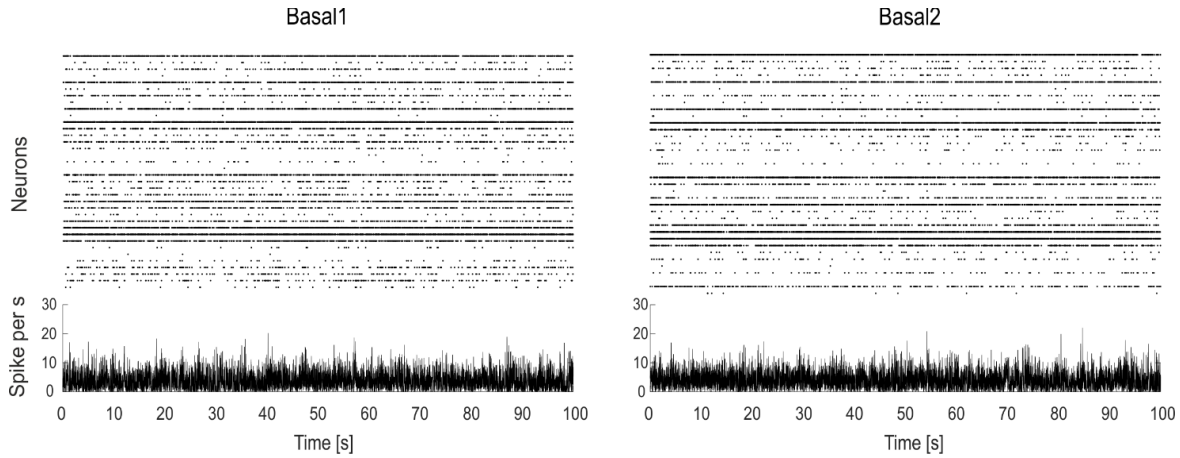

Figure 6.3.1: Firing rate analysis. Spike rasters (dotted graphs, one row per neuron) and corresponding array-wide firing rate (line graphs) measured by summing all spikes detected on the entire array in a 1-ms window during a 100-s time frame during Basal1 (left) and Basal4 (right) in a single animal subjected to the ADS protocol.

No changes in firing were found even after evaluating the cross-day changes in the instantaneous firing rates (Figure 6.3.2).

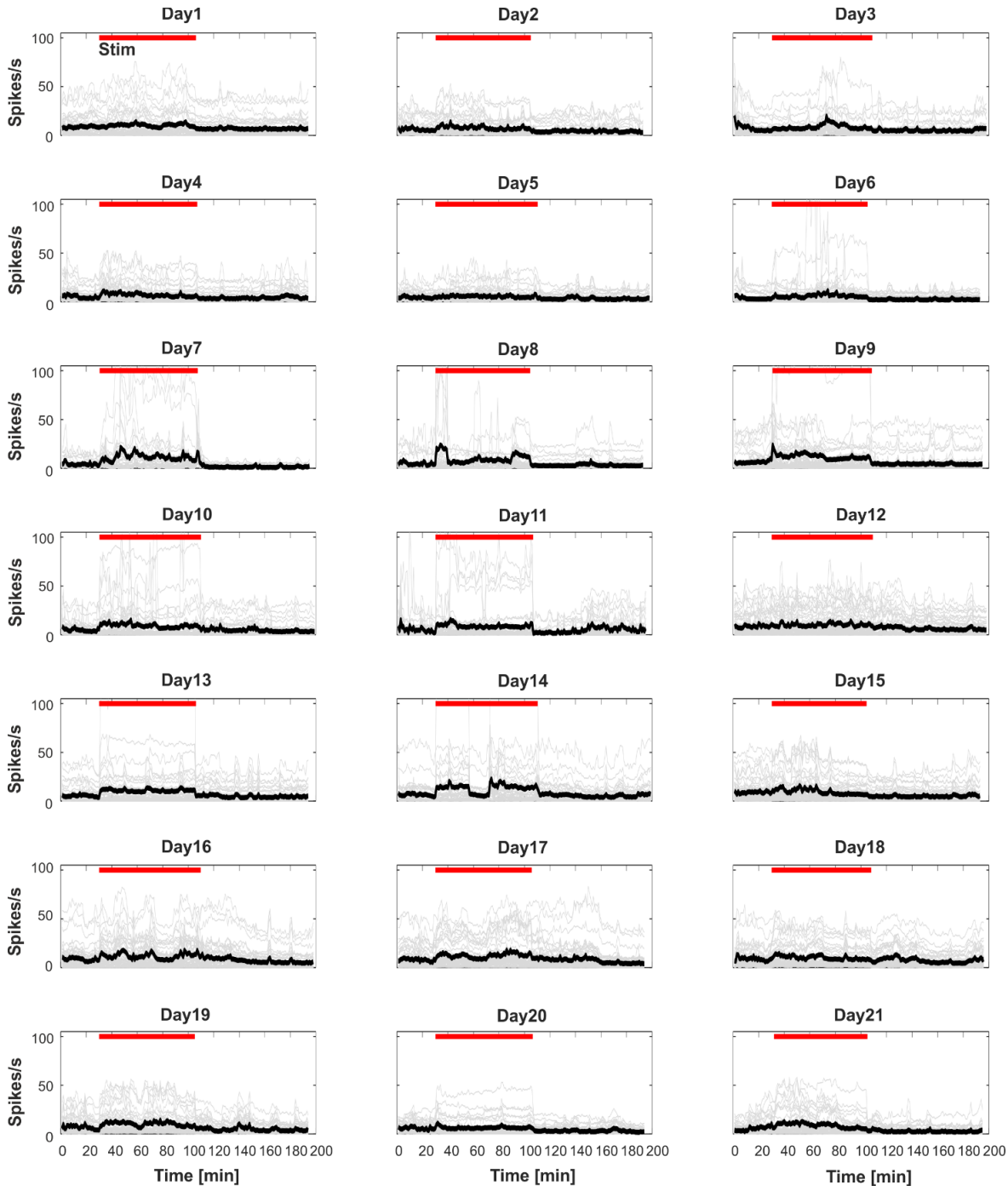

Figure 6.3.2: Firing rate changes across days. Each box represents the instantaneous firing rate (IFR) in 1 min bind of all single units (gray line) and the average IFR (black line) calculated during each of the 21 days of recordings over the entire duration of the experiment. Red line indicates the Stim phase.

Notably, no experimental condition (ADS and RS) differed from the control experiments (CTRL) (Figure 6.3.3A). Then, we quantified the number of units (i.e., neurons) whose firing rates increased, decreased or remained constant after the stimulation protocol (i.e., Basal2) with respect to the baseline period of recordings (i.e., Basal1) as shown in Figure 6.3.3B. All stimulation protocols induced a significantly greater number of units showing constant firing rates (No Change) compared to Basal1 (Figure 6.3.3C), showing that the behavior was the same as that of the control group.

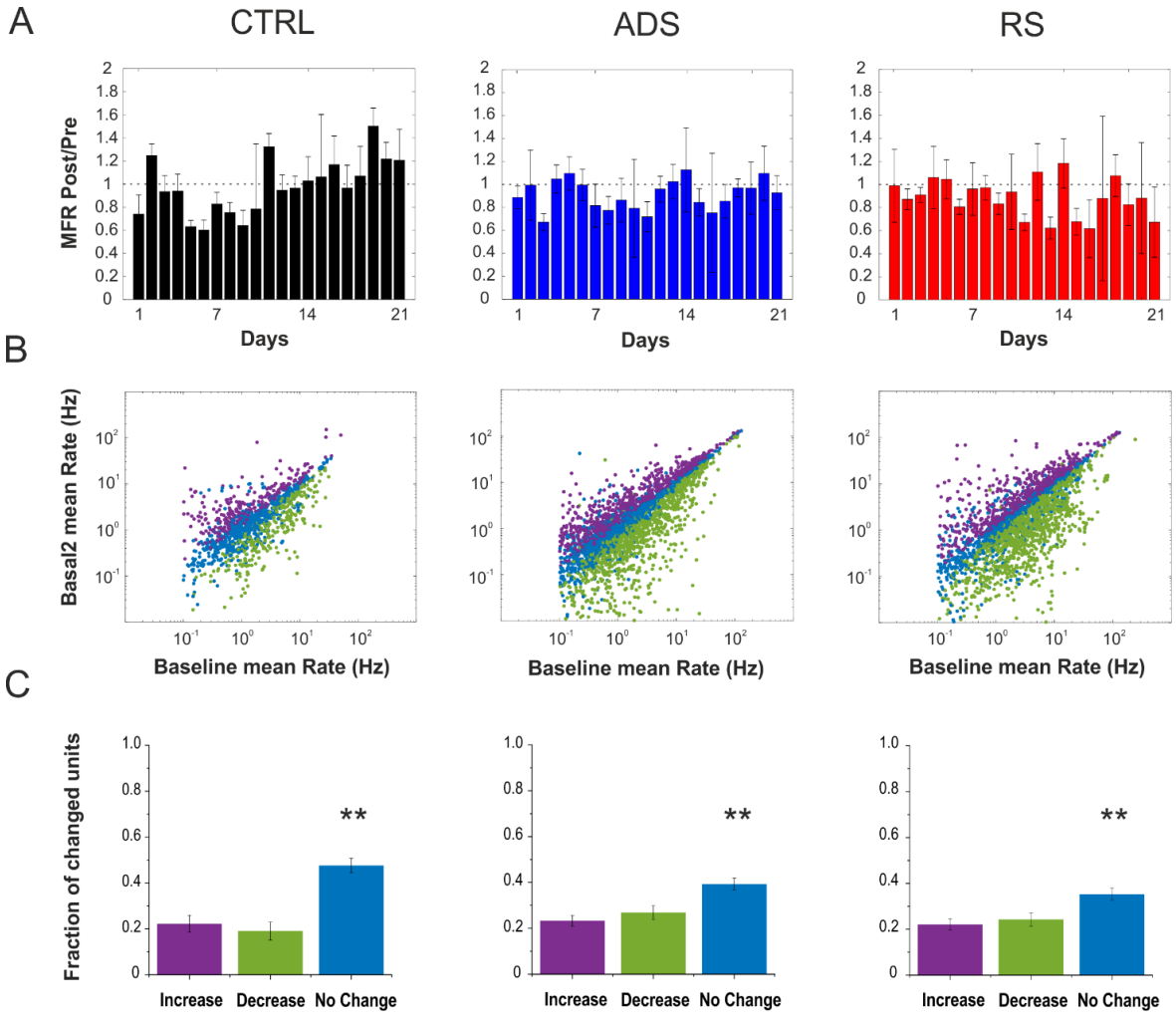

Figure 6.3.3: A) Quantitative representation of the Mean Firing Rate (MFR) changes induced by the stimulation. Each unit's firing calculated after the stimulation was divided by its value calculated during Basal1. B) Per unit correlation between the baseline firing rates (x-axis, Basal1) and the firing rates after the stimulation session (y-axis, Basal2) calculated per group (CTRL, ADS, and RS). Colors represent units that significantly increased (magenta), decreased (blue) or remained stable (green). C) Average fraction of units that significantly changed their firing with respect to the baseline period of recording (Basal1) calculated in all three experimental groups (**p <

0.01; Kruskal-Wallis one-way analysis of variance of ranks with Dunnett's multiple comparison test. Error bars represent the SEM). The data are reported as the median ± SEM (standard error of the median).

6.3.2. ADS produces more significant stimulus-associated responses than RS

The evoked response to the stimulation was analyzed using both post-stimulus time histograms following each stimulation pulse and I/O pairwise correlation (see Materials and Methods). We used a fixed length blanking window (5 ms, Figure 6.3.4A). As shown in Figure 6.3.4B, the interstimulus intervals used for the RS groups comprised a range of values comparable to those in the ADS group; in contrast to the Healthy Anaesthetized experiments, the bias between the interstimulus intervals calculated for ADS and RS was not present towards 200 ms but was evident at approximately 100 ms (higher for RS) and between 200 ms to 1 s (higher for ADS). Figure 6.3.4C display the IFR and ISR traces (in black and orange, respectively) over 1 s of recordings. To consider the correlations that were effectively induced by the stimulation, only the significant MX values with positive lags were considered in the following analysis (see Materials and Methods, I/O pairwise correlation). Figure 6.3.4D shows the functions of the significant evoked responses calculated in the two stimulation groups (ADS and RS). The PSTH derived from the neural recordings in the RFA by discriminating the spiking activity during the 28 ms after each S1 stimulus pulse was computed for both ADS and RS groups (Figure 6.3.4E). Even if the trend of the evoked activity did not differ between the stimulation protocols, a significant difference was found by quantifying the number of stimulus-associated spikes (in terms of the PSTH area) in the ADS and RS groups (Figure 6.3.4F). Furthermore, the spiking activity in response to ADS was significantly more correlated to the stimulation than that in response to RS (Figure 6.3.4G).

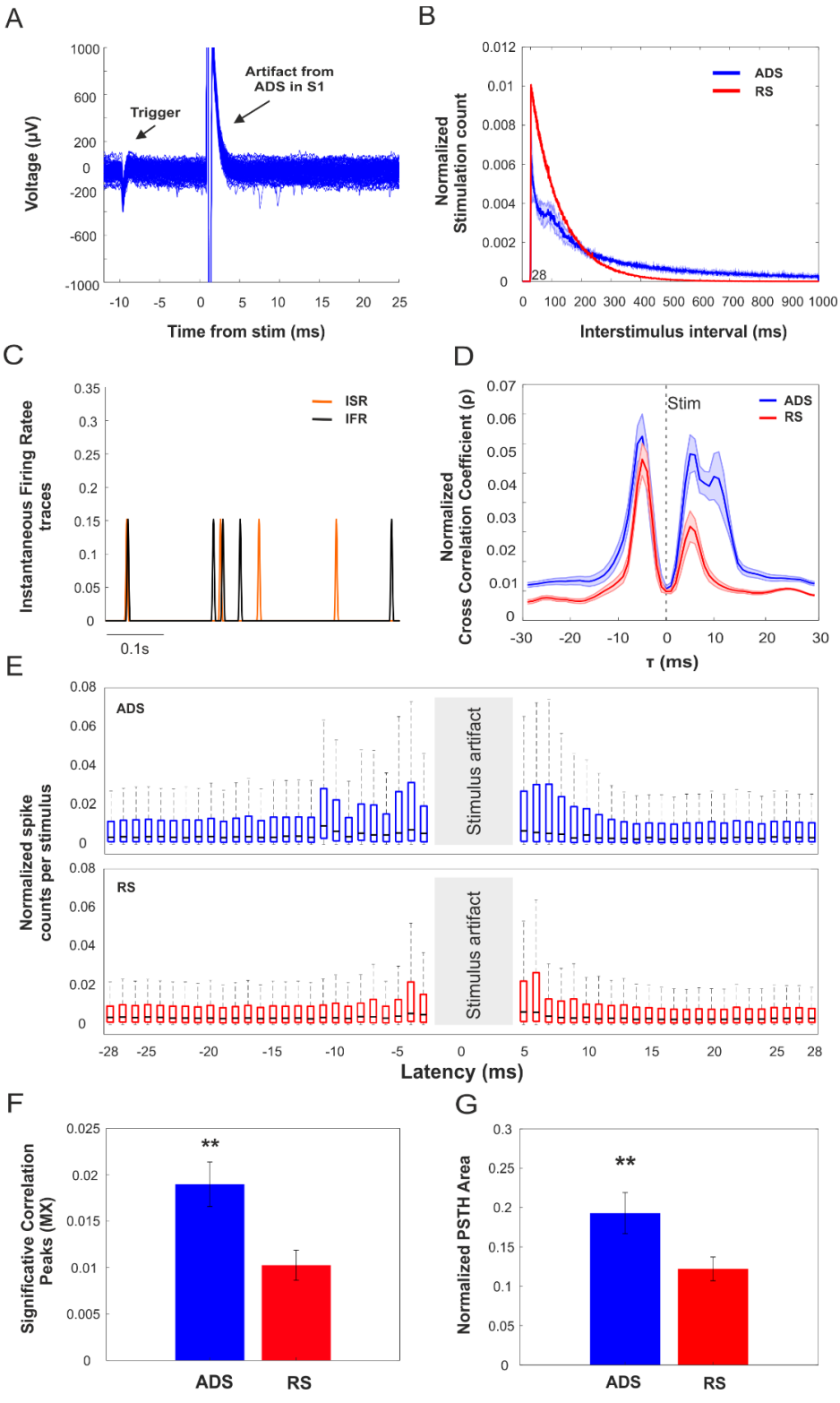

Figure 6.3.4: A) Sample trace of recordings from the RFA showing stimulus artifacts from ADS delivered to S1 and activity of the trigger unit. In total, 100 superimposed traces are shown. B) Stimulation interval distribution

(mean±STD, 1 s) in both representative ADS and RS subjects. Stimulation counts were normalized to the session length. C) Instantaneous firing rate (IFR, black trace) and instantaneous stimulation rate (ISR, orange trace) in a representative experiment. In total, 1 s of activity is reported. D) Correlation traces of the significant evoked responses in the two groups (ADS, blue and RS, red Post-stimulus spiking histograms (median±Sterr of median) derived from the neural recordings in the RFA by pooling all 21 days of stimulation sessions in the two ICMS groups (ADS, blue and RS, red). E) Histograms portraying the average number of action potentials discriminated from the neural recordings within 1-ms bins in 28 ms windows before and after each stimulation pulse. Data pooled across subjects per group and normalized to the total number of either ADS or RS events. F) Normalized PSTH areas (median±Sterr of median) in the two groups of ICMS. Input and output correlations). G) Averaged correlation values (median±Sterr of median) in the two groups of ICMS (**p < 0.001; Mann-Whitney Rank Sum test. Error bars represent SEM).

6.3.3. ICMS induces changes in LFP oscillatory activity

The power of LFP was calculated at each electrode during each specific experimental phase (i.e., Basal1, Stim, and Basal2). ICMS produced an increase in the LFP power during the Stim phase (Figure 6.3.5A) with respect to Basal1 and the Control group, particularly in the higher frequency bands (θ, β and γ, Figure 6.3.5A, B, values greater than 1 in figure 6.3.5C, Center). On the other hand, a significant decrease of power was found for delta (δ, Figure 6.3.5A, B, values lower than 1 in figure 6.3.5C, Center). No differences were found during the baseline period of recording as shown in Figure 6.3.5C (Left). A different effect is shown during Basal2, where a comparable the level of power with respect to Basal1 was observed in all groups, except for an increase of the delta band in the ADS group and a decrease of the high gamma in the RS (θ and high γ, Figure 6.3.5C, right).

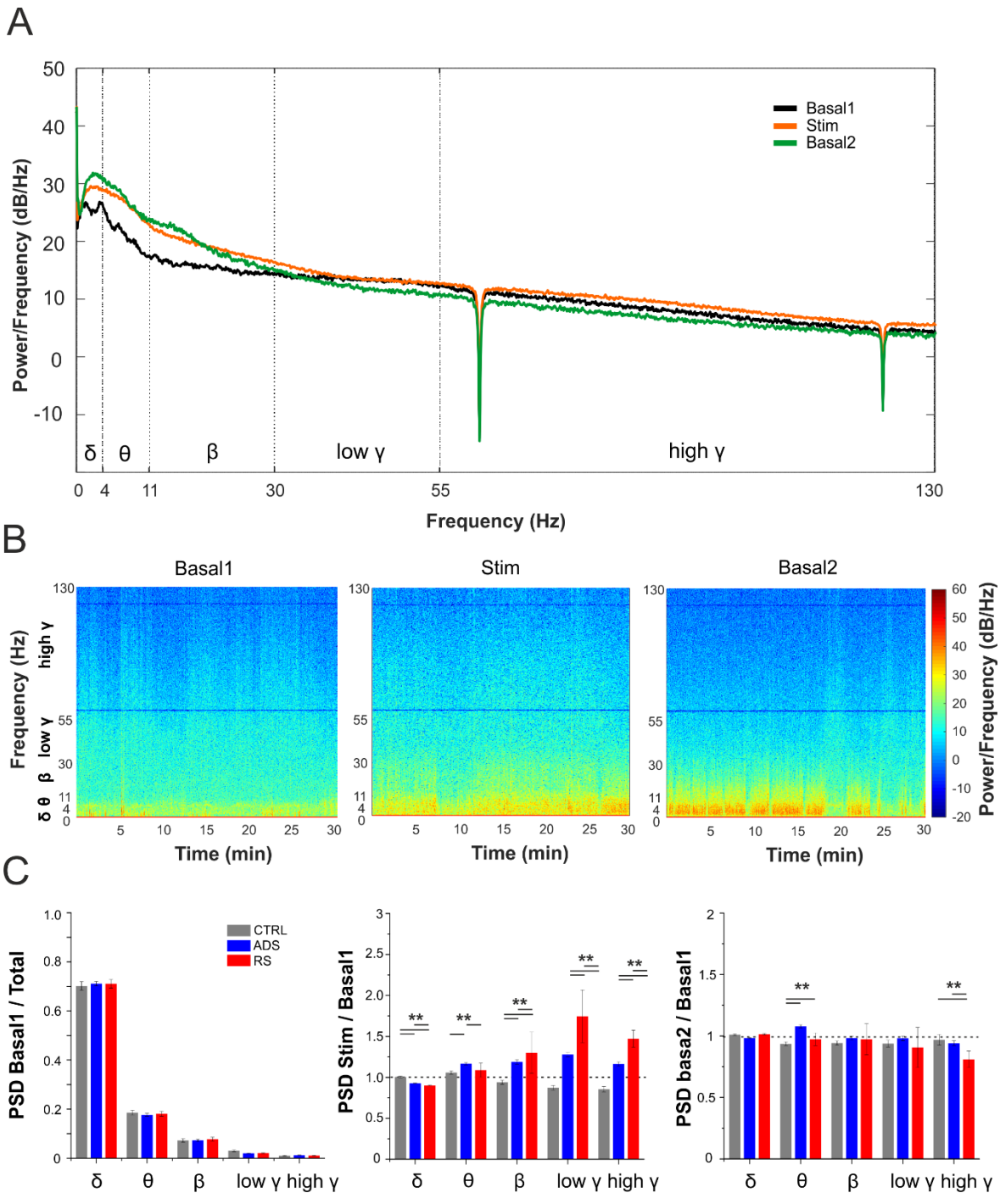

Figure 6.3.5: A) PSD calculated during different experimental phases at a representative electrode following ADS. B) Spectrogram showing the time variation in PSD in the different LFP bands. C) Column bar representing the integrated normalized PSD per frequency band during different experimental phases in all experimental groups (CTRL, ADS and RS) (**p < 0.01; Kruskal-Wallis one-way analysis of variance of ranks with Dunn's all pairwise multiple comparison test. Error bars represent the SEM). The data are reported as the median ± SEM (standard error of the median).

6.4. Discussion

ICMS of the somatosensory area (S1) has been previously shown to be effective in altering the intracortical activity of the RFA in healthy anesthetized rats in a single recording session (see Chapter 4) (Averna *et al.*, 2018; Averna *et al.*, 2019). That study demonstrated that ICMS, regardless of the type of stimulation (ADS or RS), induced an increase in the firing rate during a subsequent period of recording and that ADS (but not RS) facilitated incremental increases in stimulus-associated activity over time, thus suggesting that this protocol may lead to a stronger association over more prolonged stimulation sessions.

It has already been demonstrated that at the population level, the spatiotemporal structure of spikes firing in the awake cortex cannot be directly inferred from activity recorded in the anesthetized cortex, even when considering the same neuronal population (Greenberg *et al.*, 2008). Therefore, this study aimed to investigate the effect induced by ICMS on a cortical network not affected by anesthesia by considering awake behaving animals over 21 days of recording.

To determine the impact of ICMS on distant cortical regions under these experimental conditions, either ADS or RS (either activity-triggered stimulation (closed-loop) or randomized stimulation (open-loop)) was applied to the forelimb somatosensory area (S1FL) while recording the resulting activity in the RFA. To contrast to the findings in the Healthy Anesthetized animals (see Chapter 4), ICMS (both ADS and RS) did not induce any changes in the firing rate during the basal period after the stimulation compared to the non-stimulated controls (Figure 6.3.1, 6.3.2, 6.3.3). Based on an examination of the stimulation sessions, ADS induces a greater level of stimulus-associated activity than RS (Figure 6.3.4F), and furthermore, such evoked activity was demonstrated to be much more correlated with the stimulation train (Figure 6.3.4G). The analysis in the low frequency domain (LFPs) showed an increase in the LFP power during the stimulation phase (Figure 6.3.5A) in the higher frequency

bands (θ, β and γ, Figure 6.3.5A, B, values greater than 1 in figure 6.3.5C, center) in both ICMS groups (ADS and RS). An increase of the theta band was shown also during Basal2, but just for the ADS group. On the contrary, RS resulted to be effective in decreasing the power in the high gamma frequency band (Figure 6.3.5D, right).

The fact that no differences were found in the firing rate in the awake animals with respect to the healthy anesthetized cases could be explained by the different population-wide firing properties, such as the synchronization and relationship between the correlation and the firing rate, which are typically modulated by anesthesia (Greenberg *et al.*, 2008). This, in fact, represents a different starting point for the two experimental groups (anesthetized and awake).

Both ICMS protocols in the S1 produced an evoked spiking activity in the RFA (Figure 6.3.4E), but ADS was more effective in both evoking direct neuronal responses (Figure 6.3.4F) and recruiting stimulus-correlated activity (Figure 6.3.4G), thus suggesting its greater efficacy. Indeed, ADS is hypothetically more suited to inducing spike-timing-dependent plasticity due to the near synchronization between the recording and stimulation regions in this study. Despite the greater number of stimulation pulses and the higher mean firing rate observed during the stimulation phase (see Appendix, Figure A1 A, B), the RS treatment induced an overall decrease in correlated activity after the stimuli (Figure 6.3.4D) and a lower level of stimulus-associated activity than ADS (Figure 6.3.4F and 6.3.4G), thus suggesting a general inhibitory effect produced by this protocol.

The changes in the LFP were shown to be induced by ICMS during both the stimulation session (Stim, Figure 6.3.5C, center) and the subsequent period of recording (Basal 2, Figure 6.3.5C, Right). The increases in power observed during the stimulation reflect both a greater degree of local (RFA) communications (gamma bands (Womelsdorf *et al.*, 2007)) and enhanced synchronization between distant regions (theta and beta bands (Von Stein *et al.*, 2000)). Even in this case, ADS produced a different level of power during the basal period after the stimulation (Basal 2) with

respect to RS, inducing an increase of the delta band which is related to synaptic plasticity processes (Huerta & Lisman, 1993; Wespatat *et al.*, 2004), thus suggesting a more sustained effect of the stimulation.

These results further confirm the ability of Hebbian-inspired protocols to modulate electrophysiological activity by potentiating cortico-cortical connections between distant cortical locations in healthy brains. Thus, these findings suggest that ADS can be successfully used for neuroprosthetic applications in the case of brain lesions.

List of Selected pubblications

Presentations at international conference

Averna A, Guggenmos D, Pasquale V, Semprini M, Nudo RJ and Chiappalone M. *Long-term effect of intracortical microstimulation in awake behaving rats*. **Poster presentation**. Sixth National Congress of Bioengineering (GNB)– June 25-27, 2018. Milan, Italy.

References

Adkins-Miur, D.L., Jones, T. A. (2003) Cortical electrical stimulation combined with rehabilitative training: Enhanced functional recovery and dendritic plasticity following focal cortical ischemia in rats. *Neurological Research*, **25**, 780-788.

Averna, A., Guggenmos, D., Pasquale, V., Semprini, M., Nudo, R. & Chiappalone, M. (Year) Neuroengineering Tools For Studying The Effect Of Intracortical Microstimulation In Rodent Models. 2018 40th Annual International Conference of the IEEE Engineering in Medicine and Biology Society (EMBC). IEEE, City. p. 3076-3079.

Averna, A., Pasquale, V., Murphy, M., Rogantin, M.P., Van Acker, G., Nudo, R., Chiappalone, M. & Guggenmos, D. (2019) Differential effects of open- and closed-loop intracortical microstimulation on firing patterns of neurons in distant cortical areas. *bioRxiv*, 534032.

Blatt, M., Wiseman, S. & Domany, E. (1996) Superparamagnetic clustering of data. *Physical review letters*, **76**, 3251.

Greenberg, D.S., Houweling, A.R. & Kerr, J.N. (2008) Population imaging of ongoing neuronal activity in the visual cortex of awake rats. *Nat Neurosci*, **11**, 749.

Guggenmos, D.J., Azin, M., Barbay, S., Mahnken, J.D., Dunham, C., Mohseni, P. & Nudo, R.J. (2013) Restoration of function after brain damage using a neural prosthesis. *Proceedings of the National Academy of Sciences of the United States of America*, **110**, 21177-21182.

Huerta, P.T. & Lisman, J.E. (1993) Heightened synaptic plasticity of hippocampal CA1 neurons during a cholinergically induced rhythmic state. *Nature*, **364**, 723.

Jackson, A., Mavoori, J. & Fetz, E.E. (2006) Long-term motor cortex plasticity induced by an electronic neural implant. *Nature*, **444**, 56-60.

Kleim, J.A., Barbay, S. & Nudo, R.J. (1998) Functional reorganization of the rat motor cortex following motor skill learning. *J Neurophysiol*, **80**, 3321-3325.

Kleim, J.A., Bruneau, R., VandenBerg, P., MacDonald, E., Mulrooney, R. & Pocock, D. (2003) Motor cortex stimulation enhances motor recovery and reduces peri-infarct dysfunction following ischemic insult. *Neurol Res*, **25**, 789-793.

Kleim, J.A., Bruneau, R., VandenBerg, P., MacDonald, E. (2003) Motor cortex stimulation enhances motor recovery and reduces peri-infarct dysfunction following ischemic insult. *Neurological Research*, **25**, 789-793.

Rieke, F. (1999) *Spikes: exploring the neural code*. MIT press.

Rieke, F., Warland, D. & de Ruyter, v.S. R., & Bialek, W.(1997). Spikes: Exploring the neural code. *MITpress, Cambridge, Massachusetts*.

Slomowitz, E., Styr, B., Vertkin, I., Milshtein-Parush, H., Nelken, I., Slutsky, M. & Slutsky, I. (2015) Interplay between population firing stability and single neuron dynamics in hippocampal networks. *Elife*, **4**.

Von Stein, A., Chiang, C. & König, P. (2000) Top-down processing mediated by interareal synchronization. *Proceedings of the National Academy of Sciences*, **97**, 14748-14753.

Wespatat, V., Tennigkeit, F. & Singer, W. (2004) Phase sensitivity of synaptic modifications in oscillating cells of rat visual cortex. *Journal of Neuroscience*, **24**, 9067-9075.

Womelsdorf, T., Schoffelen, J.-M., Oostenveld, R., Singer, W., Desimone, R., Engel, A.K. & Fries, P. (2007) Modulation of neuronal interactions through neuronal synchronization. *science*, **316**, 1609-1612.

Conclusions

The study reported in this PhD thesis aimed to characterize, in depth, the electrophysiological correlates of the anatomical and behavioral recovery induced by the following particular Hebbian-inspired intracortical microstimulation protocol: activity-dependent stimulation (ADS) (Jackson *et al.*, 2006; Guggenmos *et al.*, 2013). This technique utilizes the neural activity recorded at one site as a trigger for electrical stimulation at another site, and indeed, ADS has shown success in promoting behavioral recovery by re-establishing an artificial connection between the somatosensory and pre-motor cortex following primary motor cortical injury (Guggenmos *et al.*, 2013). To test the ability of ADS to alter the physiological cortical firing patterns, three different in vivo experimental procedures involving both healthy and injured cortical networks were conducted.

The first experimental design described in Chapter 4 proved that in healthy anesthetized animals, intracortical microstimulation (ICMS) in different somatosensory regions (S1FL and S1BF) produces different effects on the recorded activity in the premotor cortex equivalent in rats (RFA) (Averna *et al.*, 2018; Averna *et al.*, 2019). In particular, the two different ICMS protocols tested, i.e., ADS and a randomized version of ADS (RS), were shown to produce an increase in the firing rate and a consequent decrease in the interspike intervals of the recorded units. Interestingly, ADS was more effective in facilitating incremental increases in evoked activity over time compared to RS.

Second, the ability of ADS to reconnect the sensory-motor loop following a M1 ischemic lesion in anesthetized rats was determined (Chapter 5). A stroke lesion in M1 was found to decrease the integrated power of the LFPs within both the RFA and S1 and modulate the cortico-cortical connectivity by increasing the number of functional connections between the two distant brain regions. ADS treatment after the ischemic lesion induced a significant increase in the LFP power in both the RFA and S1, thus reestablishing the local cortical activity in the two areas. Moreover, this treatment manipulated both intra-cortical and inter-cortical connectivity. ADS enhanced the LFP

intra-cortical correlations (especially within S1) and increased the number of functional inter-cortical connections in the θ and α bands, suggesting a reorganization of the information flow among these cortical regions (RFA and S1).

The final experimental design (Chapter 6) was aimed at investigating the effect induced by ICMS on a cortical network that was not affected by anesthesia, thus considering healthy awake behaving animals over 21 days of recording. The main difference from the healthy anesthetized experiment was the absence of changes in the firing rate of the recording units after the stimulation. However, interestingly, ADS was more effective in both evoking direct neuronal responses and recruiting stimulus-correlated activity, thus suggesting its greater efficacy. This result was further confirmed by analysis of the low frequencies of the neuronal signals (LFP). Here, ADS produced a different degree of power during the period of recording after the stimulation with respect to RS, inducing an increase in the theta band, which is related to synaptic plasticity processes (Huerta & Lisman, 1993; Wespatat *et al.*, 2004).

Taken together, these results suggest that both RS and ADS contribute to inducing the electrophysiological changes associated with behavioral recovery, but by somewhat different mechanisms. In general, ICMS is likely to modulate neuronal growth processes, leading to adaptive plasticity that could account for at least some of the major changes in the electrophysiological activity observed under the experimental conditions considered. However, under the closed-loop condition (ADS), the intrinsic firing pattern drives the cortical network to the greatest neuronal activity changes, thus suggesting its better ability to make the most of the functional connection between S1 and the RFA.

Although limited in scope, this study provides valuable insight into the electrophysiological mechanisms underlying behavioral recovery after brain injury as demonstrated in the study conducted by Guggenmos *et al*. (Guggenmos *et al.*, 2013). Moreover, the differences in the electrophysiological responses between the ADS and RS treatments are beginning to be revealed. The knowledge that open- and closed-loop

stimulation protocols can impact neuroplasticity in both healthy brains and in the absence of acute brain injury has clinical significance. This finding perhaps opens the possibility of using closed-loop approaches in patients living with disabilities due to previous stroke or TBI and the discovery of treatment options for a variety of conditions in which neural communication is disrupted regardless of whether the conditions are due to disease, injury or idiopathic causes.

References

Averna, A., Guggenmos, D., Pasquale, V., Semprini, M., Nudo, R. & Chiappalone, M. (Year) Neuroengineering Tools For Studying The Effect Of Intracortical Microstimulation In Rodent Models. 2018 40th Annual International Conference of the IEEE Engineering in Medicine and Biology Society (EMBC). IEEE, City. p. 3076-3079.

Averna, A., Pasquale, V., Murphy, M., Rogantin, M.P., Van Acker, G., Nudo, R., Chiappalone, M. & Guggenmos, D. (2019) Differential effects of open- and closed-loop intracortical microstimulation on firing patterns of neurons in distant cortical areas. *bioRxiv*, 534032.

Guggenmos, D.J., Azin, M., Barbay, S., Mahnken, J.D., Dunham, C., Mohseni, P. & Nudo, R.J. (2013) Restoration of function after brain damage using a neural prosthesis. *Proceedings of the National Academy of Sciences of the United States of America*, **110**, 21177-21182.

Huerta, P.T. & Lisman, J.E. (1993) Heightened synaptic plasticity of hippocampal CA1 neurons during a cholinergically induced rhythmic state. *Nature*, **364**, 723.

Jackson, A., Mavoori, J. & Fetz, E.E. (2006) Long-term motor cortex plasticity induced by an electronic neural implant. *Nature*, **444**, 56-60.

Wespatat, V., Tennigkeit, F. & Singer, W. (2004) Phase sensitivity of synaptic modifications in oscillating cells of rat visual cortex. *Journal of Neuroscience*, **24**, 9067-9075.

Chapter 7 Appendix

Table A1: Results of the mixed procedure test on the logarithmic firing rate log(MFR): differences of Least Squares Means (the marginal means are estimated over a balanced population) calculated for the Stim*Area*t effect. Significant p-values are colored: p-value .01-.05 (weak evidence) yellow, p-value <.01 (very strong evidence) red.

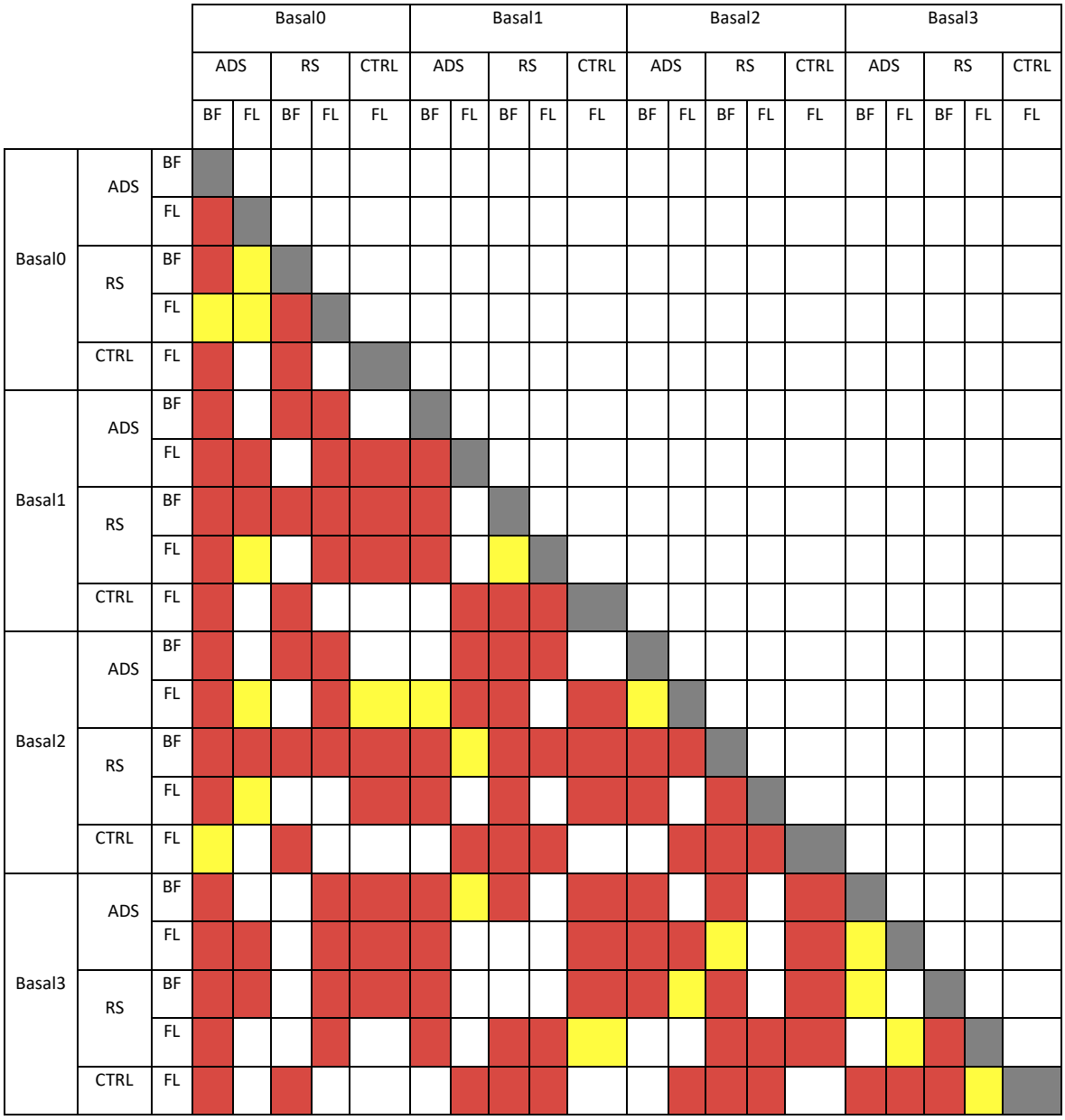

Table A2: Results of the mixed procedure test on the LvR: differences of Least Squares Means (the marginal means are estimated over a balanced population) calculated for the Stim*Area*t effect. Significant p-values are colored: p-value .01-.05 (weak evidence) yellow, p-value <.01 (very strong evidence) red.

			Basal0					Basal1					Basal2					Basal3				
			ADS		RS		CTRL	ADS		RS		CTRL	ADS		RS		CTRL	ADS		RS		CTRL
			BF	FL	BF	FL	FL	BF	FL	BF	FL	FL	BF	FL	BF	FL	FL	BF	FL	BF	FL	FL
Basal0	ADS	BF																				
		FL																				
	RS	BF																				
		FL																				
	CTRL	FL																				
Basal1	ADS	BF																				
		FL																				
	RS	BF																				
		FL																				
	CTRL	FL																				
Basal2	ADS	BF																				
		FL																				
	RS	BF																				
		FL																				
	CTRL	FL																				
Basal3	ADS	BF																				
		FL																				
	RS	BF																				
		FL																				
	CTRL	FL																				

Table A3: Results of the mixed procedure test on the PSTH: differences of Least Squares Means (the marginal means are estimated over a balanced population) calculated for the Stim*Area*t effect. Significant p-values are colored: p-value .01-.05 (weak evidence) yellow, p-value <.01 (very strong evidence) red.

			Stim1				Stim2				Stim3			
			ADS		RS		ADS		RS		ADS		RS	
			BF	FL	BF	FL	BF	FL	BF	FL	BF	FL	BF	FL
Stim1	ADS	BF												
		FL												
	RS	BF												
		FL												
Stim2	ADS	BF												
		FL												
	RS	BF												
		FL												
Stim3	ADS	BF												
		FL												
	RS	BF												
		FL												

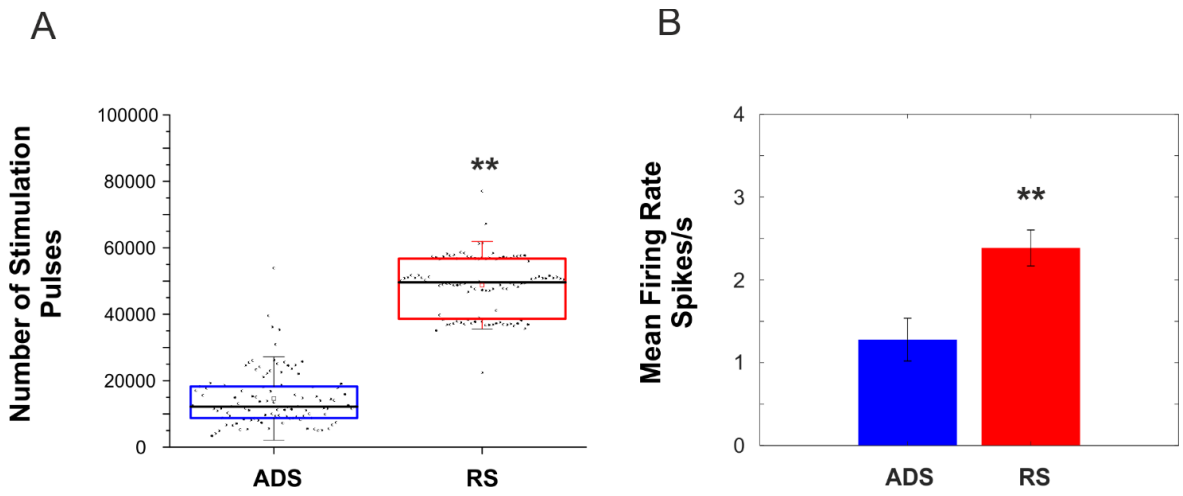

Figure A1: A) number of pulses provided by the two stimulation protocols, ADS (blue) and RS (red). B) Mean Firing Rate (median±STerr of median) calculated during the stimulation phase (Stim) for the two groups. Data pooled across subjects for each group. (**p < 0.001; Mann-Whitney Rank Sum test. Error bars represent SEM)

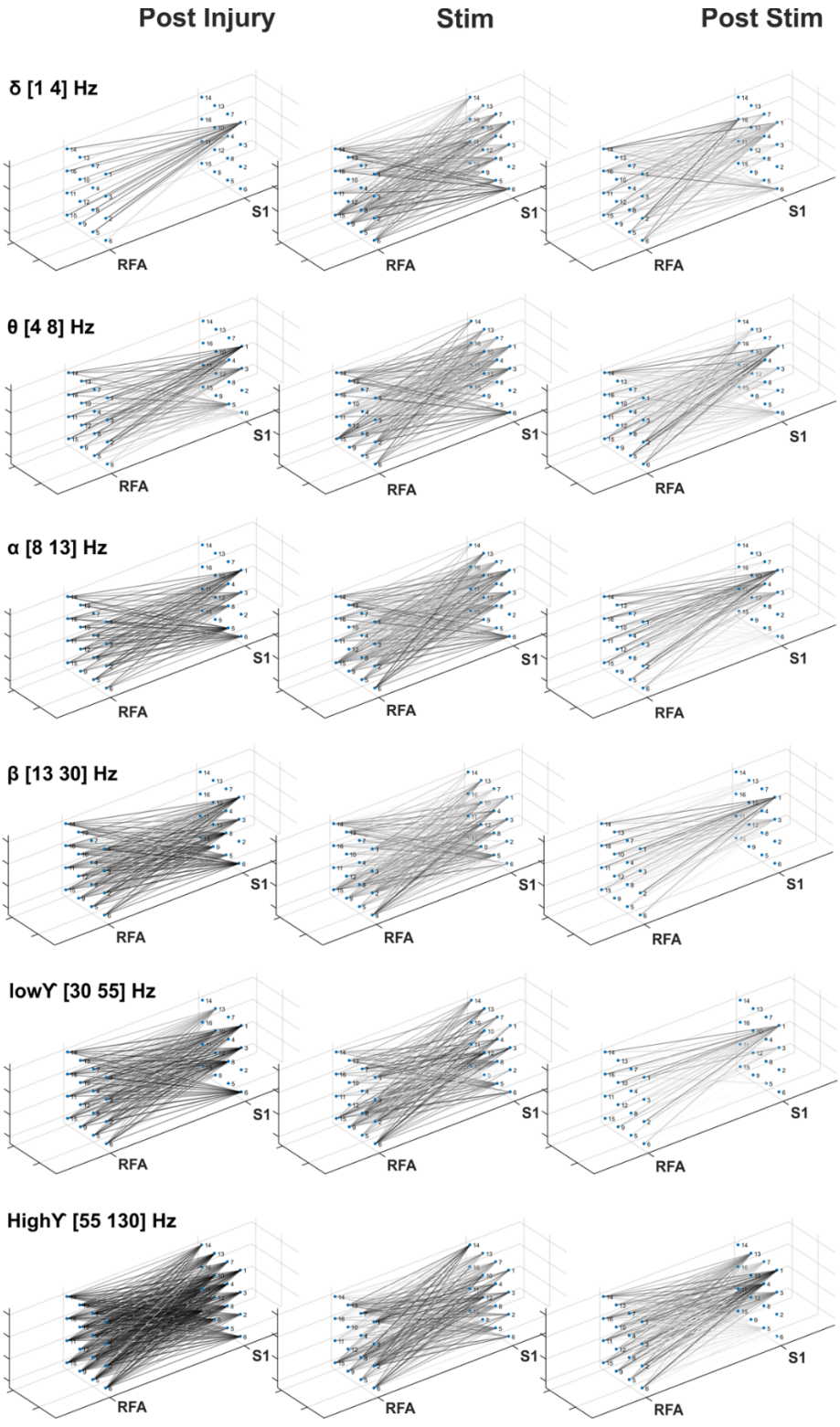

Figure A2: Graphical depiction of the number of functional connections calculated in a representative experiment before (Post Injury), during (Stim) and after (Post Stim) ADS divided per each frequency bands.